

**Tau seeding in a HEK cell model is influenced by aggregation
inducers and cellular chaperones**

By

Emily McNamara

A thesis submitted in partial fulfillment of the requirements for the degree of
Master of Science

Department of Biochemistry

University of Alberta

© Emily McNamara, 2022

Abstract

The tau protein is a microtubule associated protein whose misfolding and subsequent aggregation have been associated with a group of neurodegenerative diseases known as tauopathies. Studying tau in a lab setting has been crucial for the advancement of knowledge and technology used to treat people afflicted with tauopathies. The use of recombinant tau aggregates has and continues to play an important role in these advancements. Recombinant tau can be induced to aggregate using a variety of different inducers, however our lab focuses on heparin, polyphosphate, and arachidonic acid. Here, we explore the ways in which these three different inducers influence the ability of their resulting aggregates to seed tau aggregation in a HEK cell model. Additionally, we reveal structural differences existing between aggregates generated with different inducers that may dictate their abilities to seed cellular aggregation. Our findings reinforce the importance of structure in relation to tau templating and spread, and may inform studies on tau strains. They also give us insight into how commonly used aggregation inducers may affect experimental outcomes. We also used recombinant tau aggregates in cellular seeding assays to explore the effects that certain cellular components, specifically chaperone proteins, have on tau aggregation. One chaperone in particular, DNAJA2, is known to have inhibitory effects on tau aggregation *in vitro* and has increased expression in mild cognitive impairment and Alzheimer's disease. Given this information, we focused on establishing a cell line capable of overexpressing this chaperone, as well as analyzing the ability of tau to seed in cells where DNAJA2 is knocked down. Our results indicate that a decrease in DNAJA2 expression in cells leads to an increase in cells positive for tau aggregates.

Preface

Original work in this thesis was performed by Emily McNamara. The custom scripts for image analysis of cellular seeding was developed by Coleman Dean (Department of Physics, University of Alberta). Allan Yarahmady of the Mok lab assisted in purifying the recombinant tau protein (wildtype and mutant P301L) used in both *in vitro* and cellular assays. Pallabi Sil Paul of the Kar lab (Department of Biochemistry, University of Alberta) obtained ThT fluorescence images of heparin, polyphosphate, and arachidonic acid induced R-tau aggregates. Dr. Nicolas Touret (Department of Biochemistry, University of Alberta) supplied fluorescent secondary antibody, live cell microtubule binding stain, and technical guidance for imaging experiments.

Additionally, lentiviral vectors used in transfection were supplied by Dr. Olivier Julien (Department of Biochemistry, University of Alberta).

Acknowledgements

First and foremost, I would like to thank my supervisor Dr. Sue-Ann Mok for being an excellent mentor throughout my time here. Your patience, knowledge, support, and creativity has not only guided this project, but has taught me how to be a better scientist and person.

I owe a huge thanks to my committee members; Dr. David Westway, for his guidance and expertise, and Dr. Holger Wille, for his wonderful feedback and most importantly for taking me on as a summer student all those years ago and getting me hooked on protein folding. Additionally, thanks to Dr. Paul LaPointe for taking their time to be my external examiner, your advice is much appreciated.

My project could not have been accomplished without the coding and technical skills of Coleman Dean and Klinton Schmeit, the collaborative work of Pallabi Sil Paul from the Kar lab, and for the fluorescent antibodies and imaging assistance from Dr. Nicolas Touret.

Additionally, many of my figures were obtained using core facilities at the University of Alberta with the help of their incredible staff. A huge thank you is warranted for Dr. Xuejun Sun at the Cell Imaging Facility, Aja Rieger from the Flow Cytometry Facility, and Greg Plummer from the Imaging Core.

I will forever be grateful to all of my past and present lab mates, especially Angelle Britton, Kerry Sun, Heather Baker, and Hallie Ng, for their insight, conversations, and kinship. Biggest thanks to my fellow lab mate and masters student Allan Yarahmady who has been by my side for many years and has given me a large amount of his time, purified tau protein, garlic bread, and friendship. Also thank you to members of the Westaway, Wille, and Julien lab for your advice and friendship, and to Dr. Jonathan Parrish and Dr. Adrienne Wright for passing down their knowledge and teaching skills to me.

Lastly, thank you to my family and to my friends especially, Kale McLagan, Cody Miller, Luam Araya, Bridgette Hartley, Raelynn Brassard, Natalie Van Deusen and Claudia Holody for their unconditional love and support. Without you guys and daily Prozac, this degree would not have been possible.

Table of contents

List of Figures.....	x
List of Tables.....	xi
List of Abbreviations.....	xiii
Chapter One: Introduction.....	1
1.1 Introduction.....	2
1.2 Tau protein.....	3
<u>1.2.1 Cell structure and function.....</u>	<u>3</u>
<u>1.2.2 Protein misfolding and aggregation.....</u>	<u>5</u>
<u>1.2.3 Tau aggregation in disease.....</u>	<u>7</u>
<u>1.2.4 Tau cell-to-cell transmission and templating.....</u>	<u>11</u>
1.3 Factors modulating tau aggregation and spreading.....	14
<u>1.3.1 Chaperone proteins and proteostasis.....</u>	<u>14</u>
<u>1.3.2 Chaperone proteins and aging.....</u>	<u>15</u>
<u>1.3.3 DNAJA2 cellular function.....</u>	<u>17</u>
1.4 Recombinant tau aggregates.....	19
<u>1.4.1 Function of recombinant tau aggregates.....</u>	<u>19</u>
<u>1.4.2 Recombinant tau aggregates for use in seeding assays.....</u>	<u>21</u>
<u>1.4.3 Inducers of tau aggregation.....</u>	<u>23</u>
1.5 Thesis aims and hypothesis.....	26
Chapter Two: Materials and Methods.....	36
2.1 Reagents.....	37

2.1.1 <u>List of antibodies</u>	37
2.2 Constructs	38
2.2.1 <u>Recombinant tau vector</u>	38
2.2.2 <u>shRNA vectors</u>	38
2.2.3 <u>Cumate inducible expression vector</u>	38
2.3 General lab techniques	39
2.3.1 <u>SDS polyacrylamide gel electrophoresis (SDS-PAGE)</u>	39
2.3.2 <u>Western blots</u>	39
2.4 <i>In vitro</i> assays with recombinant tau aggregates	40
2.4.1 <u>Recombinant tau expression and purification</u>	40
2.4.2 <u>Recombinant tau aggregate generation</u>	40
2.4.3 <u><i>In vitro</i> aggregation assay</u>	41
2.4.4 <u>Analysis of aggregation assay</u>	42
2.4.5 <u>Protease digestion of tau aggregates</u>	42
2.4.6 <u>Tau aggregate labeling</u>	43
2.5 Mammalian cell culture	43
2.5.1 <u>HEK293 P301L cells</u>	43
2.5.2 <u>Lentiviral transfection</u>	44
2.5.3 <u>Generation of single cell clones</u>	44
2.5.4 <u>Cell lysis using M-PER lysis buffer</u>	45
2.6 Cellular assays with recombinant tau aggregates	45
2.6.1 <u>Cellular seeding assay</u>	45
2.6.2 <u>Imaging analysis</u>	46

<u>2.6.3 DNAJA2 immunofluorescence</u>	46
<u>2.6.4 Fluorescent MT labeling</u>	47
<u>2.6.5 Recombinant tau uptake</u>	48
Chapter Three: Results	55
3.1 Characterizing the HEK293 P301L-tau cell model	56
<u>3.1.1 Doxycycline induces the expression of GFP tagged mutant P301L-tau in our HEK cell model</u>	56
<u>3.1.2 Optimizing conditions for a tau seeding assay in our HEK293 P301L cells</u>	57
3.2 Seeding ability of differently induced fibrils	58
<u>3.2.1 Confirmation that multiple small molecule inducers promote tau aggregation</u>	58
<u>3.2.2 Comparison of cellular seeding efficiency of tau aggregates produced by different inducers</u>	59
<u>3.2.3 Efficiency of tau aggregation based on inducer <i>in vitro</i></u>	60
<u>3.2.4 Evidence of structural differences between tau aggregates generated by heparin, polyP or Ara</u>	62
<u>3.2.5 PolyP induced aggregates can seed tau monomer without the addition of an inducer</u>	63
<u>3.2.6 Heparin, polyP, and Ara induced aggregates can be internalized by our cells</u>	64
3.3 Effect of DNAJA2 on tau aggregation in cells	66
<u>3.3.1 Transfection and induction of cumate inducible expression vector</u>	66
<u>3.3.2 Selection of clones positive for cumate inducible expression vector</u>	67
<u>3.3.3 DNAJA2 and Hsp27 knockdowns lead to an increase in the percentage of cells seeded</u>	67

Chapter Four: Discussion	90
<u>4.1 R-tau aggregates generated with various inducers have different seeding abilities in cells</u>	91
<u>4.2 DNAJA2 knockdown leads to increased aggregation in cells</u>	94
Chapter Five: Conclusion and Future Directions	97
<u>5.1 Conclusions</u>	98
<u>5.2 Future directions</u>	99
Bibliography	100
Appendix A: Signal from 10% seeding material in capillary gel electrophoresis	123
Appendix B: Trypsin resistant seeding product of polyP aggregation reaction	126
Appendix C: <i>In vitro</i> seeding with differently induced aggregates in conjunction with their respective inducer	129
Appendix D: ThT staining of differently induced aggregates	132

List of tables

2.1. List of primary and secondary antibodies used in Western blots, Dot blots, and immunofluorescence assays.....	37
3.1 Cell seeding optimization parameters for our HEK 293 cell model.....	72

List of figures

1.1 Schematic structure of the six MAPT protein isoforms derived from alternative splicing.....	29
1.2 Schematic representation of aggregation motifs in MAPT.....	30
1.3 The core structure of tau aggregates can vary between tauopathies.....	31
1.4 Unique prion protein strains propagate biochemical signatures and distinct disease phenotypes.....	32
1.5 Tau replicates in a prion-like manner by templating.....	33
1.6 Schematic representation of DNAJA2 structure.....	34
1.7 Small molecule inducers of tau aggregation.....	35
2.1 Display of line fitting curve equation efficiency.....	49
2.2 Schematic of cellular seeding assay.....	50
2.3 Parameters for cellular seeding assay analysis.....	51
2.4 Gating parameters for Alexa fluor 647-tau aggregate uptake experiment.....	52
2.5 Mean internalization of Alexa fluor 647-labeled aggregates.....	54
3.1 HEK293 P301L cell model expressed GFP-tau upon addition of doxycycline.....	69
3.2 GFP-tau expressed in cells associates with microtubules.....	70
3.3 Cell seeding requires the addition of lipofectamine.....	71
3.4 Confirmation that multiple small molecule inducers promote tau aggregation.....	73
3.5 Quantification of total tau in aggregation reactions.....	74
3.6 Comparison of cellular seeding efficiency of tau aggregates generated with different inducers.....	75
3.7 Efficiency of tau aggregation based on inducer <i>in vitro</i>.....	77

3.8 Efficiency of tau aggregation based on seed concentration <i>in vitro</i>	79
3.9 Evidence of structural differences between tau aggregates generated with heparin, polyP, or Ara	80
3.10 PolyP induced aggregates can seed tau monomer without the addition of an inducer .	82
3.11 Heparin induced aggregates are internalized by cells	83
3.12 PolyP induced aggregates are internalized by cells	84
3.13 Ara induced aggregates are internalized by cells	85
3.14 HEK293 cell transfection with cumate inducible expression vector	86
3.15 Single cell clones contain the cumate inducible expression vector, and express GFP-tau	87
3.16 Characterization of the shRNA transfected HEK293 cell lines	88
3.17 Seeding in HEK293 cells transfected with shRNA constructs	89

List of abbreviations

Terms

3R = three-repeat

4R = four-repeat

A β = Amyloid beta

AD = Alzheimer's disease

AGD = Argyrophilic Grain disease

Ara = arachidonic acid

BSE = Bovine Spongiform Encephalopathy

CBD = Corticobasal Degeneration

CBD1 = client binding domain 1

CBD2 = client binding domain 2

CFTR = Cystic Fibrosis transmembrane conductance regulator

CJD = Creutzfeldt-Jakob Disease

CSF = cerebrospinal fluid

CTE = Chronic Traumatic Encephalopathy

CWD = Chronic Wasting Disease

FTLD = Frontotemporal Lobar Degeneration

GGT = Globular Glial Tauopathy

HEK = human embryonic kidney

Hsp = heat shock protein

IDP = intrinsically disordered protein

iPSC = induced pluripotent stem cell

KA = kinetic assay

MAPT = microtubule associated protein tau

MCI = mild cognitive impairment

MT = microtubule

MTBD = microtubule binding domain

NFT = neurofibrillary tangle

NI = N-terminal inserts

NDD = neurodegenerative disorder

PHF = paired helical filament

PN = proteostasis network

PolyP = polyphosphate

PrP^C = cellular prion protein

PrP^{Sc} = infectious prion protein

PSP = Progressive Supranuclear Palsy

R-tau = recombinant tau protein

R1-4 = repeat regions 1-4

SF = straight filament

shRNA = small hairpin RNA

TBI = traumatic brain injury

TD = trypsin digest

WT = wildtype

Reagents

DMEM = Dulbecco's Modified Eagle Medium

Dox = doxycycline

D-PBS = Dulbecco's phosphate buffered saline

DTT = dithiothreitol

FBS = fetal bovine serum

FSG = fish skin gelatin

Hygro = hygromycin

PBS = phosphate buffered saline

PFA = paraformaldehyde

Puro = puromycin

Ri = rock inhibitor

TBS = tris buffered saline

ThT = Thioflavin T

CHAPTER ONE: INTRODUCTION

1.1 Introduction

Proteins are fundamental building blocks of life. They are present in every living species from humans to viruses (Whitford, 2005). Each protein has a role in our body that keeps us alive and properly functioning, for example the protein hemoglobin's role is to transport oxygen from our lungs to our muscle tissue, allowing us to perform physical activity (Whitford, 2005). The structure of a protein plays a key role in dictating its specific functions (Moran et al., 2013). The way in which a protein is organized and subsequently folded gives it a specific shape that allows it to carry out its destined roles (Moran et al., 2013). When a protein does not undergo proper folding and becomes 'misfolded' it can no longer perform its designated roles, potentially resulting in the loss of function or the gain of a new function (Mroczko et al., 2019).

Neurodegenerative disorders (NDD's) are a group of progressive and often fatal diseases (Liu et al., 2017) that are characterized by defects in cognition and dementia (Soto, 2003). Furthermore, each NDD can be linked to the misfolding, and subsequent aggregation, of a specific protein (Soto, 2003). In particular, tauopathies are a group of NDDs that are associated with the misfolding and aggregation of the microtubule associated protein - tau (MAPT) (Kovacs, 2018). Tauopathies include but are not limited to Pick's disease, corticobasal degeneration (CBD), chronic traumatic encephalopathy (CTE), progressive supranuclear palsy (PSP), and the highly recognized Alzheimer's disease (AD) (Götz et al., 2019). While these diseases can be commonly linked by the misfolding of the tau protein, the way in which tau misfolds is unique in each disease (Falcon et al., 2019; A. W. P. Fitzpatrick et al., 2017; Zhang et al., 2020).

Tauopathies can affect anyone, however its greatest risk factor is age (Hipp et al., 2014). As such, it is becoming more important to study these diseases due to the substantial increase in the aging population in recent years (Fuster, 2017). In 2016, over 500 000 Canadians were afflicted with

dementia, and it is estimated that by the year 2030, this number will climb to 912 000 (Alzheimer Society of Canada, 2016).

Being able to study tau misfolding and aggregation in a lab setting is essential to the advancement and development of technologies used to treat people afflicted with tauopathies. At the bench, patient samples are considered as the go-to materials for studying specific disease states (Hosokawa et al., 2021). However, aggregates generated from recombinant tau protein (R-tau) are also effective research tools that give us insight into how structure and mutations influence the progression of disease pathology (Goedert et al., 1999; Sanders et al., 2014). For our purposes, R-tau aggregates can be used in *in vitro* assays to look at specific interactions between tau and other proteins, or they can be used in cellular assays to analyze how various cellular components, such as chaperone proteins, play a role in tau aggregation and spread.

1.2 Tau protein

1.2.1 Cellular structure and function

The tau protein is a soluble microtubule associated protein (MAPT) primarily expressed in neurons (Hernández & Avila, 2007). As its name suggests it is thought to associate with, stabilize, and promote the outgrowth of microtubules (MT) (Hernández & Avila, 2007). It is also possible for tau to interact with the neuronal cell membrane (Cantero et al., 2010; Melková et al., 2019). MTs are long tube-like structures composed of tubulin heterodimers that play essential roles in intracellular transport, cell division, and structural integrity (Kadavath et al., 2015). In addition to MT stability, the tau protein is also thought to play a role in neuronal activity, stabilization of DNA, and recruiting cellular components (such as FYN kinase) to the plasma membrane (Gunawardana et al., 2015).

The tau protein is derived from the MAPT gene, located on chromosome 17 in humans, and is composed of 352-441 amino acids, depending on its splicing pattern (**Figure 1.1**) (A. W. P. Fitzpatrick et al., 2017). Differential splicing of the MAPT mRNA gives rise to 6 different isoforms of tau, which differ in their number of N-terminal inserts (N1, N2) and repeat-regions (R1, R2, R3, R4) (A. W. P. Fitzpatrick et al., 2017; Kadavath et al., 2015; Park et al., 2016). Splicing of exons 2 and 3 give rise to 0, 1 or 2 N-terminal inserts, though it should be noted that N2 cannot exist without N1 (Hernández & Avila, 2007; Park et al., 2016). Subsequently, splicing of exon 10 gives rise to tau isoforms with 3 or 4 repeats (Hernández & Avila, 2007; Park et al., 2016). Given this information, the 6 tau isoforms are as follows: 0N4R, 1N4R, 2N4R, 0N3R, 1N3R, 2N3R, with 3R isoforms being highly expressed during fetal development and infancy, and 3R and 4R isoforms being expressed in adults (Baas & Qiang, 2019; Kadavath et al., 2015; Mroczko et al., 2019). Sequences within the repeat-regions have been identified as facilitating tau's binding to MTs, and are aptly referred to as the microtubule binding domain (MTBD) (Kadavath et al., 2015; Mroczko et al., 2019).

Tau is classified as an intrinsically disordered protein (IDP), meaning that it does not possess a rigid fold in its native state (Mroczko et al., 2019). It is suggested that tau possesses little to no regular secondary structure, including α -helices or β -sheets (Mandelkow et al., 1996). Instead, cytoplasmic tau is thought to behave as a random coil, and has even been suggested to fluctuate between an ensemble of temporary folds, including one that resembles a paperclip and shields the core region (Jeganathan et al., 2006). It is also considered to be a highly soluble protein due to the presence of many charged residues and very few hydrophobic residues (von Bergen et al., 2005).

1.2.2 Protein misfolding and aggregation

Despite being highly soluble, it is possible for tau to undergo a misfolding process wherein its individual tau monomers assemble together to form aggregates (Götz et al., 2019; Kovacs, 2018; von Bergen et al., 2005). Two short motifs within the tau sequence that promote aggregation have been identified in R2 and R3: a VQIINK sequence located in R2 from residues 275-280, and the VQIVYK sequence located in R3 from residues 306-311 (A. W. P. Fitzpatrick et al., 2017; von Bergen et al., 2000) (**Figure 1.2**). Interestingly, tau lacking these two aggregation-prone sequences was not capable of assembling into aggregates (Falcon et al., 2015). Large intracellular tau aggregates, known as neurofibrillary tangles (NFTs), are a pathological hallmark of over a dozen neurodegenerative diseases (Kovacs, 2018). All six isoforms of tau have been associated with NFTs (Berriman et al., 2003; A. W. P. Fitzpatrick et al., 2017).

Tau aggregates can be highly ordered within their core regions, adopting a rigid amyloid structure (A. W. P. Fitzpatrick et al., 2017; A. W. Fitzpatrick & Saibil, 2019). The term amyloid refers to a highly ordered cross- β (β -sheets running in parallel to one another) aggregate structure that is 100-200 angstroms in diameter (Soto & Pritzkow, 2018). The exact catalyst for tau misfolding in cells is not entirely understood, though theories suggest that hyperphosphorylation could play an initial role (Hernández & Avila, 2007; Lee et al., 2005; Ward et al., 2012). Tau contains 85 possible phosphorylation sites (Drepper et al., 2020). Normally, it is estimated that tau is occupied by 8 ± 5 phosphate groups, whereas hyperphosphorylated tau is thought to be occupied by 14 ± 6 (Drepper et al., 2020). While hypophosphorylated tau protein has been shown to bind to MT's with greater stability, hyperphosphorylated tau appears to have a lower binding capacity, promoting its free accumulation in the cytoplasm, and potential association with other tau molecules (Lee et al., 2005). Additional factors such as oxidative stress and acetylation have also been suggested to play

a role in the initiation of the misfolding event (Lee et al., 2005; Min et al., 2015; Mroczko et al., 2019). While the exact catalyst remains unknown, there is some data regarding the structural output of the misfolding process. During the misfolding process, tau can form multiple species such as dimers, oligomers, or large amyloid aggregates (Soto & Pritzkow, 2018). Large amyloid aggregates feature a core region (which can vary between tauopathies) with a characteristic cross- β structure (A. W. P. Fitzpatrick et al., 2017). The tightly packed nature of the hydrophobic core region also renders it resistant to protease digestion (Glabe, 2001; Soto & Castaño, 1996).

Some studies have found that aggregated tau alone is not sufficient to cause toxicity (Cowan & Mudher, 2013). Early studies in transgenic mice expressing an inducible form of human 0N4R tau with a disease-associated mutation (P301L) showed cognitive improvements and a reduction in cell loss when the expression of mutant tau was ceased, despite the lingering presence of large and small aggregates (Cowan & Mudher, 2013; SantaCruz et al., 2005; Spires et al., 2006). An additional study using this mouse model found that the application of a tau hyperphosphorylation inhibitor was able to prevent motor impairments even though the NFT load was not affected, suggesting that NFTs may not be the cause of such toxicity (Cowan & Mudher, 2013; Le Corre et al., 2006).

In contrast to these findings, there is evidence that suggests tau aggregates are toxic (Braak & Braak, 1991; Eckermann et al., 2007; Mocanu et al., 2008). Tau aggregates appear to generate a toxic environment for the cells through many means such as leading to physical obstructions and blocking cellular events, causing toxic signaling (von Bergen et al., 2000), inhibiting protein folding and vesicular transport, and overall disrupting the proteostasis network (PN) (A. Yu et al., 2019).

Early on in the study of tauopathies, NFTs were linked to disease progression in a correlative manner, with increased quantity and spread of NFTs being found in the brains of patients with a more advanced disease state (Braak & Braak, 1991; Cowan & Mudher, 2013). Specifically, the characterization of the Braak stages found a common pattern of tau (and A β) distribution throughout various brain regions of AD patients, which correlated with disease and symptom progression (Braak & Braak, 1991). However, studies in transgenic mice expressing tau with either pro-aggregation mutations, or anti-aggregation mutations have directly linked tau aggregation to pathology by showing that only mice expressing tau with pro-aggregation mutations experienced tau aggregation, which later led to cell death (Cowan & Mudher, 2013; Eckermann et al., 2007; Mocanu et al., 2008).

Furthermore, ongoing debate exists as to whether tau oligomers or larger aggregates are the primary toxic material for cells. Tau oligomers have been suggested to be the main source for propagation of aggregation in the initial disease pathology (Ghag et al., 2018; Meraz-Ríos et al., 2010; Patterson et al., 2011; Ward et al., 2012), possibly due to their hydrophobic nature (Lasagna-Reeves et al., 2012). Additionally, it has been noted that tau oligomers are increased in diseases like AD and also precede the formation of NFTs (Patterson et al., 2011). Conversely, larger aggregates can gain pathological function by destabilizing MTs from lack of binding ability and in turn lead to the excess production of new tau (Lovestone, 2002), and induction of apoptosis (Meraz-Ríos et al., 2010; Nie et al., 2007).

1.2.3 Tau aggregation in disease

Due to its clear association with neuronal cell death, tau misfolding and subsequent aggregation has been linked to numerous diseases collectively known as tauopathies (A. W. Fitzpatrick &

Saibil, 2019). This set of diseases includes but is not limited to: Alzheimer's disease, Pick's disease, Progressive Supranuclear palsy, Corticobasal Degeneration, Globular Glial Tauopathy (GGT), Argyrophilic Grain disease (AGD), and Frontotemporal Lobar Degeneration with Tau inclusions (FTLD-tau) (Götz et al., 2019). This group can be further divided into primary and secondary tauopathies (Vaquer-Alicea et al., 2021). In primary tauopathies, such as CBD or PSP, aggregated tau is the most pronounced pathological feature defining the disease (Vaquer-Alicea et al., 2021). In secondary tauopathies, other aggregated proteins may precede tau aggregation and play a role in defining the disease, such as the A β protein in AD, or environmental factors may play a significant role in initiating disease pathology, which occurs with severe head trauma in CTE (Vaquer-Alicea et al., 2021).

The numerous mutations associated with FTLD-tau provide the strongest evidence that aggregating tau is pathogenic. Mutations can occur along tau via mis-splicing, point missense mutations, and deletions (Park et al., 2016; von Bergen et al., 2001). Although many mutations are not yet well studied, work in this field has offered some insight into how tau can be rendered more pathogenic. For example, some mutations lead to an increased propensity for tau to aggregate, other splicing mutations can lead to an imbalance in the production of 4R versus 3R isoforms (Kar et al., 2007). Perhaps the most well-studied mutant is the P301L mutant that is associated with FTLD-tau (Berriman et al., 2003; Crowther & Goedert, 2000; Götz et al., 2019; Park et al., 2016). P301L tau is known to be extremely aggregation prone due to mutating the proline at position 301 to a leucine, which promotes its assembly into β -sheets (von Bergen et al., 2001). As such, P301L is widely used in lab settings, including our own, as a tool to efficiently study tau aggregation from *in vitro* to *in vivo* studies (Kang et al., 2021; SantaCruz et al., 2005; Spires et al., 2006).

While each tauopathy can be defined by distinct sets of clinical symptoms and pathology, they share a common characteristic of overall cognitive decline and the accumulation of aggregated tau (Soto, 2003). As previously mentioned, all isoforms of tau are capable of forming aggregates, however the proportions of different aggregated isoforms can vary between diseases (Götz et al., 2019). For example, the predominant isoform in Pick's disease is 3R tau, while for CBD, PSP, AGD, and GGT it is 4R tau, and AD and FTLD-tau contain both 3R and 4R tau (Götz et al., 2019; Kovacs, 2018; Park et al., 2016). Additionally, AD is accompanied by the presence of another aggregating protein, amyloid-beta ($A\beta$), which precedes the appearance of tau aggregates in disease progression (A. W. Fitzpatrick & Saibil, 2019). One of the more interesting aspects of tauopathies is that the structure and associated components of the tau filaments vary between diseases (Falcon et al., 2019; A. W. P. Fitzpatrick et al., 2017; Zhang et al., 2020). A recent wealth of cryo-EM structures now reveal the packing of tau aggregate cores with atomic resolution (A. W. P. Fitzpatrick et al., 2017; A. W. Fitzpatrick & Saibil, 2019). In AD, two major amyloid structures have been elucidated: paired helical filaments (PHF) and straight filaments (SF) (A. W. P. Fitzpatrick et al., 2017). While they both possess the same fold, the difference between PHFs and SFs is the way the proteins come together to form an interface (A. W. P. Fitzpatrick et al., 2017). In PHFs, the proteins form a symmetrical interface and pack together through residues 332-336 (PGGGQ), whereas SFs form an asymmetrical interface by packing together between residues 317-324 and 312-321 (A. W. P. Fitzpatrick et al., 2017).

The difference in tau filament structures between tauopathies can be largely attributed to differences in their core regions (Falcon et al., 2018, 2019; A. W. P. Fitzpatrick et al., 2017; Zhang et al., 2020) (**Figure 1.3**). In AD and CTE, there are eight β -sheets present in the core region that span across residues 306-378, and 305-379 respectively (Falcon et al., 2019; A. W. P. Fitzpatrick

et al., 2017; Zhang et al., 2020). Conversely, in Pick's disease and CBD there are eleven β -sheets spanning residues 254-378, and 274-380 respectively (Zhang et al., 2020). The architecture of the core region can also vary, with AD, CBD, and CTE taking on a similar yet not identical C-shape, and the core region of 3R tau in PD not resembling a C-shape at all (Falcon et al., 2019; Zhang et al., 2020). Additionally, both CBD and CTE have non-proteinaceous inclusions associated with their core regions, which are absent in AD and Pick's disease (Zhang et al., 2020).

The existence of different tau aggregate structures that vary with disease is reminiscent of another protein that causes NDDs: the prion protein. In fact, the idea of infectious strains in protein-misfolding diseases was first explored with the prion protein (Vaquer-Alicea et al., 2021). Upon a misfolding process, the cellular prion protein (PrP^C) is converted into the infectious form of prion protein (PrP^{Sc}), which is associated with numerous progressive, transmissible, and fatal diseases that include the well known Bovine Spongiform Encephalopathy (BSE) or 'mad cow', Creutzfeldt-Jakob Disease (CJD), and Chronic Wasting Disease (CWD) (Requena & Wille, 2017). Infectious prions, like tau, are composed of a protease-resistant amyloid core that renders the protein aggregation-prone (Prusiner et al., 1998; Requena & Wille, 2014). The infectious nature of PrP^{Sc} stems from its ability to serve as a template for PrP^C, thereby converting PrP^C monomers into PrP^{Sc} and propagating aggregation (F. E. Cohen & Prusiner, 1998; Requena & Wille, 2017). Each prion disease has a characteristic set of symptoms, incubation time, and transmissibility (Aguzzi et al., 2007; Vaquer-Alicea et al., 2021). Interestingly, when infectious prion protein is isolated from a particular diseased organism and introduced into an identical host, it has the ability to transmit its unique biochemical signatures to novel PrP^C via templating, and propagate its distinct disease phenotype (**Figure 1.4**) (Aguzzi et al., 2007). It is therefore said that prions have unique 'strains' that explain how the same protein sequence can promote multiple diseases (Vaquer-Alicea et al.,

2021). Upon protease digestion, only the protease-resistant regions of the core will remain detectable and depending on the strain of infectious prion protein, the presentation of these core regions may differ (Aguzzi et al., 2007). Tau (and other amyloid forming proteins) may also have prion-like properties (Vaquer-Alicea et al., 2021). This difference in structure between the core regions may give rise to different disease specific ‘strains’, with some diseases (notably AD) having more morphological homogeneity than others (Sanders et al., 2014). The idea of strains can give us insight into how particular tauopathies differ in phenotype and disease progression, all while being linked to the tau protein.

1.2.4 Tau cell-to-cell transmission and templating

While aggregated tau exhibits toxic properties within individual cells, its most potent pathogenic property may be its ability to spread between cells and propagate aggregation (Brunello et al., 2020; J. J. Chen et al., 2019; Clavaguera et al., 2015). Tau aggregates are thought to act as ‘seeds’ and are crucial for driving pathology. In a literal sense, a seed serves as a starting point for growth, leading to the production of more seeds and further propagation. In the context of tau, it is unclear exactly what tau species serves as a seed. There is evidence suggesting that tau monomers can serve as seeds (Mirbaha et al., 2018), in addition to oligomers (Gerson & Kaye, 2013) and short fibrils (Jackson et al., 2016). Importantly, the seeds can survive degradation inside the cell, and can be spread between cells.

Studies have suggested that tau propagates in a prion-like manner, wherein the seed taken up by a non-infected cell acts as a template for healthy monomeric tau to misfold and adopt the same aggregate conformation, perpetuating continuous cycles of aggregation (Brunello et al., 2020; Hosokawa et al., 2021; Lasagna-Reeves et al., 2012).

The way in which tau is taken up into the cytoplasm of neighbouring neuronal or glial cells may be accomplished using a variety of different pathways including but not limited to: direct secretion through the plasma membrane upon interaction with specific receptors (such as heparan sulphate proteoglycans) (Rauch et al., 2018), entry using ectosomes, endosomes or exosomes (Dujardin et al., 2014), or direct transfer to the cytosol via tunneling nanotubes (Brunello et al., 2020).

Interestingly, the structural properties or source of the tau aggregate ‘seed’ have been shown to directly modulate their pathogenic effects in cells and animal models (Sanders et al., 2014), similar to the concept of prion strains. For example, both R-tau aggregates and tau aggregates derived from brain samples are not only able to induce seeding in both cell (Frost, Jacks, et al., 2009) and mouse models (Clavaguera et al., 2009), but can also propagate their unique aggregate features such as morphology, size, and seeding capacity (Sanders et al., 2014).

When R-tau aggregates were added to HEK293 cells expressing YFP-tagged tau MTBD, the cells were able to continue to replicate the resulting aggregates through various generations (Sanders et al., 2014). Throughout the generations, these aggregates maintained their size, morphology, seeding ability and structure (Sanders et al., 2014). Studies in cells also revealed that when brain samples from patients with various tauopathies were used as seeding material, the tau isoform expressed by the cell needed to match the isoform involved in the tauopathy in order to generate a significant seeding effect (Woerman et al., 2016). For example brain samples from patients with Pick’s disease (a tauopathy involving primarily 3R tau) were only able to propagate in cells expressing 3R tau isoforms, and not in cells expressing 4R tau isoforms (Woerman et al., 2016). The reverse was true for brain samples from patients with AGD (a tauopathy involving primarily 4R tau), and AD brain samples propagated robustly only in cells expressing 3R and 4R tau isoforms (Woerman et al., 2016). When mouse models expressing 4R human tau were injected

with brain homogenates from patients with AGD, PSP and CBD, the resulting silver-staining of tau inclusions in the hippocampal brain region revealed that morphologies of the inclusions formed in the mice resembled those of the initial inoculate (Clavaguera, Akatsu, et al., 2013). More recently, a mouse model capable of expressing both 3R and 4R tau was found to successfully propagate Pick's disease aggregates that managed to retain their aggregate features (Hosokawa et al., 2021). The observations that the aggregates in individual tauopathies have distinct structural features raises the possibility that their structures may also modulate their biological effects.

Initial studies on tau spread were carried out in mutant-P301S-tau mouse models (P301S is an FTLD-tau associated mutation), where brain tissue from infected mice was injected into healthy mice, which led to them becoming sick and dying (Brunello et al., 2020; Clavaguera et al., 2009). While P301S tau was found at the injection site it was also found in surrounding brain regions, suggesting the occurrence of spread (Brunello et al., 2020; Clavaguera et al., 2009). Further studies have been conducted on this phenomenon using brain samples from human AD patients (Clavaguera, Akatsu, et al., 2013; Lasagna-Reeves et al., 2012) and mice with traumatic brain injury (TBI) (Zanier et al., 2018), wherein both samples were able to propagate in mouse models. The generation of preformed R-tau aggregates *in vitro* were a critical step in tau research. Injection of R-tau aggregates into mice induces aggregation and spread throughout the brain, making it a useful tool to study spread in tauopathies (X. Chen et al., 2020; Min et al., 2015; Wang et al., 2021). Experiments conducted with these aggregates have suggested that tau propagates from cell-to-cell based on synaptic connectivity and physical proximity (Brunello et al., 2020; Calafate et al., 2015; Iba et al., 2013).

1.3 Factors modulating tau aggregation and spreading

1.3.1 Chaperone proteins and proteostasis

Tauopathies and other NDDs are characterized by the presence of aggregates containing misfolded protein, however not all misfolded or aggregated proteins lead to pathology (Mok et al., 2018). Our cells have thousands of proteins, and each one needs to be properly folded and functioning in the face of changing cellular conditions (Hipp et al., 2014, 2019; Margulis et al., 2020). The homeostasis of proteins, called proteostasis, is maintained by an extensive network of chaperone proteins, as well as proteolytic degradation machinery, and regulatory proteins (Hipp et al., 2014, 2019; Margulis et al., 2020). Following translation, newly synthesized unfolded proteins find themselves in a crowded cellular environment with lots of potential to undergo a misfold, especially with exposed hydrophobic regions (Kim et al., 2013). Similarly, proteins that have been exposed to a stressor, like heat, may become denatured in the cytoplasm, exposing hydrophobic regions and increasing their risk of entering a misfolded state (Kim et al., 2013). Chaperones can reversibly bind to unfolded or misfolded client proteins, and assist in their proper folding (Brehme et al., 2014; Kim et al., 2013). More specifically, chaperones act by overcoming free-energy barriers that would otherwise lead these proteins to assembling into more energetically stable oligomers or aggregates (Hartl et al., 2011; Jahn & Radford, 2005; Kim et al., 2013). The primary components of the chaperone network are called heat shock proteins (Hsp), examples of which include Hsp70 and Hsp90 (Margulis et al., 2020; Mok et al., 2018). Hsps utilize ATP hydrolysis in order to form reversible interactions with their client proteins (Margulis et al., 2020). The functions of Hsps can be assisted by co-chaperones, which have a variety of roles. For example, one group of co-chaperones called Hsp40s, are known for their ability to dictate the Hsp70 client specificity of newly synthesized or damaged client proteins, as well as determine the

folding/degradation/localization outcome of said client (Margulis et al., 2020; Mok et al., 2018). However, they are also capable of directly binding to client proteins, independently of Hsp70s (Cyr, 1995; Meacham, 1999). Relevant to the work of this thesis, a study by Mok et al. (2018) identified multiple chaperones that were able to directly inhibit tau aggregation, including the Hsp40 co-chaperone, DNAJA2 (see section 1.3.3) (Mok et al., 2018).

1.3.2 Chaperone proteins and aging

Despite having a clear defence system in place for misfolded and aggregated proteins, it is unclear how and why disease associated proteins evade the cell's protective mechanisms.

The most significant risk factor for NDDs is aging (Brehme et al., 2014; Hipp et al., 2014). Perhaps a hint as to why certain misfolded proteins are able to evade proteostasis defense systems is that as we age, there is a decline in the expression of chaperone proteins (Brehme et al., 2014; E. Cohen et al., 2006; Hsu et al., 2003; Mok et al., 2018). This decline of protective proteostasis is correlated with the accumulation of toxic protein species (Ben-Zvi et al., 2009). Interestingly, even though overall chaperone levels become impaired with aging, aged organisms do increase the expression of subsets of chaperones with known anti-aggregation activity (Söti & Csermely, 2000; Söti & Csermely, 2002). It would be more accurate to say that chaperone expression becomes unbalanced in aging and NDDs, with certain chaperones having increased expression, certain with decreased expression and some remaining unchanged (Brehme et al., 2014; Nachman et al., 2020). This concept has been reinforced in AD, which is known to exhibit increased levels of Hsp27 (Renkawek et al., 1993) and Hsp28 (Shinohara et al., 1993). Additionally the co-chaperone 'DNAJA2' is significantly upregulated in mild cognitive impairment (MCI), a cognitive state often preceding AD, and to a lesser extent in AD (Mok et al., 2018). Since chaperones are key regulators

of the PN that assists in the proper folding and refolding of proteins, this increased expression of chaperones during aging or age-related disorders might be beneficial in regulating toxic protein buildup. When Hsp27 was overexpressed in transgenic mice expressing human P301L tau prior to NFT formation, it was able to rescue the neuronal dysfunction that occurred later on in mice expressing only endogenous levels of Hsp27 (Abisambra et al., 2010).

Some evidence supports that certain chaperones actually end up causing more pathology in diseases such as AD, despite their known roles in preventing protein aggregation (Nachman et al., 2020; Stege et al., 1999). α B-crystallin, a small Hsp whose expression is increased in AD, has a role in preventing A β aggregate formation *in vitro*, however when overexpressed in cells alongside A β it leads to cell death, suggesting that it may play a role in stabilizing smaller more toxic and seeding prone A β species and preventing them from assembling into larger aggregates (Stege et al., 1999). Similarly, Hsp70, Hsp110, Hsp40 complexes have been found to have disaggregase activity in the context of aggregated tau protein, however by attempting to eliminate larger amyloid aggregates, it may play a role in generating many smaller, more potent seeds (Nachman et al., 2020). There has also been evidence that chaperones become entangled within NFTs (Cisse et al., 1993; Perez et al., 1991), possibly suggesting that their interactions with toxic proteins may contribute to pathology, or even that their potentially protective roles may be blocked by being sequestered into aggregates.

While there are many suggestions that increased levels of specific chaperones can be helpful in NDDs, there is also evidence that states the contrary. As of now, it is not clear how chaperone levels affect disease progression and more detailed mechanistic studies in the context of disease-causing aggregating proteins such as tau are needed.

1.3.3 DNAJA2 cellular function

According to a large-scale study analyzing purified chaperone interactions with tau, DNAJA2 was found to be a potent inhibitor of tau aggregation *in vitro*, and was found to be active against multiple aggregation-prone mutants (Mok et al., 2018). Additionally, DNAJA2 was found to be upregulated in patients with MCI or AD, possibly suggesting a protective role in early disease state (Mok et al., 2018). Notably, DNAJA2 is capable of binding to multiple tau species *in vitro* including monomeric tau, oligomeric tau, and small or large aggregates (Irwin et al., 2021). This interaction occurs in the client binding regions of DNAJA2 and is suggested to prevent aggregate growth through the addition of tau monomers, as well as reduce the speed of the aggregate nucleation process (Irwin et al., 2021). More specifically, client-binding domain 1 (CBD1) of DNAJA2 is largely associated with binding to tau monomers, while client binding domain 2 (CBD2) is primarily associated with binding to aggregation-prone tau species (Irwin et al., 2021). The interaction between tau and DNAJA2 occurs via tau's aggregation-prone sequences in R2 and R3 (**Figure 1.2**) at residues 275-280 and 305-314 respectively (Irwin et al., 2021). Despite having been suggested to play a role in disaggregation, DNAJA2 has not been identified as part of the metazoan disaggregase complex (Rampelt et al., 2012). Currently, the way in which DNAJA2 affects tau aggregation in a human cell model has yet to be analyzed.

DNAJA2 is a cytoplasmic co-chaperone, meaning that it interacts with other chaperones, specifically Hsc70, and helps to dictate client binding specificity (Piette et al., 2021; Terada & Mori, 2000). This co-chaperone is in the family of Hsp40s, also called 'J-domain proteins', which is a group of chaperones that interact with a variety of different Hsp70s (Piette et al., 2021). DNAJA2 belongs to the 'A' class of this family, which is the most ubiquitous alongside class 'B' (Craig & Marszalek, 2017; Jiang et al., 2019; Piette et al., 2021). The J-domain is a highly

conserved alpha-helical region comprising roughly 70 residues and located at the N-terminal region of the protein (**Figure 1.6**) (Jiang et al., 2019; Kampinga & Craig, 2010). Additionally, it allows for the interaction of Hsp40s with Hsp70s to initiate ATP-hydrolysis (Baaklini et al., 2012; Kampinga & Craig, 2010). Following the J-domain, there is a glycine/phenylalanine (G/F) rich region that plays a role in function and specificity (Jiang et al., 2019; Yan & Craig, 1999), along with 4 zinc-binding motifs that are exclusive to Class A Hsp40s and assist in autonomous binding and refolding of unfolded proteins (Linke et al., 2003; H. Y. Yu et al., 2015). Hsp40s have two client binding domains (CBD1 and CBD2), that promote client protein binding and interaction with Hsc70 (**Figure 1.6**) (Jiang et al., 2019; Rosenzweig et al., 2019). Both CBD1 and CBD2 are composed primarily of β -barrel structures, and bind distinctly to client proteins using hydrophobic and charged surfaces (Jiang et al., 2019). Human DNAJA2 has a preference for binding smaller aggregates to assist in their disassembly and solubilization, while other Hsp40s may have a preference for larger aggregates (Nillegoda et al., 2015; Rosenzweig et al., 2019). Finally, Hsp40 proteins have a dimerization domain at their C-terminus that allows them to form functional dimers in the cytosol (Jiang et al., 2019). In addition to interacting with Hsc70, DNAJA2 and other Hsp40s have also been found to interact with each other via charge based interactions in their J domains (Nillegoda et al., 2017), and can act autonomously (Craig & Marszalek, 2017). The overexpression of certain Hsp40s on their own, including DNAJB8, were shown to suppress client protein aggregation (Craig & Marszalek, 2017; Hageman et al., 2010).

It is important to note that Hsp40s, including DNAJA2, can function on a variety of different clients, and can have different effects on the same client. We've established that DNAJA2 can bind to both monomeric and aggregation-prone tau (Irwin et al., 2021), however its substrate binding is not limited to tau. A second substrate example for DNAJA2 is the Cystic Fibrosis

transmembrane conductance regulator (CFTR), a membrane protein involved in Cystic Fibrosis (Kim Chiaw et al., 2019). At endogenous levels, DNAJA2 binds to CFTR to assist in its folding process, however at overexpressed levels the co-chaperone promotes CFTR degradation (Kim Chiaw et al., 2019). The ability of Hsp40s to carry out a variety of roles on a variety of proteins suggests that they may have multiple effects on the PN, and specifically on tau homeostasis.

1.4 Recombinant tau aggregates

1.4.1 Function of recombinant tau aggregates

Considering its strong links to human disease, it is very important for us to be able to study tau effectively in a lab setting. The ability to study the misfolding, aggregation, spread and pathology of this protein requires us to obtain samples of pathological tau. Patient brain samples are a prevalent source of aggregate material when studying tauopathies. These samples are obtained post mortem, and while they are extremely physiologically relevant, their abundance is limited and samples are often difficult to obtain.

A reliable alternative to patient samples is the *in vitro* generation of aggregates using purified, R-tau protein. This method is efficient as it uses bacterial cells to express the desired protein, which is then purified and concentrated for use in a variety of assays (Morozova et al., 2013). The remarkable aspect of this system is that it not only works for wildtype (WT) tau, but also for any of the tau mutants, providing us with a useful tool to study tau's aggregation-prone mutants. This technique is widely used, and our lab in particular is currently developing a high-throughput method of purifying hundreds of possible R-tau mutants.

R-tau can be induced to form aggregates *in vitro* (Morozova et al., 2013). Conditions can be replicated by other researchers and give consistent results between experiments. These aggregates

have been successfully studied in *in vitro* (Min et al., 2015; Mok et al., 2018; Morozova et al., 2013), cellular (J. J. Chen et al., 2019; Guo & Lee, 2013), and mouse model assays (Clavaguera, Lavenir, et al., 2013).

Though current preparations of R-tau aggregates may have structural differences compared to the aggregates found in patient samples (S. H. Scheres et al., 2020; Zhang et al., 2019, p.), they have served (and continue to serve) as an indispensable tool for the advancement of knowledge and technology surrounding tauopathies. Currently, new conditions are being established to generate and select R-tau aggregates that are indistinguishable from the aggregates found in patient brains, making them an even more relevant tool for studying various tauopathies (Lövestam et al., 2022; Scheres & Lövestam, 2022). R-tau aggregates have played an important role in identifying the roles of the various repeat regions (Arrasate et al., 1999), and have even acted as antigens in the development of antibodies against tau (Agadjanyan et al., 2017). In fact, it was through the use of these aggregates that we were able to establish the role that mutations had in aggregate assembly and disease pathology, including the role of the P301L mutation in FTLD-tau (Arrasate et al., 1999; Goedert et al., 1999).

Studies with R-tau also revealed that mutations, including P301L, can lead to structurally distinct tau species (Frost, Ollesch, et al., 2009). Interestingly, R-tau with a P301L/V337M double mutation was able to alter the subsequent aggregation of WT tau in a seeding assay (Frost, Ollesch, et al., 2009). This gave rise to aggregates that were conformationally distinct from WT aggregates but that resembled those of P301L/V337M aggregates, further suggesting the idea of tau strains and templating (Frost, Ollesch, et al., 2009).

Using a recombinant protein in assays allows us a certain degree of control when it comes to what goes into biochemical reactions. This aspect has been beneficial in studying specific protein-

protein interactions, or aggregation inhibitors (Crowe et al., 2007; Mok et al., 2018; Pickhardt et al., 2005; Taniguchi et al., 2005; Zhang et al., 2019). Several aggregation inhibitors have already been identified using R-tau, including anthraquinones (Pickhardt et al., 2005), polyphenols, and porphyrins (Taniguchi et al., 2005). A particularly compelling study used R-tau in conjunction with various chaperone proteins to analyze their effect on tau aggregation (Mok et al., 2018). Strikingly, they found that DNAJA2 was a potent inhibitor of not only WT tau aggregation, but also the aggregation of certain tau mutants (Mok et al., 2018). Needless to say, R-tau offers us an efficient way to study tau structure, mutations, aggregation, and spread.

1.4.2 Recombinant tau aggregates for use in seeding assays

R-tau aggregates can be used for both *in vitro* and cellular seeding assays. Similar to how inducers speed up R-tau aggregation, adding a preformed aggregate, known as a ‘seed’, to a reaction with monomeric tau will accelerate the monomer’s assembly into aggregates (Fuster-Matanzo et al., 2018).

An *in vitro* seeding assay gives us the benefit of having control over the components of the reaction. This type of assay can allow us to look specifically at seeded tau aggregation, or seeded tau aggregation in the presence of other proteins, such as chaperones (Mok et al., 2018), or potential aggregation inhibitors (Crowe et al., 2007; Taniguchi et al., 2005). *In vitro*, tau aggregation can be monitored using a fluorescent, amyloid binding dye called Thioflavin T (ThT), where an increase in ThT signal suggests an increase in aggregate formation (Friedhoff, Schneider, et al., 1998).

A cellular seeding assay is slightly different from an *in vitro* seeding assay. Here, pre-formed tau aggregates are added to cells extracellularly and are subsequently taken up by the cells via

endocytosis or other mechanisms (Fuster-Matanzo et al., 2018; Guo & Lee, 2013). Lipofectamine, a liposomal reagent, is commonly used in seeding to aid in the uptake of tau aggregates into cells, thereby increasing the concentration of seeds in the cell available for templating new aggregation (Nonaka et al., 2010; Polanco et al., 2021). Like *in vitro* assays, cell assays allow us to look at protein-protein interactions and aggregation inhibitors, but they do so in the context of the cellular environment. Thus, when compared to the *in vitro* assay, a cell assay has a lot more factors that are beyond our control, however it offers a more biologically relevant environment for an aggregation assay to take place. Fortunately, our lab has an excellent system in place for both *in vitro* and cellular seeding assays.

It has been confirmed that soluble tau expressed in cells will undergo aggregation upon the addition of preformed R-tau aggregates (Guo & Lee, 2011). Cell seeding assays have proven to be useful tools in studying propagation and templating in tauopathies. The importance of endolysosomal escape in tau's propagation between cells was established using a cell seeding assay involving R-tau aggregates and human cells with knockdowns in the endosomal sorting complex required for transport (J. J. Chen et al., 2019). The ability of cells to degrade tau aggregates upon the suppression of endogenous tau expression was also explored using human cell seeding models (Guo et al., 2016). These models also reinforced that aggregation would swiftly resume if the expression of endogenous tau was activated (Guo et al., 2016). The unique qualities of aggregates and their abilities to propagate depending on the seed of origin have also been characterized using cell seeding assays, giving us insight into spread and potential tau strains (Sanders et al., 2014). Building on the concept of spread, live-imaging of endogenous tau aggregates generated in cells revealed their dynamic structures that can be transmitted during cell division, furthering their propagation (Guo et al., 2016).

1.4.3 Inducers of tau aggregation

Due to its incredibly soluble nature, R-tau takes a long time to assemble into aggregates on its own *in vitro* (Ramachandran & Udgaonkar, 2011). Polyanionic molecules including RNA, polyphosphate, polyglutamate, heparin and fatty acids have been used to recruit tau and reliably promote its assembly into an amyloid structure (Friedhoff, Schneider, et al., 1998; Kampers et al., 1996; Wickramasinghe et al., 2019; Wilson & Binder 1997; Zhang et al., 2019). While the exact mechanism behind how polyanionic inducers play a role in tau's assembly into aggregates is not fully understood, it is speculated that the negatively charged inducers may neutralize tau's positively charged regions and allow for much closer proximity of the tau molecules (Shammas et al., 2015), or they may act as a scaffold onto which tau can use to assemble into amyloid structures (Wickramasinghe et al., 2019). Evidence suggests, however, that tau's process of assembly into amyloid aggregates is nucleation-dependent, meaning that the initial formation of small aggregates constitutes a lag phase before rapid elongation of aggregates begins (Friedhoff, von Bergen, et al., 1998; Guo & Lee, 2011). Aggregation inducers, specifically heparin, have played a crucial role in establishing the existence of the lag phase, and also the differences in lag phases between different mutants (Friedhoff, Schneider, et al., 1998; Friedhoff, von Bergen, et al., 1998; Shammas et al., 2015).

These inducers offer us a set of tools to make amyloid tau structures for the use in a variety of different assays. Our lab has focused primarily on three inducers: heparin, polyphosphate, and arachidonic acid.

i. Heparin

Heparin is a sulfated glycosaminoglycan that occurs naturally in our bodies (Paudel & Li, 1999). It has been used medically as an anticoagulant for the treatment of thrombosis (Alquwaizani et al., 2013). Despite being found naturally outside of the cell, this polyanion offers us a tool to study tau aggregate formation *in vitro*, and gives us insight as to what may be going on inside of the cell (Ramachandran & Udgaonkar, 2011). Incubation of R-tau with heparin allows for the assembly of R-tau into amyloid aggregates. Though its mechanism of action is not totally clear, studies suggest that it compensates for tau's positive charges and allows for tau molecules to gather in close proximity; stacking their core regions (Sibille et al., 2006). Early studies also suggested that heparin may integrate into the core of tau aggregates (Sibille et al., 2006). More recent Cryo-EM studies have hypothesized that heparin's negative charge serves to neutralize the positive charges from Lysine residues surrounding the core region, allowing for the stacking and subsequent stabilization of tau cores into amyloid structures (Zhang et al., 2019). Additionally, the disaccharide components of heparin may interact with hydrophobic regions of the tau molecule, again acting to stabilize the core region (Zhang et al., 2019). Heparin has been used successfully for many years to generate R-tau aggregates *in vitro* (Goedert et al., 1999), as well as to study various kinetic factors of aggregation, such as lag phase (Friedhoff, Schneider, et al., 1998; Friedhoff, von Bergen, et al., 1998; Shamma et al., 2015).

ii. Polyphosphate

Polyphosphate (polyP) is a naturally occurring biological polymer produced in all prokaryotes and eukaryotes (Cremers et al., 2016). As its name implies, polyP is composed of multiple (from 10 to 1000) phosphate residues that are linked together via phosphoanhydride bonds (Achbergerová & Nahálka, 2011; Cremers et al., 2016; Jiménez et al., 2017), and as such it is an intense polyanion (Morrissey et al., 2012). While polyP is found within the cytosol and in various organelles, it is also known to be secreted into the extracellular space (Cremers et al., 2016). Functionally, it has been linked with pro-inflammatory effects, and procoagulant effects (Smith et al., 2006), which is opposite to heparin (Morrissey et al., 2012). Additionally, it has been found to be upregulated during stress conditions (Cremers et al., 2016). As an inducer it functions similarly to other polyanions, however it is also suggested that polyP binds to and between R-tau monomers, thereby linking them in a scaffold-like fashion (Mok et al., 2018; Xie & Jakob, 2019). PolyP has also been used to study protein aggregation, and has been used as an inducer to initiate tau's assembly into amyloid aggregates (Cremers et al., 2016; Wickramasinghe et al., 2019).

iii. Arachidonic acid

Arachidonic acid (Ara) is a polyunsaturated fatty acid that can function as an anionic inducer of tau aggregation (Mutreja & Gamblin, 2017). Ara is obtained from a diet containing meat and eggs, and is then incorporated into cytosolic phospholipids (Tallima & El Ridi, 2018). It has been suggested that Ara plays roles in cell membrane fluidity, neuronal excitability, and apoptosis (Tallima & El Ridi, 2018). Fatty acids have gained

traction when it comes to NDDs since during disease states they appear to have an altered metabolism (Snowden et al., 2017) and increased cytosolic presence (Carlson et al., 2007; Mutreja & Gamblin, 2017; Sharon et al., 2003). In regards to *in vitro* R-tau aggregation it is suggested to function in a similar fashion to the previously mentioned polyanions, where it can act as a negatively charged ligand to induce tau's nucleation and subsequent aggregation (Carlson et al., 2007). More specifically, Ara is capable of forming micelles, which are key in promoting the assembly of monomeric tau into aggregates through recruiting tau to their negatively charged surfaces (Chirita et al., 2003). Notably, induction via Ara causes tau to assemble faster than other polyanions, including heparin (Lim et al., 2014). Ara is a widely used inducer of tau aggregation and has contributed to a variety of findings including the effects of phosphorylation, truncation and mutations on tau and tauopathies (Abraha, et al., 2000; Combs & Gamblin, 2012; Mutreja & Gamblin, 2017).

1.5 Thesis aims and hypothesis

Our lab uses three different inducers of tau aggregation: heparin, PolyP, and Ara. The initial goal was to analyze the seeding efficiency of aggregates generated with different inducers, both *in vitro* and in cellular assays. Upon applying our differently induced aggregates to our cell model of tau aggregate seeding, it was discovered that only heparin induced aggregates generated a significant seeding effect. This led us on a quest for answers to determine the reason behind the lack of cell seeding potential in polyP and Ara induced aggregates.

I hypothesize that different inducers may generate aggregates with different structures, therefore making them more or less seeding potent in cellular assays.

To explore my hypothesis, I will complete the following objectives:

1. Quantify the aggregation potential of differently induced aggregates both in our cell model and *in vitro*.
2. Analyze structures of the differently induced aggregates to uncover potential differences.
3. Analyze the ability of cells to uptake differently induced aggregates.

The results of these assays will give us insight into how aggregation inducers influence the seeding potential of their subsequent aggregates. The potential structural effect of these aggregates will also further reinforce the notion of strain, templating, and spread in tauopathies.

Additionally, I want to analyze if cellular components, specifically the co-chaperone DNAJA2, can modify tau aggregation in our cell model. Despite evidence that DNAJA2 may reduce or inhibit tau aggregation *in vitro* (Mok et al., 2018), a knowledge gap exists for how this co-chaperone modulates tau aggregation in a human cell model.

I hypothesize that an overexpression of DNAJA2 will reduce or inhibit the number of aggregates formed in our cell model upon seeding.

To explore this hypothesis, I will complete the following objectives:

1. Generate an inducible cell line that overexpresses DNAJA2.
2. Test seeding in DNAJA2 knockdown cell line.

Developing our knowledge on DNAJA2's role in tau aggregation will offer us insight into how various cellular components, especially chaperone proteins, respond to toxic protein buildup. It may also provide a reason for why certain chaperones are upregulated in specific NDDs such as MCI or AD.

Chapter One: Figures

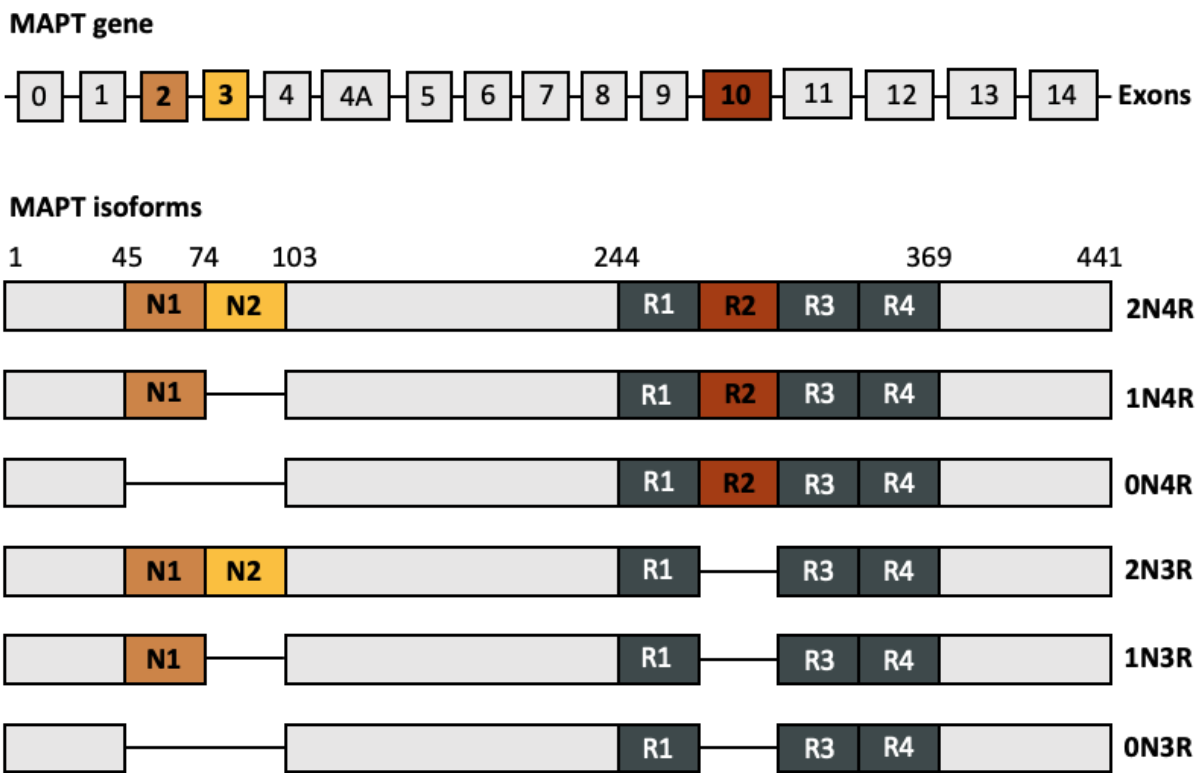


Figure 1.1. Schematic structure of the six MAPT protein isoforms derived from alternative splicing

On the top is a schematic of the 14 exons of the MAPT gene which encodes for the protein tau. Exons subject to alternative splicing are in colour. On the bottom is a schematic illustrating how alternative splicing produces the 6 tau isoforms expressed in adults. Boxed regions and lines indicate protein sequences that are included or excluded, respectively.

Splicing of exons 2 and 3 dictate the presence or absence of N-terminal inserts 1 (N1) and 2 (N2), respectively (A. W. P. Fitzpatrick et al., 2017). Splicing of exon 10 determines the presence or absence of repeat-region 2 (R2), giving rise to a protein with either 3 or 4 repeat-regions (Park et al., 2016). The repeat-regions (R1-R4) are collectively referred to as the microtubule binding domain (MTBD) (Kadavath et al., 2015; Mroczko et al., 2019). The name of each isoform is indicated (e.g. 2N4R). Adapted from Park et al. (2016) (Park et al., 2016).

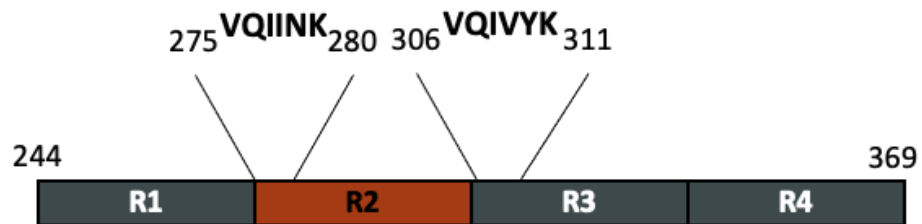


Figure 1.2. Schematic representation of aggregation motifs in MAPT

The repeat regions (R1-R4) of the microtubule binding domain of tau are shown. The relative location and amino acid sequences of the two aggregation motifs are indicated. Adapted from Von Bergen et al. (2000)(von Bergen et al., 2000).

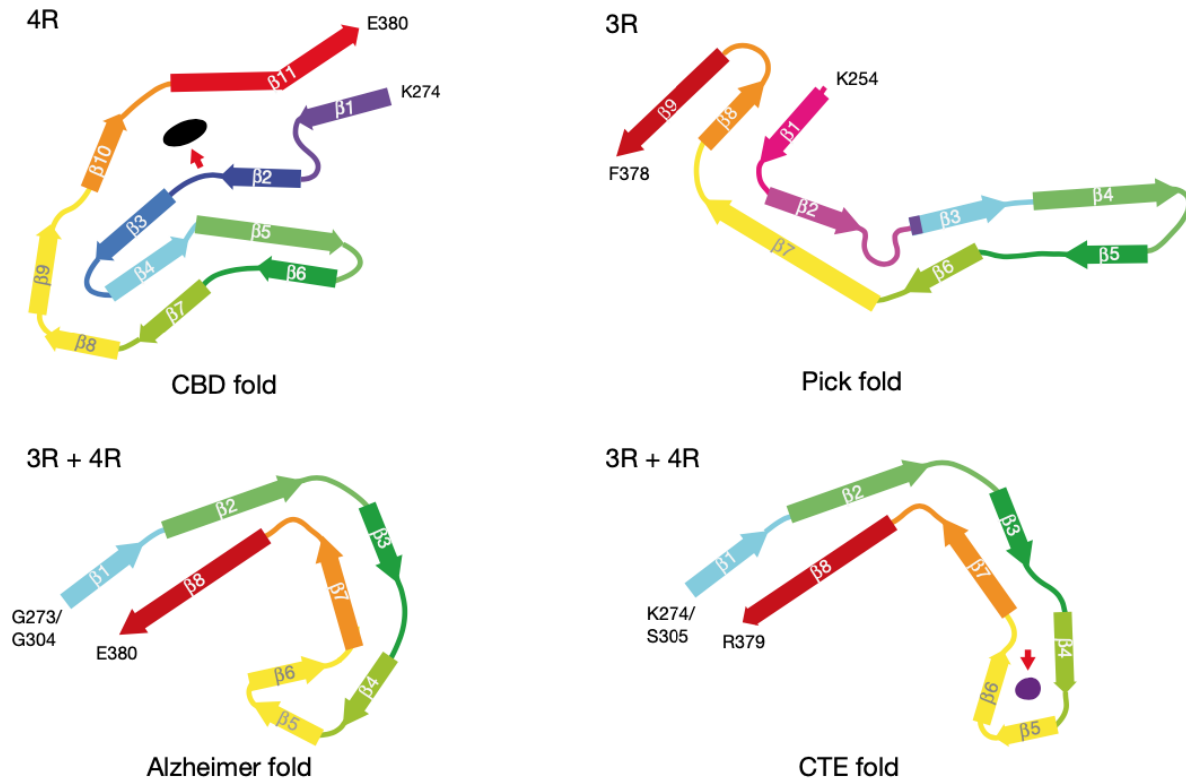


Figure 1.3. The core structure of tau aggregates can vary between tauopathies

The structure and components of tau’s core region can differ depending on the tauopathy (Zhang et al., 2020). (Top left) The core region of tau in CBD, involving primarily 4R tau, is composed of 11 B-sheets spanning residues 274-380 (Zhang et al., 2020). The CBD core takes on a narrow, C-shaped fold and has a non-proteinaceous inclusion (indicated by red arrow) (Zhang et al., 2020). (Top right) By contrast, the core region of tau in Pick’s disease, involving primarily 3R tau, is composed of only 9 B-sheets spanning residues 254-378 (Zhang et al., 2020). The Pick’s disease core is much less C-shaped than that of the CBD core, and does not contain any additional components (Zhang et al., 2020). Both AD and CTE involve 3R and 4R tau (Götz et al., 2019; Kovacs, 2018; Zhang et al., 2020). (Bottom left) The core region of tau in AD is composed of 8 B-sheets spanning residues 273/304-380, and takes on a hook shape (Zhang et al., 2020). (Bottom right) The core region of tau in CTE resembles that of AD in that it is composed of 8 B-sheets and takes on a nearly identical hook shape (Zhang et al., 2020). The CTE B-sheets span residues 273/305-379 and unlike AD, this fold includes a non-proteinaceous inclusion (indicated by red arrow) (Zhang et al., 2020). Reproduced from Zhang et al. (2020) with permission (Zhang et al., 2020).

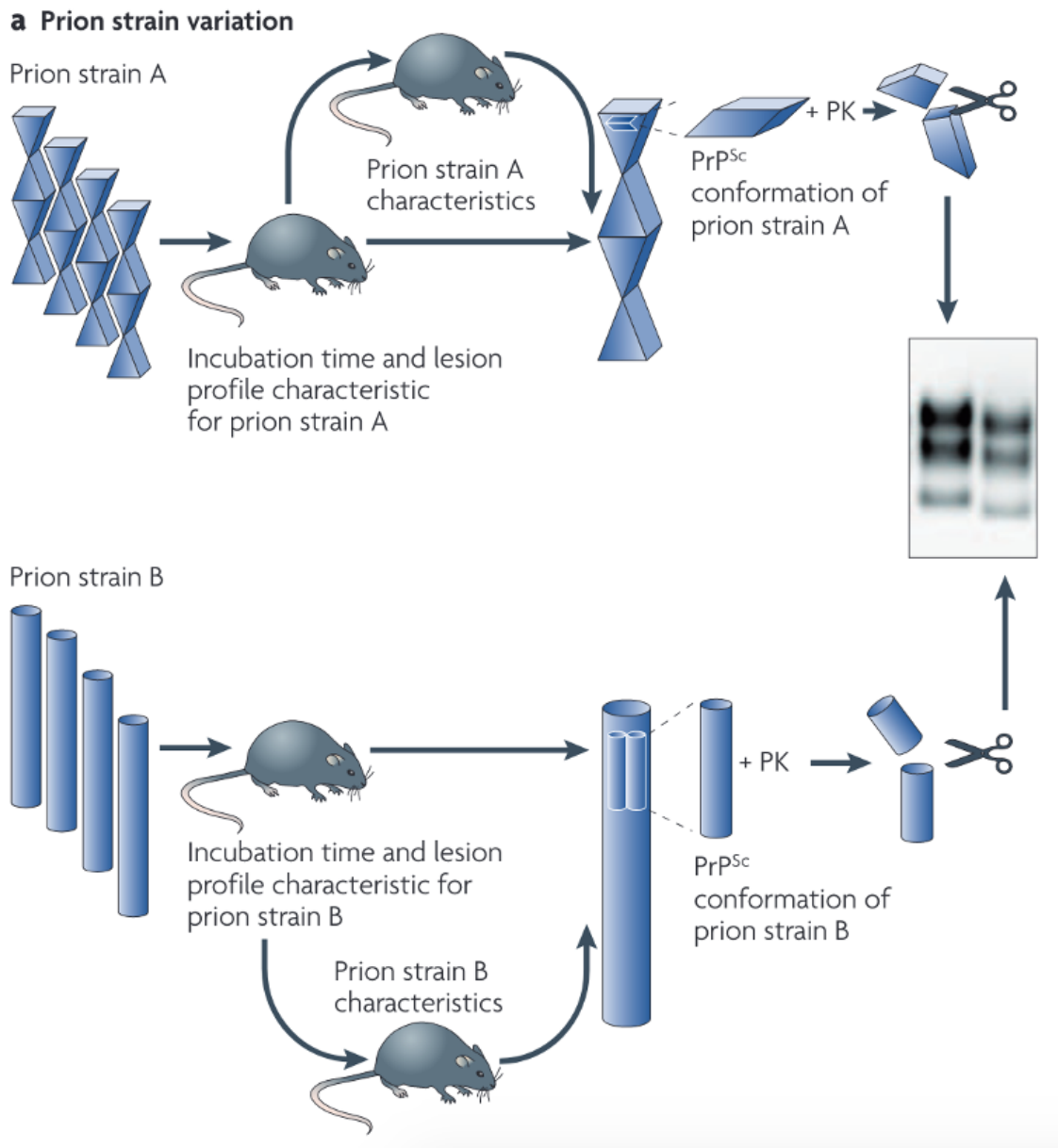


Figure 1.4. Unique prion protein strains propagate biochemical signatures and distinct disease phenotypes

The idea of infectious protein ‘strains’ was first explored with the prion protein (Vaquer-Alicea et al., 2021), and it has been suggested that PrP^{Sc} can have unique biochemical signatures, including conformation, depending on the disease (Aguzzi et al., 2007). Prion strain A (top) and B (bottom) occupy different hosts and give rise to a different set of disease characteristics including incubation time, aggregate morphology, and symptom progression (Aguzzi et al., 2007). When strain A or B is inoculated into a new host, their unique characteristics are transmitted, and the resulting PrP^{Sc} is identical to that of the original inoculate (Aguzzi et al., 2007). Upon protease digestion, resistant regions of the core have distinct mobility when subjected to electrophoresis (Aguzzi et al., 2007). Reproduced from Aguzzi et al. (2007) with permission (Aguzzi et al., 2007).

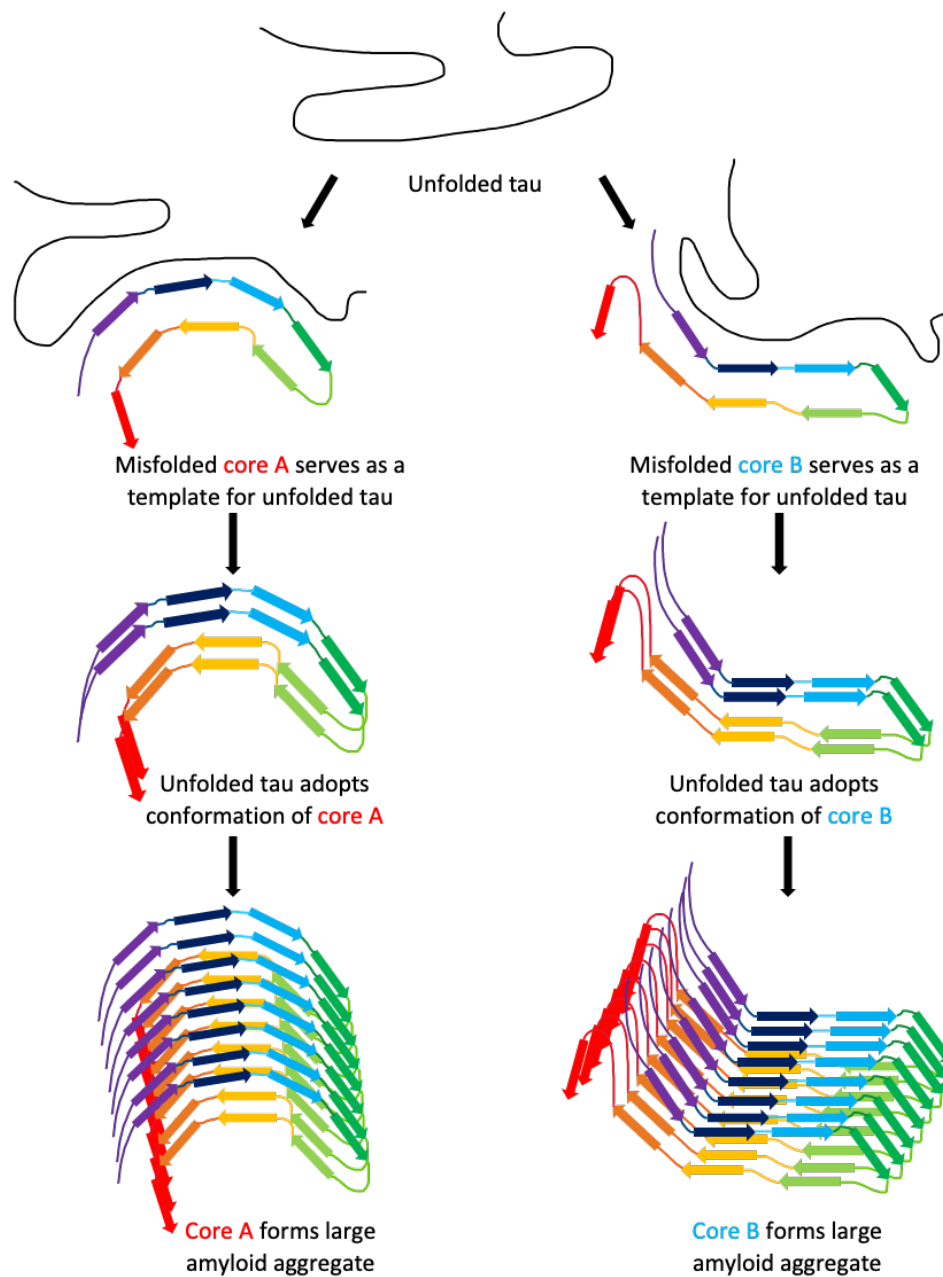


Figure 1.5 Tau replicates in a prion-like manner by templating

Studies have suggested that tau replicates in a prion-like manner by serving as a template for unfolded, monomeric tau to undergo a misfolding process and perpetuate the cycle of aggregation (Brunello et al., 2020; Hosokawa et al., 2021; Lasagna-Reeves et al., 2012). Interestingly, the structural properties of the template will be transmitted to the newly misfolded monomer, giving rise to specific tau ‘strains’ that possess unique traits such as morphology, size and seeding capacity (Sanders et al., 2014). When unfolded tau is exposed to the misfolded core region of tau molecule A or B, it will take on the fold of its template, thus propagating its distinct phenotype and pathology (Sanders et al., 2014).

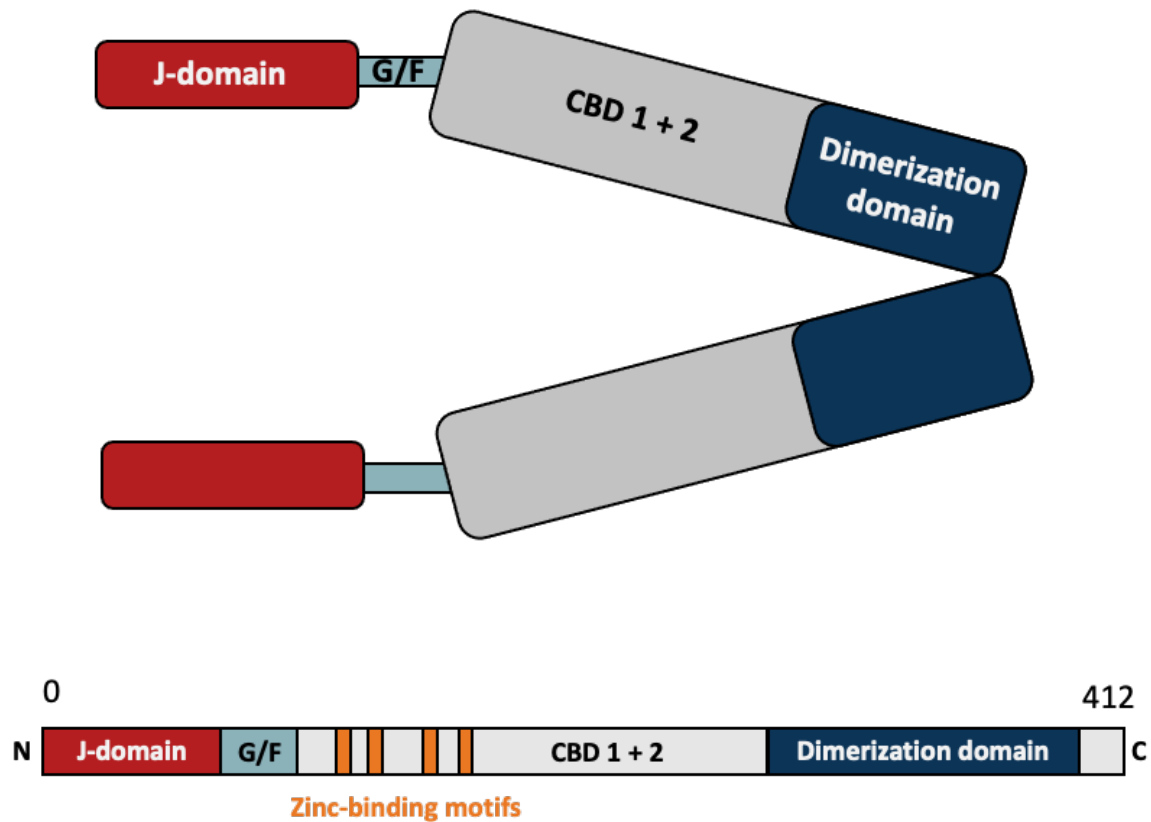


Figure 1.6. Schematic representation of DNAJA2 structure

Human DNAJA2 is 412 amino acids long, and is composed of various domains (Baaklini et al., 2012). The N-terminus makes up the highly conserved J-domain that is made up of roughly 70 residues (Jiang et al., 2019; Kampinga & Craig, 2010). Following the J-domain there is a G/F rich region, and four zinc binding motifs (Baaklini et al., 2012; Jiang et al., 2019). DNAJA2 has two CBDs that participate in binding to substrates and dictate client specificity (Jiang et al., 2019). Finally, on the C-terminal end of the protein there is a dimerization domain, which allows the DNAJA2 monomers to form functional dimers in the cytoplasm (*top*) (Baaklini et al., 2012; Jiang et al., 2019). Adapted from Baaklini et al. (2012)(Baaklini et al., 2012).

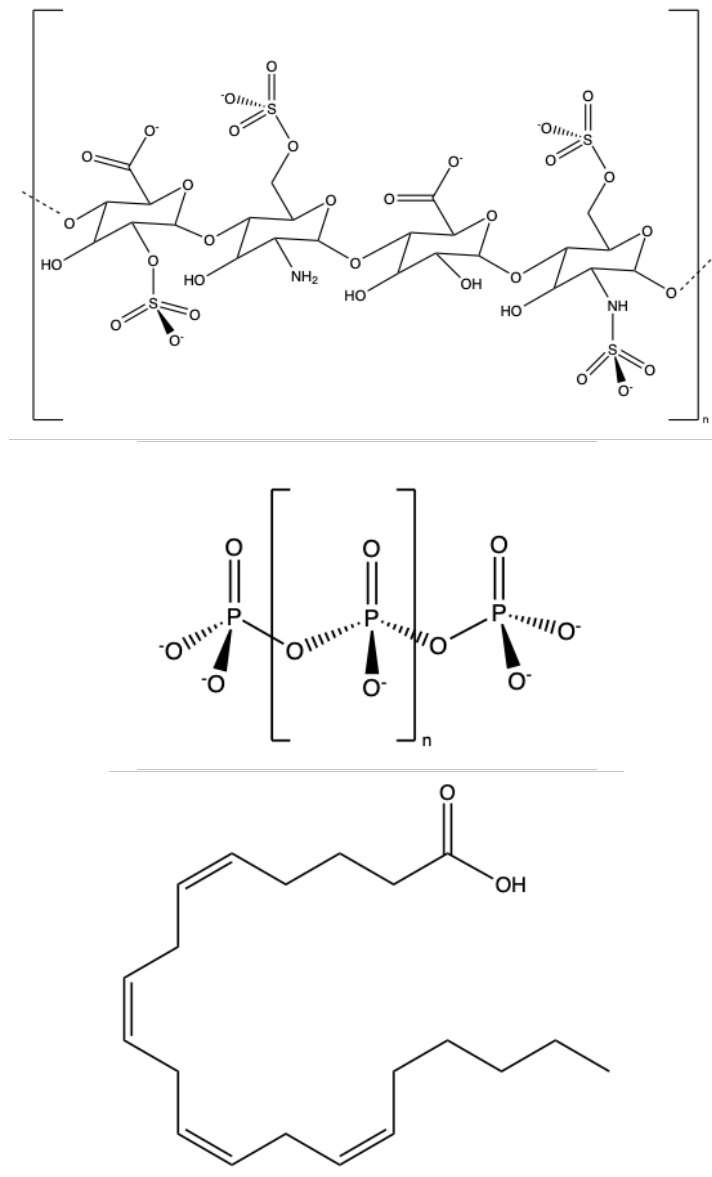


Figure 1.7. Small molecule inducers of tau aggregation

Representation of the structures for (top) heparin, (middle) polyphosphate, and (bottom) arachidonic acid. Brackets with subscript n denote repeating polymer units of variable length. Individual units of the fatty acid arachidonic acid can come together to form micelles that are thought to encourage taus assembly into aggregates (Chirita et al., 2003).

CHAPTER TWO: MATERIALS AND METHODS

2.1 Reagents

2.1.1 Antibodies

Table 2.1. List of primary and secondary antibodies used in Western blots, Dot blots, and immunofluorescence assays.

Primary antibodies	Specificity	Species	Concentration	Provider	Catalog no.
Tg5	Tau: 220 – 240 (phospho-independent, total tau)	Mouse	1:250	Peter Davies	N/A
Monoclonal α tubulin antibody	α tubulin	Mouse	1:1000	NEB	Sc-32293
Monoclonal anti- β actin antibody	Actin	Mouse	1:1000	Sigma	A5441
Purified anti-Tubulin β -3	Tubulin β 3	Rabbit	1:2000	BioLegend	TUBB3
Monoclonal DNAJA2 antibody	DNAJA2	Mouse	1:1000	Invitrogen	OTI2A2
Monoclonal anti-DNAJA2 antibody	DNAJA2	Rabbit	1:1000	Atlas Antibodies	HPA060538
Polyclonal Hsc70/HSP73	Hsc70	Rabbit	1:1000	Enzo	ADI-SPA-816-F
Secondary antibodies	Specificity		Concentration	Provider	Catalog no.
Anti-mouse IgG HRP-linked antibody	Anti-mouse IgG	Horse	1:10000	Cell Signaling Technology	7076S
Anti-rabbit IgG HRP-linked antibody	Anti-rabbit IgG	Goat	1:10000	Cell Signaling Technology	7074S
Anti-mouse Cy5 fluorescent antibody	Anti-mouse IgG	Donkey	1:500	Jackson ImmunoResearch	715-175-151

2.2 Constructs

2.2.1 Recombinant tau

Previously, the 0N4R R-tau isoform with an N-terminal 6X Histidine and thrombin cleavage-site tag was inserted into a pET28a vector harboring kanamycin resistance (Min et al., 2018). Single missense mutations in R-tau were introduced into the WT sequence via site-directed mutagenesis (Min et al., 2018).

2.2.2 shRNA vectors

ShRNA constructs are expressed in a pMK1200 vector with puromycin (puro) resistance (Kampmann et al., 2013, 2014). The constructs are under the control of the EF1A constitutive promoter. Additionally, the vector carries a fluorescent mCherry gene that is constitutively expressed in cells. Each shRNA is specifically coded to its mRNA target of interest, and the control is a scrambled sequence that does not have a target. The constructs were previously cloned as part of a larger shRNA vector repository (Dr. Martin Kampmann, UCSF) with the following corresponding ID numbers: DNAJA2 (#4184), Hsp27 (#3609), control (#4174). Following lentiviral transduction of constructs into HEK293 P301L cells, a heterogenous population of puromycin-resistant, mCherry positive cells was selected.

2.2.3 Cumate inducible expression vector

The DNAJA2 WT and mutant constructs, along with various other control constructs, were expressed in a cumate-inducible vector (QM80A-1) with puro resistance (System Biosciences). The constructs are located downstream of a CMV promoter, which is upstream of the cumate operator. In the absence of the small molecule cumate, a CymR repressor binds the operator and inhibits

gene expression. The addition of cumate will cause CymR to bind to the cumate instead of the operator, allowing for expression of the construct. Upon lentiviral transduction of constructs into HEK293 P301L cells, single cell clones were selected through puro treatment and dilution (see **section 2.5.3**). Successful integration of constructs was confirmed using Western blot.

2.3 General lab techniques

2.3.1 SDS polyacrylamide gel electrophoresis (SDS-PAGE)

6X SDS-PAGE laemmli loading buffer (0.25 M tris base, 0.28 M SDS, 40% glycerol, 20% 2-mercaptoethanol, Bromophenol blue) was added to protein samples at a final concentration of 1X and further denatured by boiling for five minutes. They were then loaded onto 4-20% 10 well Mini-PROTEAN TGX Gels (cat# 4561093, Biorad), along with 2.5 μ L of BlueElf Prestained Protein Ladder (FroggaBio,) and resolved at 200 Volts for 40 minutes. Stained gels were soaked in Coomassie blue (0.5% Coomassie blue, 50% methanol, 1% acetic acid) for 10 minutes, and de-stained by boiling in deionized water for 20 minutes. Gels were imaged using LI-cor instrument (Licor) at 700 nm for 2 minutes.

2.3.2 Western blots

Protein samples were transferred from gels to 0.1 μ m nitrocellulose membranes (GE Healthcare Life Sciences) using a BioRad Transblot Turbo Transfer System (BioRad) for 7 minutes at 25 Volts and 2.5 Amps. Membranes were blocked in 2.5% fish skin gelatin (FSG) in Tris-Buffered Saline (TBS)(Truoin Science) for 1 hour at room temperature, and subsequently incubated overnight at 4°C in primary antibody (**Table 1**). Membranes were washed 3 times with 1X TBS and incubated in HRP-linked secondary antibody (**Table 1**) for 1 hour at room temperature. Blots were

visualized with SuperSignal West Pico (Thermo Fisher Scientific) or Femto (Thermo Fisher Scientific) PLUS Chemiluminescent Substrate Kits and imaged using LI-cor instrument.

2.4 *In vitro* assays with R-tau aggregates

2.4.1 Recombinant tau expression and purification

0N4R human tau (WT, P301L) was expressed and purified as previously described (Mok et al., 2018). Briefly, BL21(DE3)-RP *E. coli* cells transformed with desired constructs were induced with 300 μ M IPTG for 1.5 hours at 37°C, in the presence of a chemical chaperone solution (1.66 mM betaine, 83 mM NaCl). Pelleted cells were resuspended in a resuspension buffer (20 mM MES pH 6.8, 1 mM EGTA, 0.2 mM MgCl₂, 1 mM PMSF, 5 mM dithiothreitol (DTT) and protease inhibitor tablet). Cells were lysed by high pressure homogenization and then boiled for 20 minutes and centrifuged to pellet cellular debris. The supernatant containing tau was purified by cation exchange with a gradient elution (20 mM MES pH 6.8, 1 mM EGTA, 1 mM MgCl₂, 2 mM DTT, and 0.1 mM PMSF, Buffer A= 50 mM NaCl, Buffer B= 1M NaCl). Protein was then concentrated using Amicon filters (3 kDa cutoff) and dialyzed overnight in D-PBS with 2 mM DTT. Protein concentration was determined using a reducing agent compatible BCA assay (Pierce). Purified tau protein was aliquoted and stored at -80°C.

2.4.2 Recombinant tau aggregate generation

Using a Posi-Click low protein-binding microcentrifuge tube (cat# C2170, Denville), the following components were added to the tube at the following final concentrations: DTT (1 mM), purified tau protein (10 μ M), heparin (cat# sc-203075, Santa Cruz Biotechnology) (0.044 mg/mL)/polyphosphate (cat# 390932500, Acros Organics) (0.1 mg/mL)/arachidonic acid (cat# A3611-

100MG , Sigma Aldrich) (150 μ M). All stock solutions were prepared in Dulbecco's Phosphate Buffered Saline (D-PBS). The final volume of the reaction was 330 μ L. Shake tubes at 790 rpm and 37°C for 36 hours.

Aggregates were loaded onto an SDS-PAGE gel, alongside purified tau standards, and quantified using ImageJ. Measurements of each gel band were taken using a common region of interest, and the total pixel density for each sample was inverted using the equation $255 - X$. The inverted background value was subtracted from each sample. Protein standard values were assembled into a scatter plot and a linear regression analysis was applied to obtain an R squared value and $y = mx + b$ equation to determine the unknown protein concentrations.

2.4.3 *In vitro* aggregation assay

A Corning black 384-well low volume round bottom plate (cat# 4511, Corning) was briefly coated with 0.01% Triton X-100 diluted in deionized water, removed from wells, then allowed to completely dry. Tau solution was prepared by calculating the total volume of tau (final concentration 10 μ M) and DTT (cat# BP172-25, Fisher) (final concentration 1 mM) required for the assay. With a total volume of 20 μ L per well, the following components were added to each well: tau solution, Thioflavin T (ThT) (cat #23064, AAT Bioquest) (10 μ M) plus the following inducers or buffer controls as indicated: 3% w/w seeding material (0.0129 mg/mL), heparin (0.044 mg/mL), polyphosphate (0.1 mg/mL), arachidonic acid (150 μ M), D-PBS, ethanol (10 % final). The plate was placed in a SpectraMax M5 plate reader (Molecular Devices) at 37°C with shaking (120 sec between reads), and fluorescence values were recorded over the course of 24 hours, at five minute intervals. ThT fluorescence was excited at 444 nm and emitted at 485 nm, with the emission cut off being 475 nm.

2.4.4 Analysis of aggregation assay/lag time

Prism GraphPad 6 was used to process the kinetic curve values obtained from the plate reader.

Curves were fitted to the following equation:

$$Y = A_0 + A_1 e^{-\frac{A_2 - t}{A_3}}$$

Y = the fluorescence value at time t

A0 = minimum fluorescence value

A1 = maximum fluorescence value

A2 - A3 = the time it takes for the elongation phase to begin (the lag time)

1/A3 = the elongation rate

Extracted lag time values were graphed using Prism, and repeated experiments were averaged (**Figure 2.1**).

2.4.5 Protease digestion of tau aggregates

Tau aggregates directly sampled from *in vitro* aggregation assays (20 μ L) were treated with a final concentration of 27 ng/ μ L MS-grade trypsin (Thermo Fisher) in D-PBS and incubated at 37°C for 3 hours with shaking at 800 rpm. Digestion reactions were stopped by the addition of sample buffer (200 mM DTT and 10X ProteinSimple sample buffer) and heating to 95°C for 5 min. Tau

fragments were resolved using the Wes capillary gel electrophoresis system (ProteinSimple) with the 2-40 kDa separation and total protein detection modules.

CompassSW software (ProteinSimple) was used to generate chromatograms representing the lane profiles of separated protease-resistant tau fragments. Chromatograms plot signal intensity versus apparent MW, calibrated using protein standards included with each run.

2.4.6 Tau aggregate labeling

Recombinant tau aggregates were labeled using Alexa Fluor-647 NHS ester dye (Thermo Fisher Scientific). Dye was added to the aggregates at a final concentration of 0.25 μ M (ratio of 1:40 of dye:protein), and aggregates were protected from light and incubated at RT for 1 hour. Samples were then spun at 100,000 x g for 1 hour at 4°C to remove excess dye, and the pellet was resuspended in $\frac{1}{3}$ of the original volume. Aggregates were quantified using SDS-PAGE gel and ImageJ analysis.

2.5 Mammalian cell culture

2.5.1 HEK293 P301L cells

HEK293 P301L cells were stably transfected to express GFP-tagged mutant P301L-tau(Kang et al., 2021). Tau expression is inducible using doxycycline at a concentration of 10 ng/mL. All HEK cells were cultured and maintained in Dulbecco's Modified Eagle Medium (DMEM) (cat# 2318848, Gibco) supplemented with 10% Avantor Seradigm Premium Grade Fetal Bovine Serum (FBS) (cat# 97068-085, VWR) and 1% penicillin/streptomycin (Gibco). Cells were routinely passaged using 0.05% trypsin (Gibco) and 1X PBS (Gibco). All cells were mycoplasma tested with PCR myco detection kit (cat# G238, ABM) every 2 months or prior to making of cell stocks.

Hygromycin (hygro) was applied to cells after every second passage to select for cells carrying the integrated GFP-tau vector.

2.5.2 Lentiviral transduction

To package desired vectors into lentivirus particles, HEKT cells were plated at a density of 750,000 cells per well of a 6-well plate. 1.35 μg of the CMV vector, 165 ng of the MD2 vector and 0.5 μg of our desired vector were added to each well along with 7.5 μL of lipofectamine 2000 (cat# 11668-027, Invitrogen) and incubated for 6 hours at 37°C before media (DMEM with 10% FBS and 1% P/S) was replaced. The color of the media was used to monitor for pH changes during packaging and the culture media containing virus particles was harvested 48 hours later. The collected culture media was centrifuged at 150 x g for 5 minutes and subsequently passed through a 0.45 μm filter to remove cells/debris (Basix). Filtered supernatant was applied to HEK293 P301L cells along with 8 $\mu\text{g}/\text{mL}$ polybrene (Millipore Sigma) to yield a transfection rate of roughly 10%, which was established using mCherry vector fluorescence that was quantified using the Cell Countess (Thermo Fisher). Culture media was replaced the following day. Lentiviral vectors were generously provided to us by the Julien Lab (University of Alberta).

2.5.3 Generation of single cell clones

Transfected cells were passaged twice prior to a one-week treatment with 1 $\mu\text{g}/\text{mL}$ puromycin (Rose Scientific Ltd). Cells were then split into four tissue culture treated 96-well plates (Falcon) at a total volume of 100 μL per well and a calculated density of 1 cell per mL. Cells were incubated at 37°C for roughly 2 weeks and checked daily for positive cell growth and/or pH change. Immediately upon observable pH change, wells were visualized under the FLoId microscope

(Thermo Fisher) to identify growth of single cell clones versus multiple clones in each well. Single clones were then transferred to larger 12-well plates for induction with cumate or freezing.

2.5.4 Cell lysis using M-PER lysis buffer

After treatment, cells were washed twice with cold 1X PBS and subsequently lysed on ice for 15 minutes in Mammalian Protein Extraction Reagent based lysis buffer (Thermo Fisher Scientific) (supplemented with 5 mM NaF, 2 mM NaVO₄, and 1 Complete MINI protease inhibitor tablet per 50 mL). Lysate was centrifuged at 13,000 rpm for 5 minutes at 4°C. Protein containing supernatant was collected and total protein concentration was measured using Pierce BCA Protein Assay Kit (Thermo Fisher Scientific).

2.6 Cellular assays with R-tau aggregates

2.6.1 Cellular seeding assay

Live cell seeding assays were optimized for use in 96-well TC-Treated Black-sided, thin-bottom, Microplates (cat# 655090, Greiner Bio-One), with a total volume of 200 µL per well. The tau aggregate solution was prepared by calculating the total volume of aggregated tau required for the assay (final concentration per well was 0.05-0.3 µM) and the final volume was adjusted with OptiMEM (Gibco). Lipofectamine solution was simultaneously prepared by calculating the total volume of Lipofectamine 2000 required for the assay (final volume per well was 0.2 µL). The final volume was adjusted with OptiMEM and the solution was allowed to incubate at room temperature for 5 minutes.

The tau aggregate solution and the lipofectamine solution were mixed and incubated for 20 minutes at room temperature. Cells were induced with 10 ng/mL doxycycline 72 hours prior to the

assay, and resuspended at a concentration of 1 million cells per mL to seed each well with 10,000 cells. The following components were added to each well: 170 μ L DMEM with 10% FBS and 1% Pen/Strep, 20 μ L of tau fibril/lipofectamine mixture (or lipofectamine/OptiMEM only mixture for control wells), 10 μ L of cell resuspension, 10 ng/mL doxycycline, and additional inducers when appropriate. Plates were imaged with ImageXpress High Content Screening Microscope (Molecular Devices) at 10X magnification 48 hours post seeding.

2.6.2 Imaging analysis

Analysis of live cell seeding assays was conducted using the MetaXpress software (Molecular Devices). A vesicle setting on the Transfluo application module was adapted to count all GFP-tau aggregates between 3 μ m and 10 μ m, of each cell. Cells were defined by the nucleus setting, which counted Hoechst stained cell nuclei between 6 μ m and 8 μ m. Greater than 1000 cells per well, assayed in triplicate, were analyzed in three independent experiments.

The outputted data from the Transfluo analysis module was further processed using a code written by Coleman Dean (Department of Physics, University of Alberta). Code was written in python and uses the NumPy package (Harris et al., 2020). It uses an automated sorting routine to identify wells containing cells with tau aggregates and sorts by the number of cells with aggregates present. The program also integrates the total count of aggregate positive cells across all wells.

2.6.3 DNAJA2 immunofluorescence

Cells grown on coverslips were treated with Hoescht stain (1 μ g/mL) an hour prior to fixation. A fixation solution containing 4% paraformaldehyde (PFA) was applied to the coverslips, which were then incubated at 37°C for 12 minutes. All following incubations are carried out at room

temperature. 1X PBS was used to gently wash the coverslips four times. Reducing agent, 0.2% NaBO₄ diluted in 1X PBS, was prepared immediately before use and applied to the coverslips for 10 minutes. Cells were washed an additional three times with 1X PBS before a 1 hour incubation in a 3% FSG blocking buffer (diluted in 1X PBS supplemented with 0.1% Triton X-100). Primary antibody diluted in blocking buffer (1:500) was loaded onto parafilm and coverslips were inverted on top of it (150 μ L per coverslip) for 45 minutes. Coverslips were washed five times with 1X PBS supplemented with 0.1% Triton X-100 (Sigma Aldrich). Fluorescent secondary antibody diluted in blocking buffer (1:500) was loaded onto parafilm and coverslips were inverted on top of it (150 μ L per coverslip) for 45 minutes and protected from light. Coverslips were washed three times with 1X PBS supplemented with 0.1% Triton X-100, and then fixed an additional time with 4% PFA for 10 minutes. Coverslips were washed a final three times with 1X PBS and then mounted on glass slides using Prolong Glass Antifade Mountant (Thermo Fisher Scientific) and allowed to cure overnight. The following day, a clear coat of nail polish was applied to the edges of the coverslip on the glass slide.

Images were obtained using the WaveFX1 confocal microscope at 60X magnification.

2.6.4 Fluorescent MT labeling

HEK293 P301L cells were induced with dox to express GFP-tau 72 hours prior to labeling. Since this labeling was done on live cells, the cells were grown on glass coverslips in a 12-well plate. 1 μ L of SPY555-tubulin probe (Cytoskeleton) was added to 1 mL DMEM/FBS media and allowed to incubate at 37°C for 1 hour. After incubation, the coverslip was removed from the plate and placed into a coverslip cell chamber for live cell imaging, and was imaged using a confocal microscope at 60X magnification. Images were processed in Omero.

2.6.5 Recombinant tau aggregate uptake

HEK293 P301L cells were induced with dox 72 hours prior to beginning the experiment. Cells were then passaged as normal, with 250,000 cells/well being added to a 12-well plate. Experimental wells were subjected to the addition of 0.1 μ M Alexa fluor 647-labeled aggregates alongside lipofectamine (1 μ L per well). Control wells were left untreated. After 4 hours of incubation at 37°C, cells were washed once with 1X PBS and trypsinized. After neutralization with DMEM/FBS and spin down at 150 x g for 5 minutes, the supernatant was removed and cell pellets were washed an additional time with 1X PBS. Finally, cells were spun again at 150 x g, and pellets were resuspended in 120 μ L of 1X PBS. Control cells were incubated on ice for 45 minutes prior to the addition of 0.1 μ M Alexa fluor 647-labeled aggregates without the addition of lipofectamine in order to block endocytosis. Aggregates were left on cells for 45 minutes on ice prior to being analyzed on the ImageStream instrument (Amnis). Additionally, 2 mM trypan blue dye was added to the cell samples 10 minutes prior to analysis in order to quench external Alexa fluor 647 signal. Data was analyzed using IDEAS version 6.3. Template for analysis was based on gating shown in **Figure 2.4**. Internalization wizard module in IDEAS 6.3 was used to analyze the internalization of Alexa fluor 647-punctae in GFP-tau expressing cells. This module provided us with a mean value of internalization where a higher value is associated with a more central localization of 647-punctae in relation to our cell (**Figure 2.5**).

Chapter Two: Figures

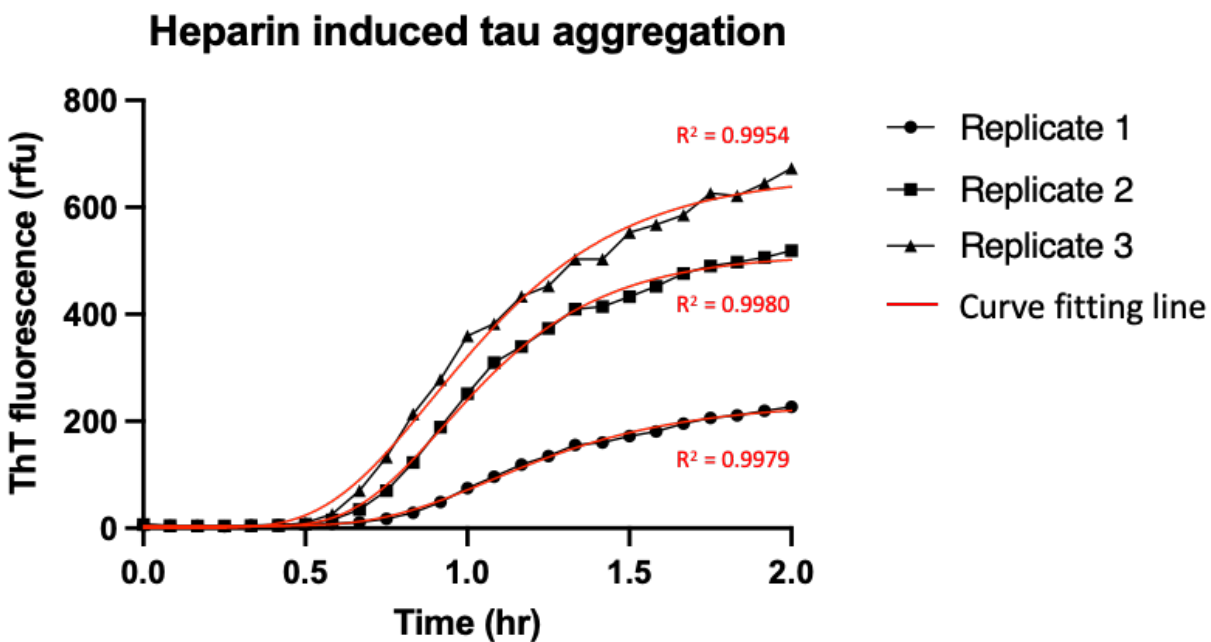


Figure 2.1. Display of line fitting curve equation efficiency

A *In vitro* kinetic assay performed on P301L tau using heparin as an aggregation inducer. The curve fitting lines acquired using nonlinear regression curve fitting equation are represented in red, along with their respective R-squared value. Replicates were done with different batches of aggregated tau on different 96-well plates.

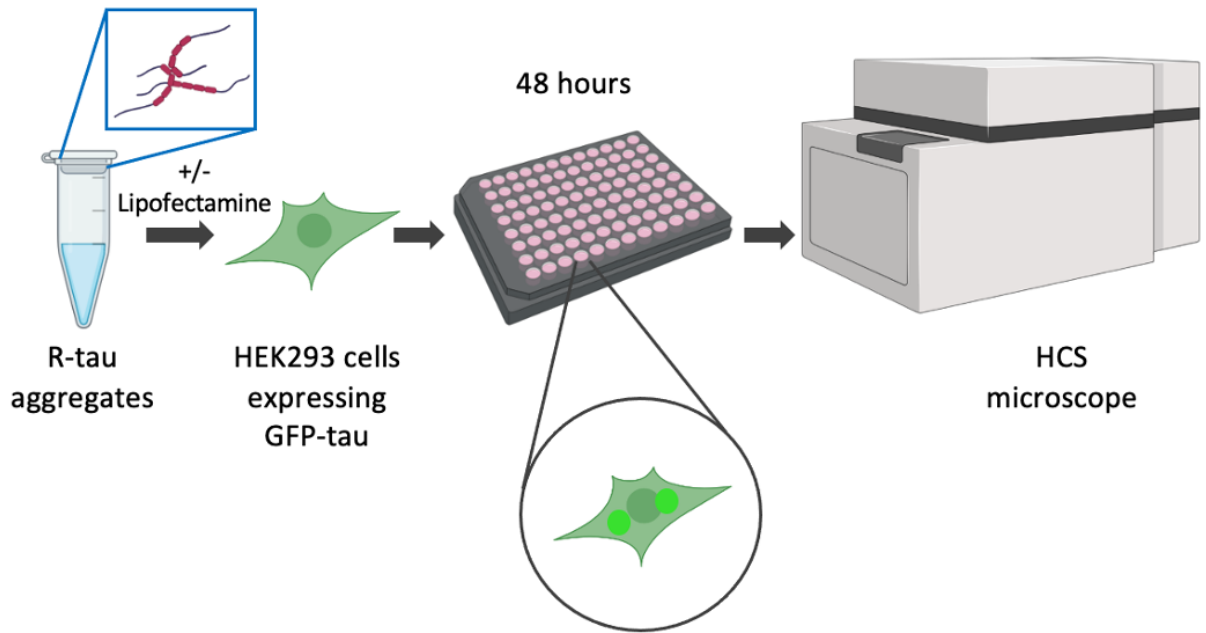


Figure 2.2. Schematic representation of cellular seeding assay

Recombinant tau (R-tau) aggregates generated *in vitro* are applied to HEK293 cells expressing GFP-tagged mutant P301L (induced to express 72 hours prior to assay) in the presence or absence of lipofectamine. Cells are left to incubate with exogenously applied aggregates for 48 hours to induce aggregation of the endogenous GFP-tau, which is visible as the presence of bright green punctae. After 48 hours, the 96-well plate containing the seeded cells is imaged using a high content screening microscope (Molecular Devices) and the resulting images are processed using MetaXpress software. Figure made using BioRender.

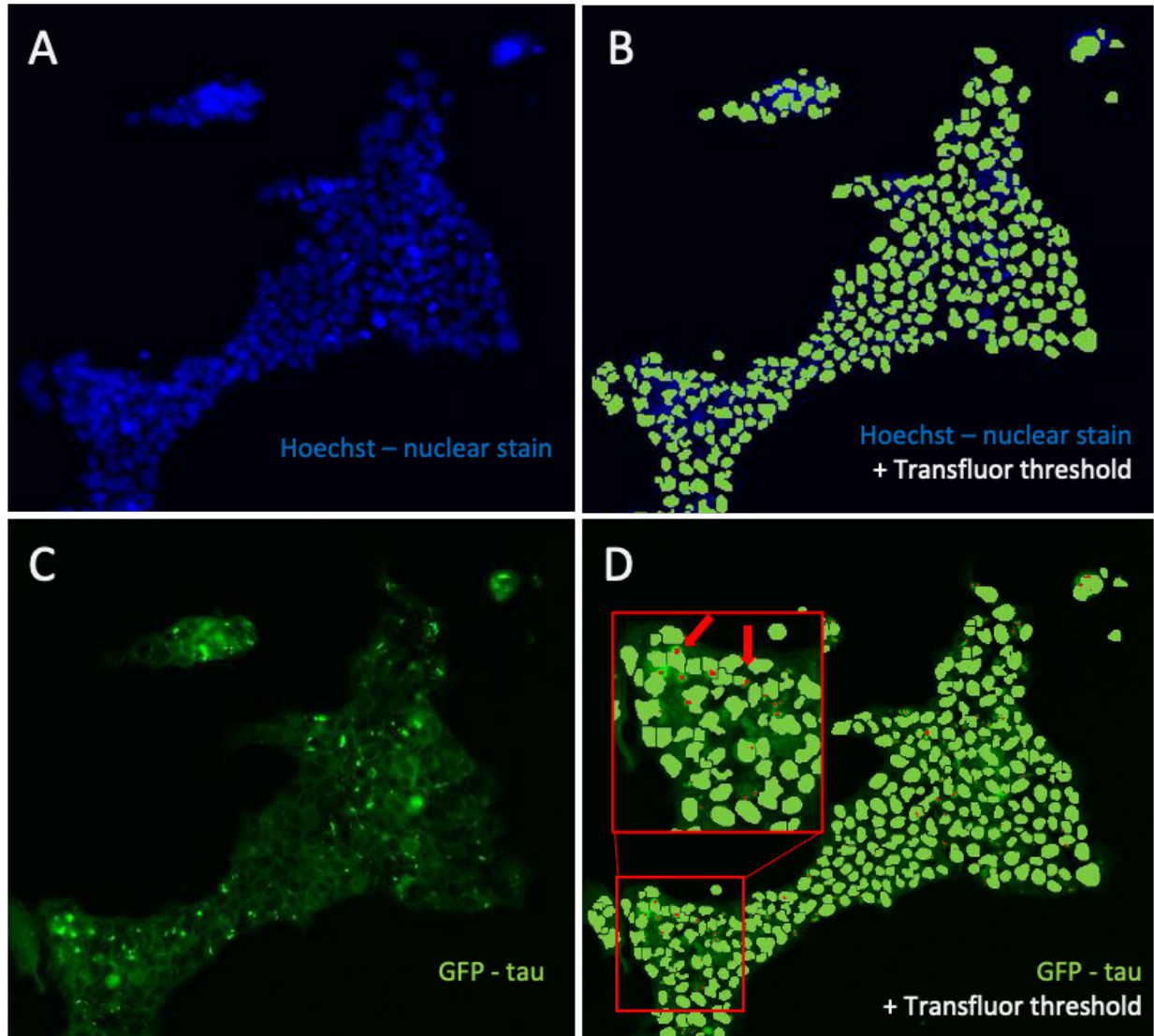
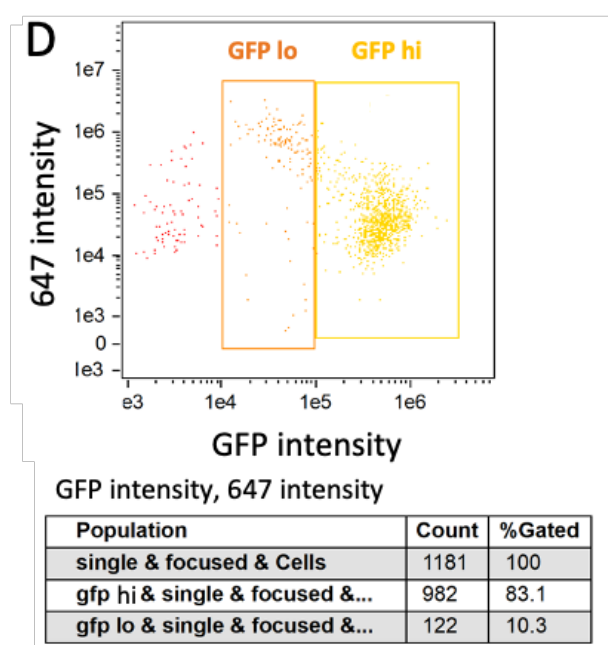
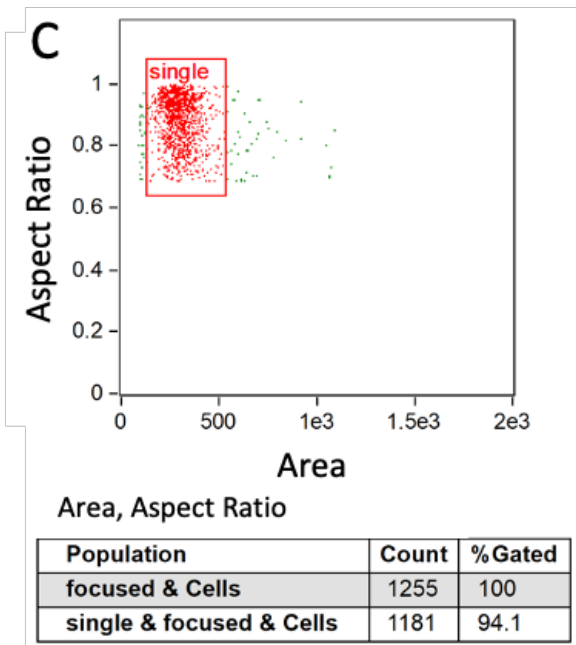
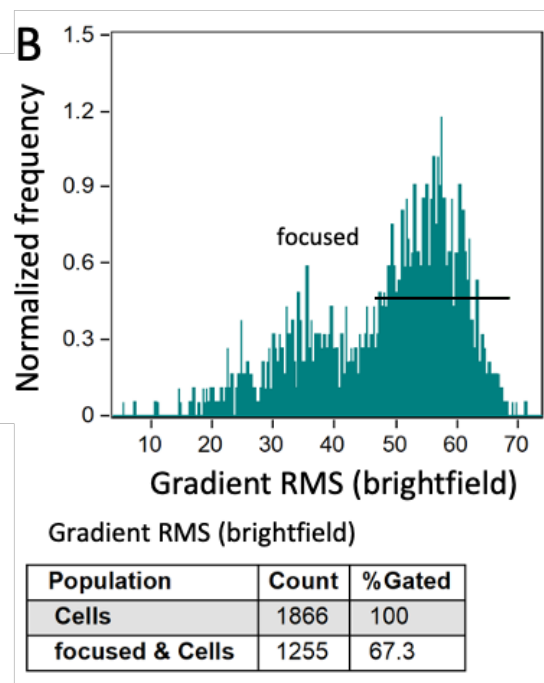
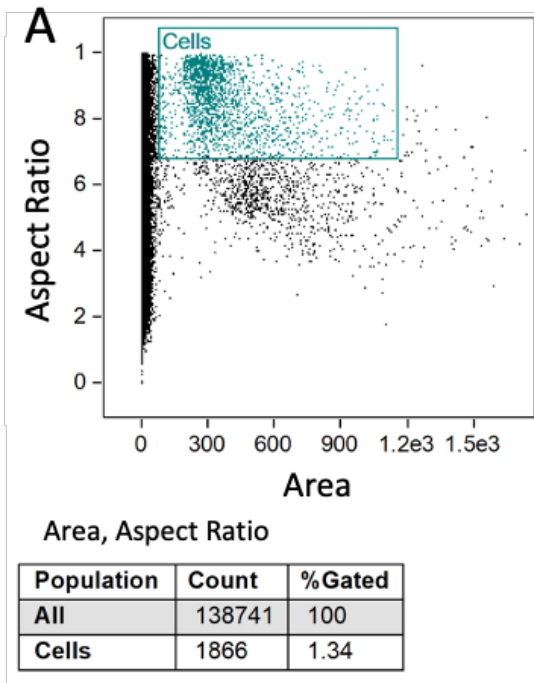


Figure 2.3. Parameters of cell seeding assay analysis

A-B Cell nuclei stained with Hoechst without (A) and with (B) the threshold. Nuclei overlaid with light green.

C-D Cells expressing GFP-tau and aggregates as GFP-punctae without (C) and with (D) the threshold. Punctae are overlaid with red, examples of which are indicated on zoomed in image with red arrows.



(Continued)

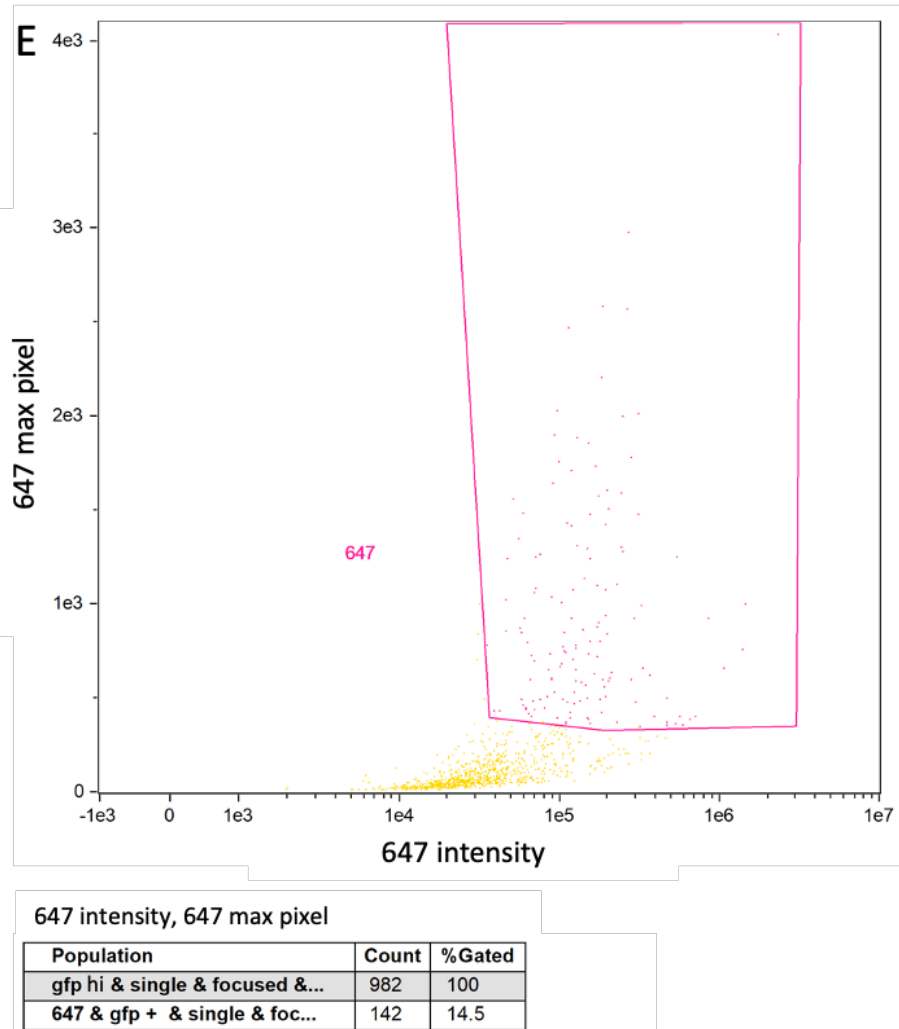


Figure 2.4. Gating parameters of Alexa fluor 647-tau cell uptake experiment

A Plot of total items counted, with aspect ratio values on the Y-axis and area values on the X-axis. Blue box captures what we identified as cells, in an effort to exclude beads, debris, and large cell clumps. Cells were 1.34 % of the total count, with most items counted being beads.

B RMS gradient of cell focus in the brightfield channel, using cells selected from plot A. Black line indicates gradient values that were selected to represent focused cells. Cells falling outside of the black line were not in focus.

C Plot of focused cells, with aspect ratio values on the Y-axis and area values on the X-axis. Red box captures what we identified as single cells.

D Plot of fluorescence intensities of single cells selected in plot C. Alexa fluor 647 intensity values are on the Y-axis and GFP-intensity values are on the X-axis. Orange box represents cells with low GFP (GFP lo) signal and high Alexa fluor 647 signal, and yellow box represents cells with high GFP (GFP hi) signal and high Alexa fluor 647 signal, which is what we focus on for the analysis.

E Plot of cellular Alexa fluor 647 intensity of GFP hi cells. Pink box represents the highest Alexa fluor 647 values selected for analysis, whereas values falling outside of this range were lower and more diffuse, not indicative of punctae.

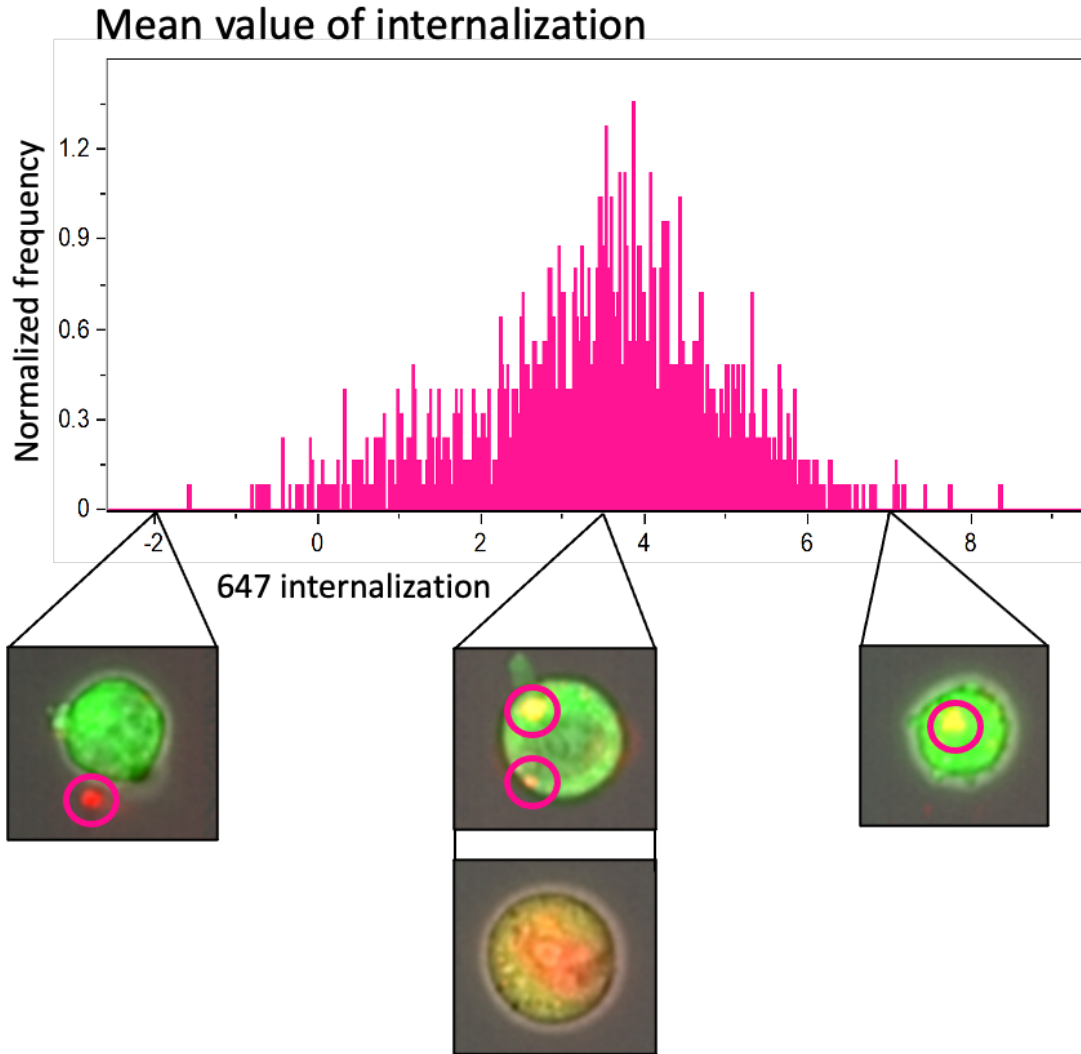


Figure 2.5. Mean internalization of Alexa fluor 647-labeled aggregates

The internalization of the Alexa fluor 647-aggregates into GFP-tau expressing cells was determined using an internalization wizard module on the IDEAS 6.3 software. This module uses a numerical system to rank Alexa fluor 647-punctae based on their proximity to the center of the GFP-tau expressing cell. Negative numbers are associated with Alexa fluor 647-punctae that have a peripheral association with the GFP signal, whereas higher numbers are associated with Alexa fluor 647-punctae that have a central localization in GFP-tau expressing cells. Diffuse Alexa fluor 647 signal is recorded as being both central and localized to the outskirts, landing them amongst the mid-section values.

CHAPTER THREE: RESULTS

3.1 Characterizing the HEK293 P301L-tau cell model

In order to study tau aggregation at a cellular level, we first needed to optimize tau expression and seeding our cell model. Our process of optimization included achieving the maximum amount of cellular tau expression, and selecting conditions for seeding that led to consistent and reliable results.

3.1.1 Doxycycline induces the expression of GFP tagged mutant P301L-tau in our HEK cell model

Our lab previously developed a stable HEK293 cell line that expresses GFP tagged to the N-terminus of mutant P301L tau (GFP-tau) under the control of a doxycycline (dox) inducible promoter (Kang et al., 2021). GFP-tau is not detected by immunoblot or fluorescence microscopy in the absence of dox (**Figures 3.1 A-E**). Upon the addition of dox, GFP-tau is detected at 24 hr (**Figure 3.1 C**). While expression is first detected after 24 hr of dox induction, it is further elevated after 48 and 72 hr post induction. Following the removal of dox, GFP-tau expression is mostly cleared after 24 hours, and is fully cleared after 48 hours (**Figure 3.1 D**). The expression levels of GFP-tau increase in a dose dependent manner with dox concentration as demonstrated by Western blotting (**Figure 3.1 E**). At 72 hr, expression is detected with treatment of dox concentrations greater than 5 ng/ml and plateaus at 10 ng/mL dox. Additionally, GFP-tau is normally localized to the MT's, where it reflects its physiological role as a MT associated protein (Hernández & Avila, 2007), but is also diffusely present throughout the cytoplasm (**Figure 3.2**). Based on these observations, we used 10 ng/mL dox to induce our cells for a period of 72 hours to ensure maximum GFP-tau expression prior to initiating further treatments. Spontaneous aggregation of GFP-tau was not detected under any cellular conditions tested.

3.1.2 Optimizing conditions for a tau seeding assay in our HEK293 P301L cells

Our first objective was to develop a tau cellular seeding assay, similar to other reported models (J. Chen et al., 2019; Guo & Lee, 2013; Sanders et al., 2014). In this assay, we apply exogenous, pre-formed R-tau aggregates to cells as seeding material, which then induces the aggregation of the endogenously expressed GFP-tau (**Figure 2.2**). Lipofectamine, which served to permeabilize the cell membrane and bypass endocytosis (Nonaka et al., 2010; Polanco et al., 2021), was needed alongside the aggregates in order to produce a seeding phenotype in this cell model (**Figure 3.3**). Aggregate formation in the cells is visible as bright green punctae as the GFP-tau detaches from the MT's and aggregates in the cytoplasm. A series of conditions were tested in order to achieve the most robust and consistent tau aggregate seeding rates in our cell model. Condition variables tested included temperature, dox concentration, time of dox pre-induction, cell number seeded, and cell time spent seeded prior to analysis (**Table 3.1**). It should be noted that P301L-tau seeds induced with heparin were used to optimize our seeding assay. During optimization, cells were seeded and then grown at both 30°C and 37°C to validate whether or not slowing their growth at 30°C would lead to higher seeding numbers. The verdict was that there is no difference after 48 hours between seeded cells grown at 30°C or 37°C, and that cells grown at 37°C looked overall more healthy.

As stated in section **3.1.1**, 10 ng/mL of doxycycline was used to induce GFP-tau expression over the course of 72 hours prior to each experiment to ensure maximum tau production, which also led to higher amount of aggregates formed compared to cells that had only been induced with dox for 24, or 48 hours. For our seeding assay, 10 000 cells were added per well of a 96-well plate to avoid over confluency, and the assay was analyzed 48 hours post seeding as aggregates had fully formed

by that time point. The final optimized seeding conditions are found in **Table 3.1**. We found that the concentrations of fibrils required to induce maximal seeding rates varied from batch to batch so we decided to test a range of concentrations in each experiment. Minimal or no GFP-tau aggregation was detected in non-seeding control groups. The very small number of punctae occasionally detected in unseeded samples (< 2 % of total cells with punctae) can be explained by the presence of debris, cellular spindles that resemble punctae during cell division, or increased GFP signal due to cells clumping together in the well.

3.2 Seeding ability of differently induced fibrils

As previously mentioned, our lab uses three specific inducers of tau aggregation: heparin, polyP, and Ara. We chose to explore the potential seeding effects (in both cellular assays and *in vitro* assays) that these inducers may have on their resulting R-tau aggregates.

3.2.1 Confirmation that multiple small molecule inducers promote tau aggregation

Tau aggregation *in vitro* can be promoted through the addition of a negatively charged aggregation inducer. While heparin is a popular and widely used inducer, both polyP and Ara are also capable of inducing tau aggregation *in vitro* (Chirita et al., 2003; Cremers et al., 2016; Mok et al., 2018; Paudel & Li, 1999; Sibille et al., 2006; Xie & Jakob, 2019; Zhang et al., 2019). We carried out an *in vitro* tau aggregation assay (Mok et al., 2018) under a set of standard conditions of 10 μ M tau in DPBS + 1 mM DTT, but varied the inducer used to initiate aggregation. Aggregation was monitored using the amyloid binding dye Thioflavin T (ThT). Consistent with previous literature (Cremers et al., 2016; Mok et al., 2018; Sibille et al., 2006; Voss et al, 2012) **Figure 3.4 A-C** demonstrates the ability of tau to aggregate in the presence of all three different inducers.

Increasing ThT signal intensity over time is detected following the addition of each of the three inducers, but does not exist when an inducer is absent. We can extract out multiple kinetic parameters from the output ThT curve for analysis, including lag time (**Fig 3.4. D**) (Mok et al., 2018). Lag time is the period of time from which the reaction starts, to when the tau begins to aggregate and ThT signal begins to increase. A shorter lag time is associated with faster aggregation (Mok et al., 2018).

Ara is the most potent inducer of tau aggregation, generating the shortest lag time of 0.06 hr (5 min), indicating that the ThT signal begins to increase prior to our first measured time point (**Figure 3.4 D**). PolyP is the next most potent, generating a lag time of 0.3 hr, followed by heparin which generates a lag time of 0.5 hr.

The amount of tau in solution in each reaction was quantified using SDS-PAGE gels and subsequent imageJ analysis (**Figure 3.5 A-B**). Known amounts of unaggregated tau were loaded on the same gel to generate a standard curve for quantification. This quantification was done to normalize the amount of tau added to subsequent *in vitro* and cellular seeding reactions. Heparin and polyP inducers appeared to consistently generate equal amounts of total tau in the aggregate reaction, however arachidonic acid had a tendency to generate lower quantities (**Figure 3.5 B**). It is possible that due to the fatty acid nature of Ara, some of the tau aggregates bound by this molecule become stuck to the walls of the tube and are thus unintentionally excluded from our sample analysis.

3.2.2 Comparison of cellular seeding efficiency of tau aggregates produced by different inducers

Tau aggregates generated using different inducers were used as seeding material for HEK293 cells that were expressing GFP-tagged mutant P301L tau. Lipofectamine, which served to permeabilize

the cell membrane and bypass endocytosis, was needed alongside the aggregates in order to produce a seeding phenotype in this cell model (**Figure 3.6 A-D**). When added to the cells, tau induced with heparin generated a seeding effect, where 0.1 μM of seeding material led to a peak of roughly $40\% \pm 3\%$ of cells having aggregates, before cells began to lose shape and grow abnormally with higher concentrations of aggregate (**Figure 3.6 E**).

Equivalent amounts of tau from aggregated reactions (based on previously described gel quantification) were assayed. Consistent with our previous results, heparin induced tau seeds generated dose-dependent increases in seeding rates that plateaued at $40\% \pm 3\%$ (**Figure 3.6 A-B**). In stark contrast to the heparin induced seeds, tau induced with polyP and Ara generated much lower seeding rates in cells, even at increasing concentrations of seeding material (**Figures 3.6 A,C-D**). While polyP induced seeds had a peak seeding rate of $5\% \pm 3\%$ of cells with aggregates at 0.1 μM , Ara induced seeds plateaued at a rate of only $3\% \pm 1\%$ at 0.05 μM , which was not significantly different from unseeded controls.

As control groups, uninduced P301L-tau monomer and ethanol-only induced P301L-tau monomer (ethanol is used to dilute Ara) were applied to cells. Neither control group exhibited a noticeable seeding effect compared to the unseeded control (**Figure 3.6 F-H**).

3.2.3 Efficiency of tau aggregation based on inducer *in vitro*

Contrary to our cellular seeding assays, we found that PolyP and Ara induced aggregates were capable of seeding tau aggregation *in vitro*. *In vitro* kinetic seeding assays were performed using mutant P301L R-tau monomer with differently induced aggregates acting as seeds (DPBS for control), plus the addition of the respective inducer. In contrast to cell seeding assays, *in vitro* seeding assays require the addition of an inducer to detect seeded aggregation (**Figure 3.7**). The

effect of seeding is observed through a reduction in lag time, which would indicate that monomeric tau is able to aggregate faster due to the addition of pre-formed aggregate seeding material. Heparin and polyP induced seeds were able to reduce lag time upon being added to the reaction compared to unseeded tau monomer, though a larger reduction in lag time was observed with heparin induced seeds, which decreased lag time by 5-fold, whereas polyP induced seeds decreased lag time by 2-fold (**Figure 3.7 A-D**).

Ara induced seeds did not show a significant reduction in lag time upon being added to the reaction when compared to unseeded monomeric tau (**Figure 3.7 E-F**). Since Ara causes rapid aggregation that is observable at our earliest time point, it would not be possible to see a reduction in lag time through the addition of seeding material. Control experiments were carried out with uninduced monomeric P301L-tau used as seed, and with ethanol-only induced seed. Both control groups had a significant effect in reducing aggregation lag time compared to unseeded monomeric tau (**Figure 3.7 G-J**), however this effect was small (1.5-fold) compared to heparin and polyP induced seed groups.

When seeds were added in increasing concentrations, heparin and polyP induced seeds appeared to decrease lag time in a dose dependent manner, which once again was observed to be more dramatic with the heparin induced seeds (**Figure 3.8 A-B**). Ara induced seeds showed no change in lag time, even at increased seed concentrations (**Figure 3.8 C**).

Compared to the heparin and polyP induced seeds, which had a significant effect on reducing lag time with just 0.05 μM of seed (**Figure 3.8 A-B**), uninduced and ethanol induced control groups did not see a reduction effect until the addition of 0.1 μM seed (**Figure 3.8 D-E**). The variable seeding ability of the differently induced aggregates in cells versus *in vitro* led us to further investigate the cause of the differential seeding effects in cells.

3.2.4 Evidence of structural differences between tau aggregates generated by heparin, polyP or Ara

We hypothesized that tau aggregates generated using different inducers may have distinct structures that could account for the effects we observe in cells. To explore this possibility we performed trypsin digest assays on our tau aggregate samples. The trypsin digest assay works by completely digesting the trypsin-sensitive portions of the protein, leaving only peptide fragments of the trypsin-resistant core. The specific structure of the trypsin-resistant core can modulate the set of peptide fragments generated, thus allowing for comparisons of different banding patterns of fragments to indicate distinct core structures. Mixtures of peptide fragments were resolved by capillary gel electrophoresis for analysis.

Chromatograms and lane view representations of separated peptide fragments demonstrated unique profiles for the differently induced aggregates. Heparin induced aggregates show intense bands at 9 and 26 kDa, and less intense bands at 4, 15, and 19 kDa (**Figure 3.9 A**). Polyphosphate induced aggregates similarly have intense bands at 9 and 26 kDa, however they differ in their less intense bands, with the 4 kDa band being more pronounced and the presence of 13 and 20 kDa bands as opposed to 15 and 19 kDa bands (**Figure 3.9 B**). Perhaps most striking are the arachidonic acid induced aggregates, with two very intense bands at 10 and 27 kDa, and two less intense bands at 4 and 19 kDa (**Figure 3.9 C**). While there is some overlap, aggregates generated with three different inducers do possess structural differences (**Figure 3.9 D, G**).

As a control, monomeric P301L tau without inducer was subjected to trypsin digestion, capillary gel electrophoresis and no bands were detected, indicating the absence of a trypsin resistant core

as expected (**Figure 3.9 E, H**). We also examined control tau aggregate reactions generated using ethanol only (the buffer used for Ara stocks). Upon trypsin digestion, these control reactions showed trypsin resistant bands, two of which (10 + 19 kDa) aligned with arachidonic acid peaks. However, it should be noted that when directly compared with Ara induced reactions, the bands were much fainter in comparison (**Figure 3.9 F, I**).

3.2.5 PolyP induced aggregates can seed tau monomer without the addition of an inducer

To determine if the aggregates generated using different inducers were capable of effectively templating monomeric tau and retaining their original aggregate structure, 10 % seed was added to monomeric P301L tau *in vitro* without the addition of an inducer. When 10 % heparin induced seeds were added to the reaction the ThT signal was already elevated, indicating that the dye was binding to the seeds (**Figure 3.10 A-B**). Within the first 0.5 hr of the reaction, there was a slight increase past the original signal but nothing more after that indicating that no significant seeding (new aggregation) occurred. In contrast, when 10 % polyP induced seeds were added to the reaction, a gradual increase in ThT signal occurred over the course of 48 hrs. The increasing presence of ThT bound material in reactions with added polyP induced seeds suggests that further seeding has occurred. Finally, when Ara induced seeds were added to the reaction, there was no increase in ThT signal and the curve resembled that of unseeded monomeric tau, indicating a lack of seeding in the reaction . It is unknown why there is a lack of initial ThT binding to Ara seeds (as seen with heparin fibrils). These results indicate that while heparin and Ara induced seeds require the presence of an inducer along with monomeric tau for further aggregation to take place, polyP induced seeds are capable of seeding on their own.

Trypsin digests were performed on all wells of the kinetic assay post seeding and were structurally compared to the original 10 % seed sample (**Figure 3.10 C-E**). No trypsin resistant fragments were detectable past the signal from the original seed in both heparin and Ara induced seeding assays (**Figure 3.10 C, E, Appendix A**). PolyP induced seeds were capable of inducing seeding, however trypsin digestion revealed that the outcome was variable, where a trypsin resistant product was only generated once out of three attempts and the resulting structure did not resemble that of the original seed (**Figure 3.10 D**). Upon adding the trypsin resistant product to cells at 0.1 μ M, it did not have a significant seeding effect compared to heparin induced seeds (**Appendix B**).

When differently induced seeds were used in conjunction with their respective inducers to seed monomeric tau, the resulting structures were identical to the original seed (**Appendix C**).

3.2.6 Heparin, polyP, and Ara induced aggregates can be internalized by HEK293 P301L cells

Finally, we set out to determine if the reason why polyP and Ara induced aggregates were not generating a significant seeding effect in our cell model was due to the fact that the cells were not able to internalize them. This was accomplished using Alexa fluor 647-labeled tau aggregates (generated with different inducers) in order to monitor their localization in our cells. Imaging flow cytometry was used to visualize the Alexa fluor 647 signal produced by the labeled aggregates and their localization upon associating/internalizing in our GFP-tau expressing cells. A higher mean value calculated for “Alexa fluor 647 internalization” (strong correlation of GFP and Alexa fluor 647 signal intensities) is correlated with positive internalization (**Figure 2.5**). As expected, R-tau aggregates generated using heparin are able to be internalized by our cells (**Figure 3.11 A, C**). Specifically, when heparin seeds are incubated with the cells for four hours alongside lipofectamine, the mean value of Alexa fluor 647 internalization is 3.1 from 676 cells assessed to

be Alexa fluor 647-positive (**Figure 3.11 A**). In contrast, when heparin seeds were added to cold cells for 45 minutes in the absence of lipofectamine (inhibition of endocytosis), the mean value was 1.7 and only 32 cells were found to be Alexa fluor 647-positive (**Figure 3.11 B**). These results are reinforced by representative images, which show central localization of Alexa fluor 647-labeled tau punctae when heparin seeds were incubated for four hours with lipofectamine (**Figure 3.11 C**), and peripheral localization of Alexa fluor 647-labeled tau punctae on cells where endocytosis is inhibited (**Figure 3.11 D**).

Similar to the results seen with the heparin induced aggregates, polyP and Ara induced aggregates are able to be internalized by our cells (**Figures 3.12 + 3.13**). In the presence of a four hour incubation with lipofectamine, Alexa fluor 647-labeled polyP induced aggregates have a mean value of internalization of 2.6, with 824 cells assessed to be Alexa fluor 647-positive (**Figure 3.12 A**), while this value drops to 2.0 when endocytosis is inhibited and only 32 cells are positive for 647 signal (**Figure 3.12 B**). Like we saw with heparin induced aggregates, polyP induced aggregates are centrally located in our cells (represented as Alexa fluor 647-labeled tau punctae), compared to the outer localization of punctae in cells where endocytosis is inhibited (**Figure 3.12 C-D**). When Ara induced aggregates are incubated with cells for four hours with lipofectamine, the mean value of internalization is 3.4 and a total of 1252 cells are positive for Alexa fluor 647 signal (**Figure 3.13 A**). When endocytosis is inhibited, the mean value drops to 1.6, with only 72 cells positive for Alexa fluor 647 signal (**Figure 3.13 B**). As with both heparin and polyP induced aggregates, the Alexa fluor 647-labeled Ara induced aggregates are located centrally in the cells (**Figure 3.13 C**), and their localization becomes more peripheral when endocytosis is inhibited (**Figure 3.13 D**).

Additionally, ThT staining of the differently induced aggregates was carried out to investigate the possibility of aggregate size playing a role in internalization. Subsequent fluorescent imaging of aggregates revealed that heparin, polyP, and Ara induced aggregates are similar in size (**Appendix D**). Aggregate sizes also appear to be relatively homogenous throughout the samples. This evidence does not support the possibility that large size variations between tau aggregates generated using different inducers accounts for the differential seeding effects we observed in cells.

3.3 Effect of DNAJA2 on tau aggregation in cells

Chaperone proteins are key regulators of protein folding and are known to have dysregulated expression in age-related disorders, which makes them excellent candidates for NDD research (Brehme et al., 2014; Nachman et al., 2020). A previous study concluded that DNAJA2 had an inhibitory effect on tau aggregation *in vitro*, and its expression was observed to be increased in both MCI and AD (Mok et al., 2018). The effects of DNAJA2 overexpression and knockdown on tau aggregate formation have not yet been studied in a human cell model.

3.3.1 Transfection and induction of cumate inducible expression vector

First we wanted to overexpress DNAJA2 in our HEK293 P301L cell line. A vector was generated to express full-length human DNAJA2 under the control of an inducible cumate promoter (see section **2.2.3**). The construct was introduced to our HEK293 cell line via lentiviral transduction. Cells with successful integration of the construct were selected using puromycin (mg/ml) for one week. Following puromycin selection, cell samples were fixed and immunostained for DNAJA2. Fluorescence microscopy showed an endogenous level of DNAJA2 in non-transfected cells, and a

significantly higher level of DNAJA2 in transfected cells that were induced to overexpress the protein (**Figure 3.14 A-B**). This level of expression was also verified via Western blot (**Figure 3.14 C**). Within the cell population, variable overexpression of DNAJA2 was observed between cells, with a significant portion of the population not appearing to show any overexpression. For our experiments, we desired a more homogeneous population of cells overexpressing DNAJA2 and thus, single cell clones were selected from the initial mixed population.

3.3.2 Selection of clones positive for cumate inducible expression vector

Individual clones were then further selected using two criteria: 1) ability to express GFP-tau in response to dox induction and 2) ability to overexpress DNAJA2 in response to cumate induction. Fluorescence microscopy was used to confirm the presence of GFP-tau expression upon doxycycline induction (**Figure 3.15 A-C**), and Western blotting was used to confirm the overexpression of DNAJA2 upon addition of cumate (**Figure 3.15 D-F**). Interestingly, only 1 out of 4 clones selected passed our selection criteria. Of the three clones that were determined to be positive for GFP-tau expression and the cumate inducible expression vector, only clones 6 and 7 were utilized in experiments since clone 4's expression of DNAJA2 was not consistent when induced.

3.3.3 DNAJA2 and Hsp27 knockdown lead to an increase in the percentage of cells seeded

Western blot confirmed that DNAJA2 was decreased in cells stably transfected with the DNAJA2 shRNA vector (**Figure 3.16 A**). This was compared to cells that had not been transfected with shRNA, thus expressing endogenous levels of the DNAJA2 protein.

Lysates from shRNA transfected cells induced with doxycycline for 72 hours were analyzed by Western blot. DNAJA2 shRNA cells, Hsp27 shRNA cells, and control shRNA cells all appear to have similar levels of GFP-tau expression (**Figure 3.16 B**).

Compared to control shRNA cells, both DNAJA2 and Hsp27 shRNA cells had a higher percentage of cells with aggregates (**Figure 3.17 A-B**). The percentage of cells with aggregates in all three cell groups increased in a dose-dependent manner with increasing fibril concentration. While control cell aggregation peaked with 16% of cells with aggregates at 0.2 μ M fibrils, DNAJA2 knockdown cells peaked with 20% of cells with aggregates at 0.1 μ M fibrils (**Figure 3.17 B**). Hsp27 knockdown cells shared a trend with the DNAJA2 knockdown cells, with both groups reaching 20% of cells with aggregates at 0.1 μ M fibrils, but they peaked at 21% of cells with aggregates at 0.2 μ M fibrils (**Figure 3.17 B**).

Chapter Three: Figures

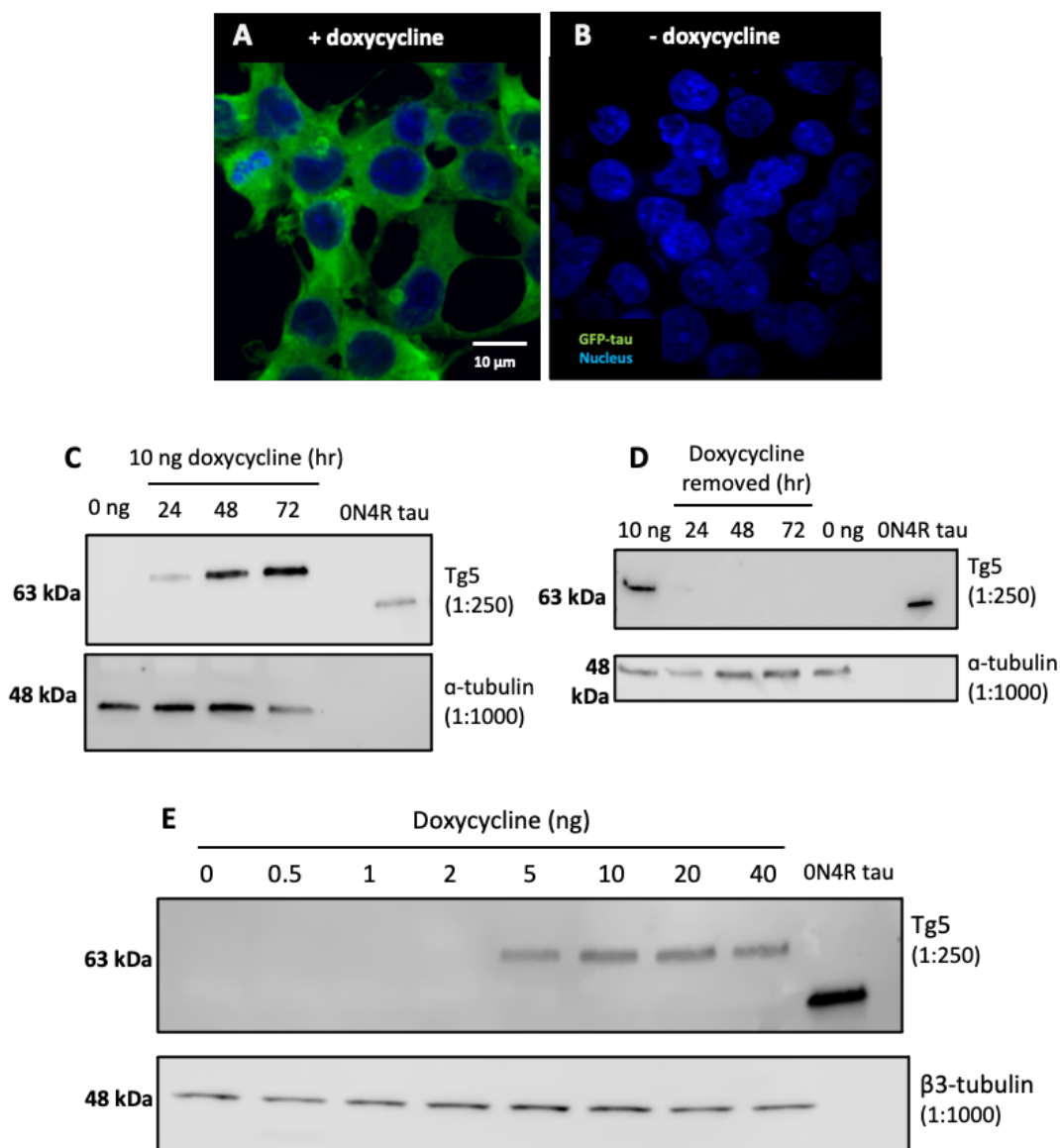


Figure 3.1. HEK293 P301L cell model expressed GFP-tau upon addition of doxycycline

A-B HEK293 cells treated with doxycycline (dox) (**A**) and without dox (**B**). Cell nuclei were stained with Hoechst (1 $\mu\text{g}/\text{mL}$) 2 hour prior to fixation and imaging. Images were obtained using WaveFxl confocal microscope at 60X magnification.

C Western blot of HEK293 cells that had been treated with 10 ng dox 24, 48, or 72 hours prior to lysis. Uninduced cells served as a negative control.

D Western blot of HEK293 cells that had been induced with 10 ng dox for 72 hours, and then dox had been removed for 24, 48, 72 hours prior to lysis. Cells induced with 10 ng dox served as a positive control.

E Western blot of HEK293 cells that had been induced with 0-40 ng dox 72 hours prior to lysis. ON4R tau serves as a positive control.

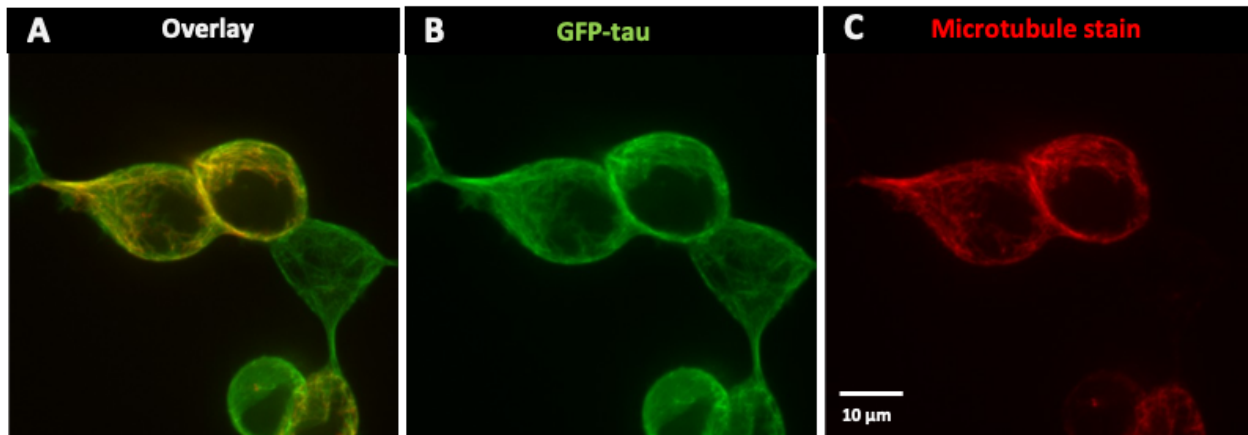


Figure 3.2. GFP-tau expressed in cells associates with microtubules

A-C HEK293 cells were induced with 10 ng dox 72 hours prior to live cell imaging. Additionally, SPY555 microtubule (MT) stain was applied 1 hour prior to imaging. Cell images were obtained using confocal microscopy at 60X magnification. The overlay image (**A**) contains signal from both GFP-tau and MT stain, and the two channels are shown individually as GFP-tau (**B**), and MT stain (**C**).

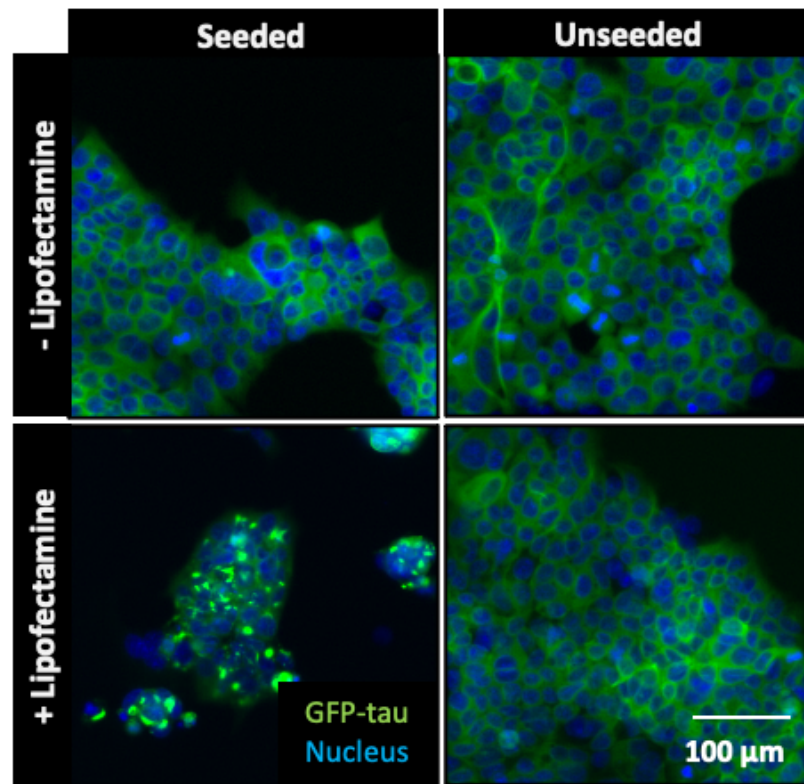


Figure 3.3. Cell seeding requires the addition of lipofectamine

HEK293 cells were induced with 10 ng dox 72 hours prior to seeding with 0.1 μ M heparin induced aggregates, or buffer control, along with the presence or absence of lipofectamine. Cells were stained with 1 μ g/mL Hoechst 2 hours prior to live cell imaging and images were acquired using a high content screening microscope (Molecular Devices) at 10X magnification.

Table 3.1. Cell seeding optimization parameters for our HEK293 cell model

Condition	Optimized value
Temperature	37 °C
Doxycycline	10 ng/mL
Doxycycline pre-induction	72 hours
Cell number seeded per well	10,000 cells
Post-seed analysis	48 hours

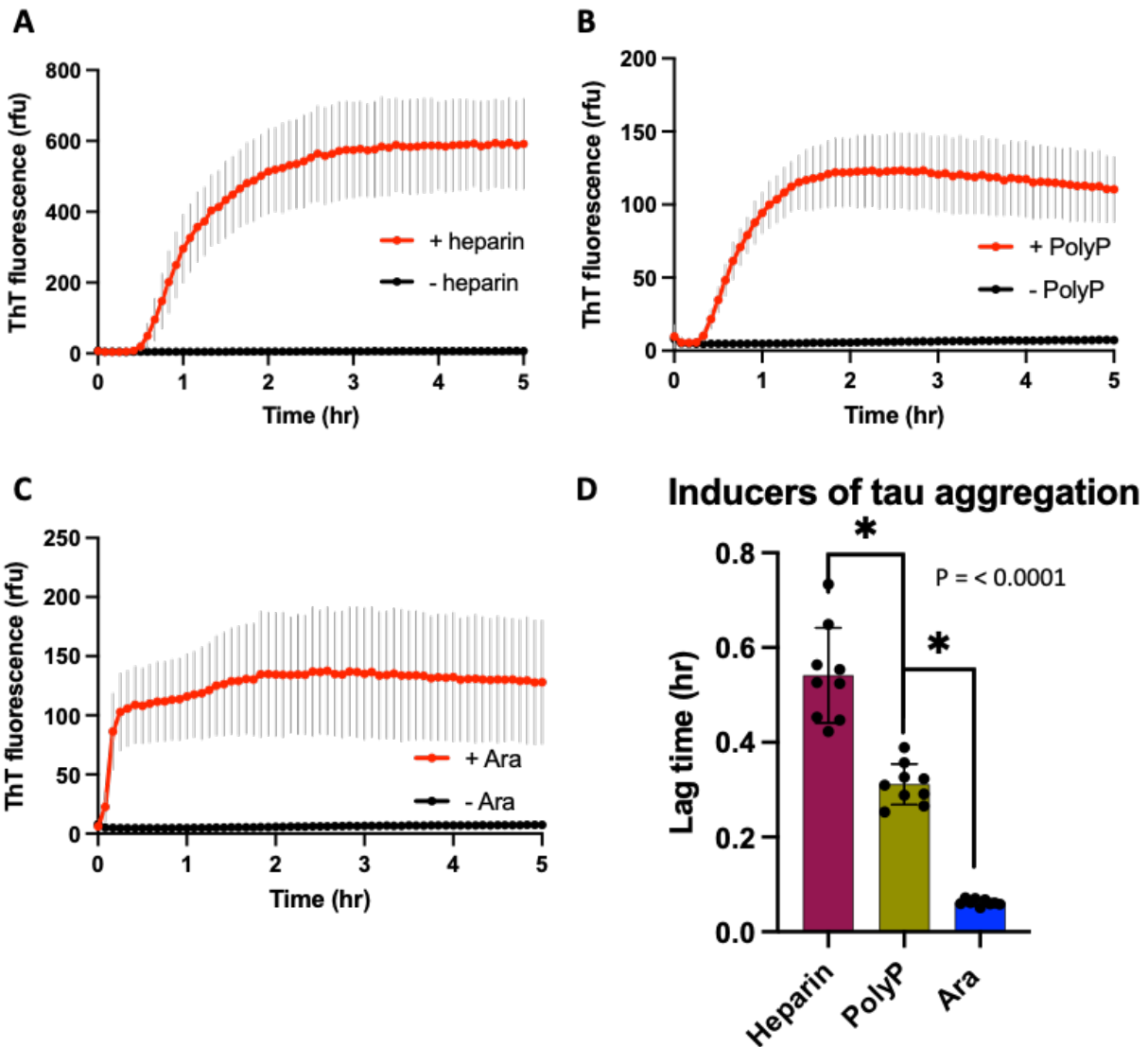


Figure 3.4. Confirmation that multiple small molecule inducers promote tau aggregation

A-C Kinetic assays performed using P301L tau monomer in the presence and absence of different small molecule inducers: heparin (A), polyphosphate (polyP) (B), arachidonic acid (Ara) (C). Tau aggregation was monitored using Thioflavin T (ThT) amyloid binding dye over the course of 24 hours. Each curve shown as mean \pm SD, with $n = 3$.

D Bar graph quantifying the differences in the lag time between P301L tau monomer aggregating with different inducers, shown in (A-C). P-value = < 0.0001 calculated using a one-way ANOVA.

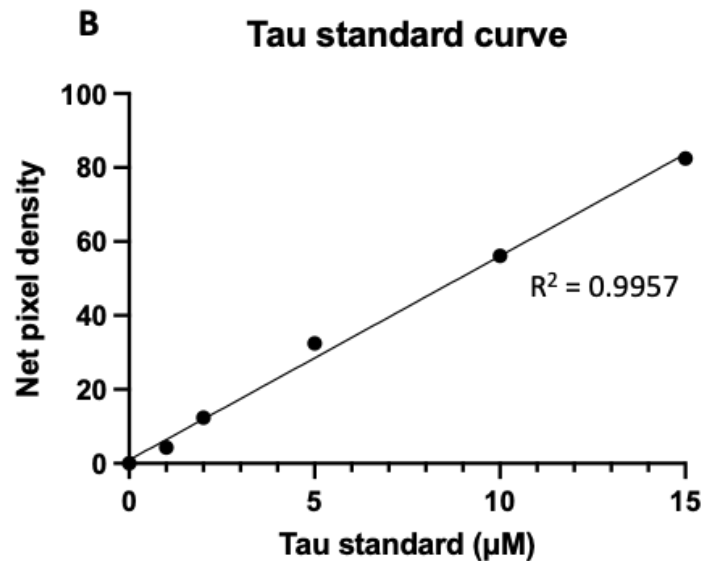
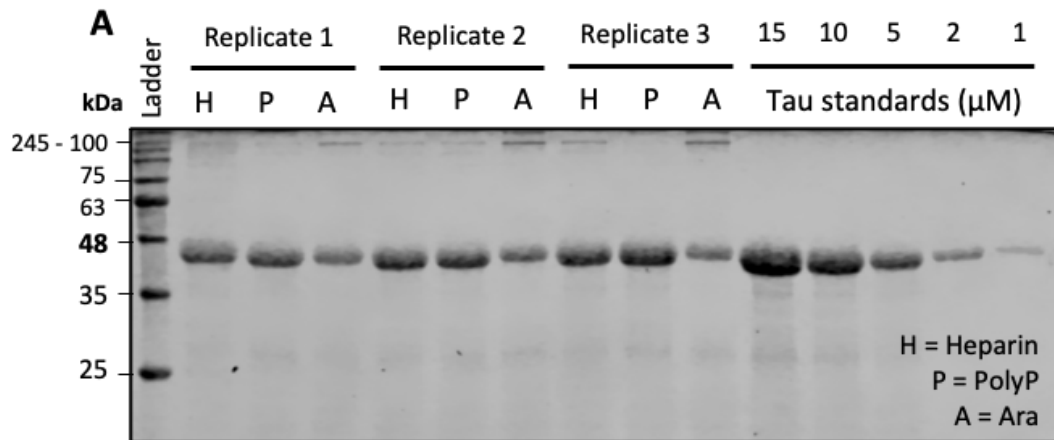
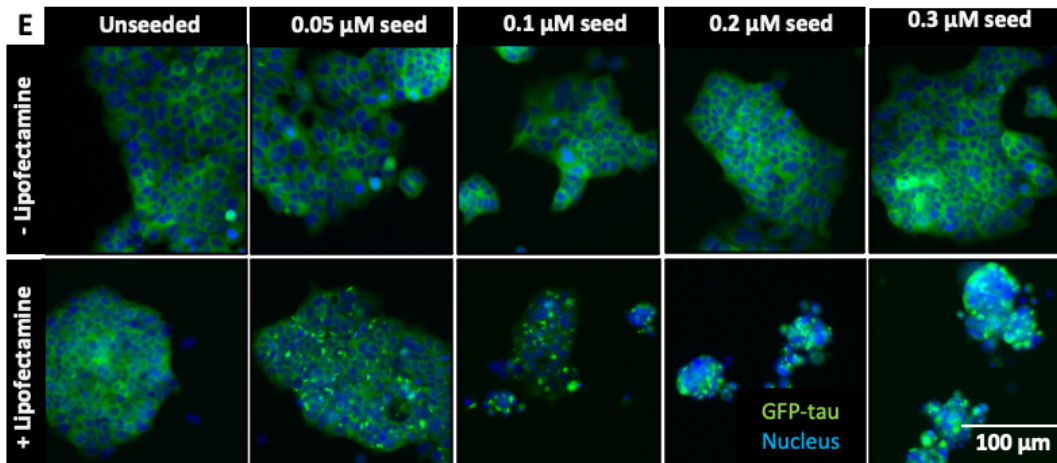
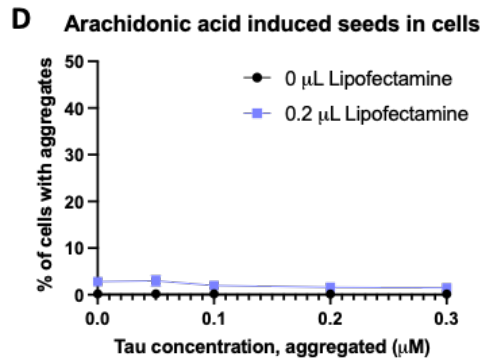
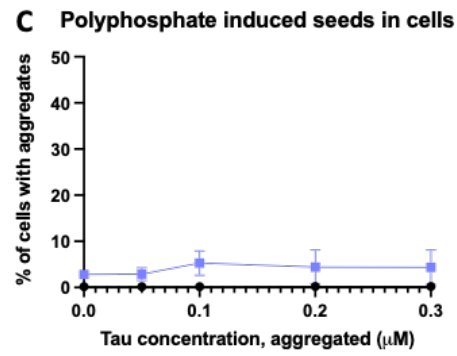
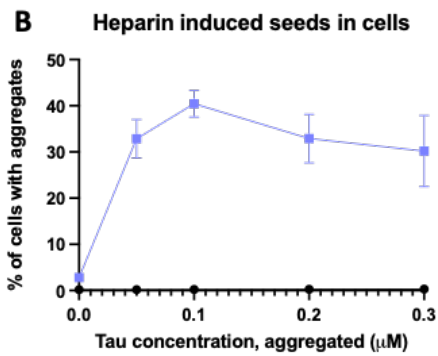
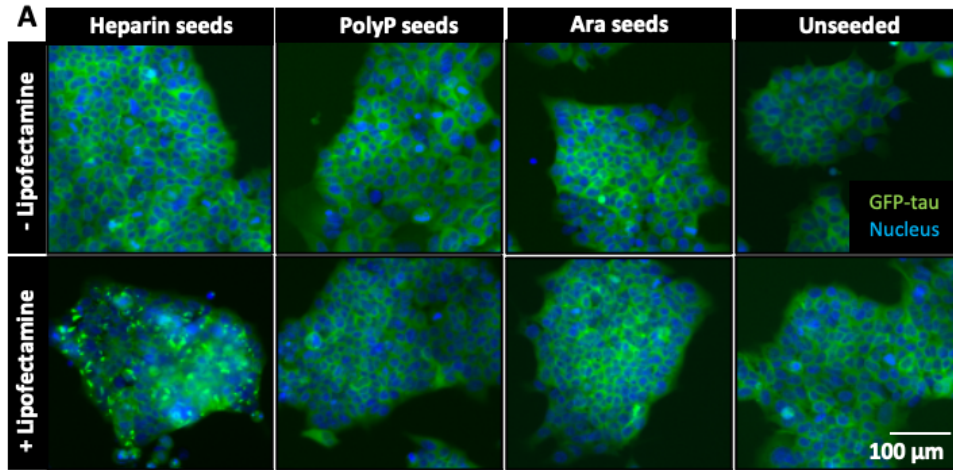


Figure 3.5. Quantification of total tau in aggregation reactions

A SDS-PAGE gel quantification of total tau in the solution of aggregation reactions produced using different inducers. Three different batches of aggregation reactions were analyzed alongside purified tau standards for consistency.

B Standard curve constructed from purified tau standards in (A), which were analyzed using inverted pixel density in ImageJ. Curve was used to normalize total tau in the solution of aggregation reactions.



(continued)

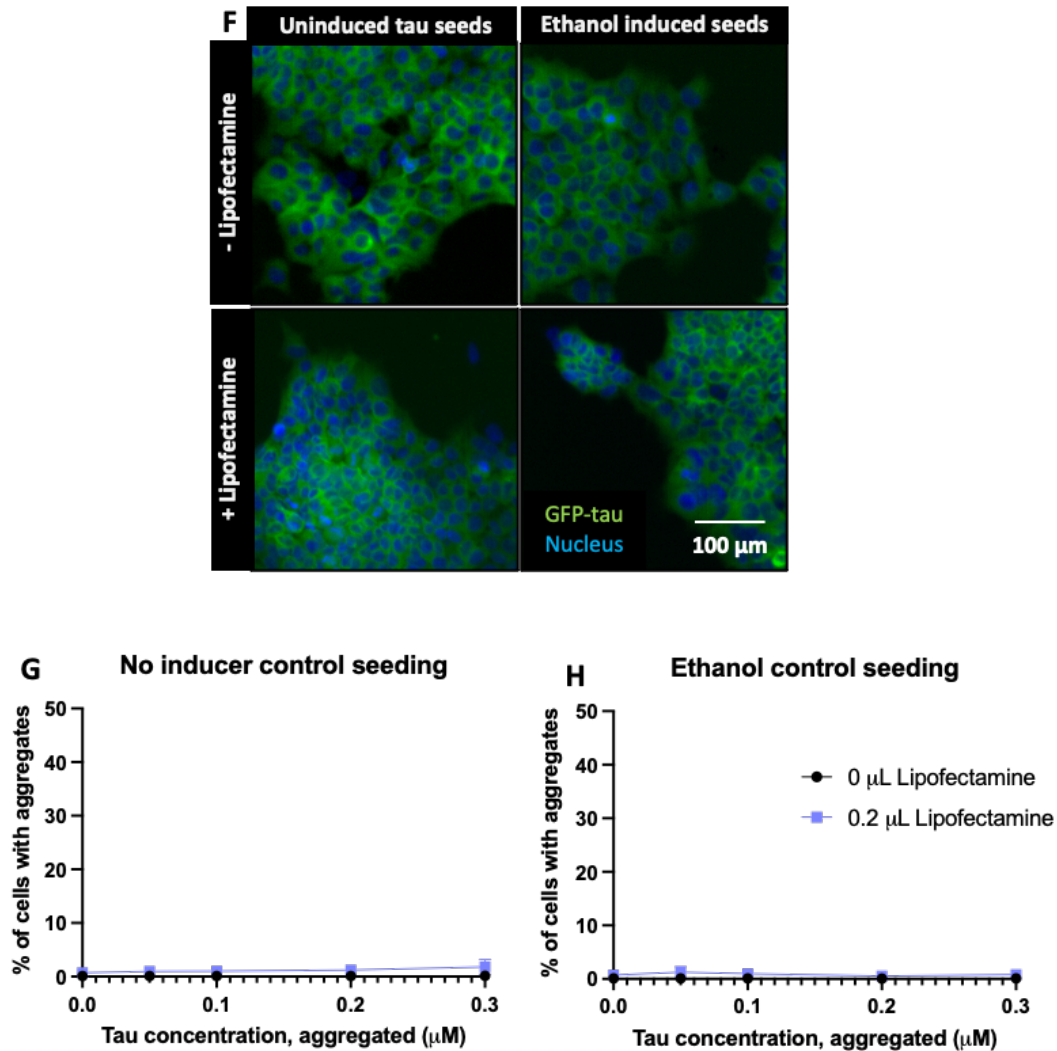


Figure 3.6. Comparison of cellular seeding efficiency of tau aggregates generated with different inducers

HEK293 cells were treated with doxycycline to induce GFP-tau expression 72 hours prior to seeding with aggregates. Cellular aggregates at 48 hours post-seeding were observed via live cell imaging. Cell nuclei were stained with Hoechst (1 $\mu\text{g}/\text{mL}$) 2 hour prior to imaging. Fluorescent microscope images were acquired using a high content screening microscope (Molecular Devices) at 10X magnification.

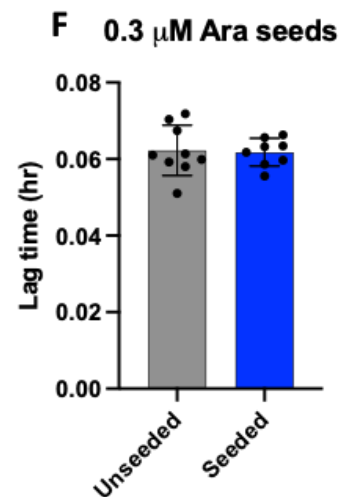
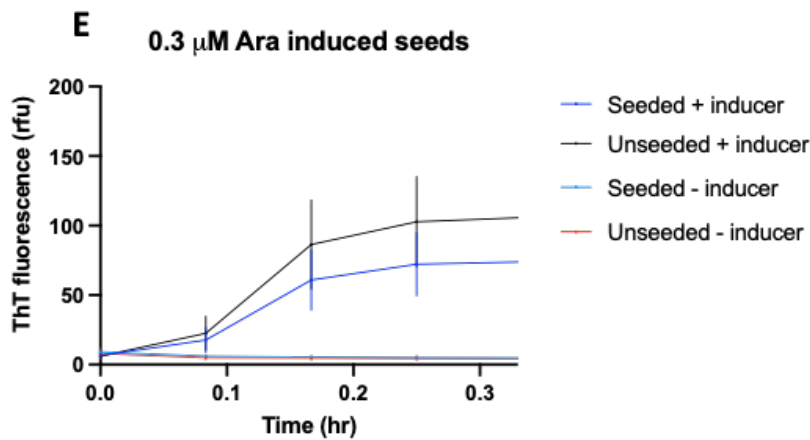
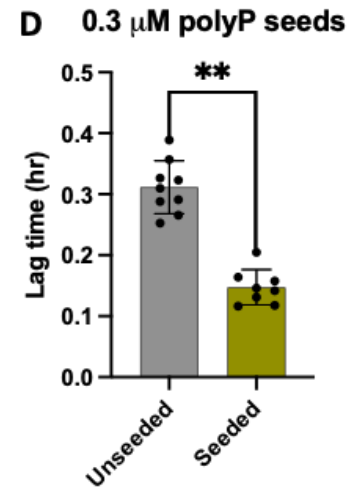
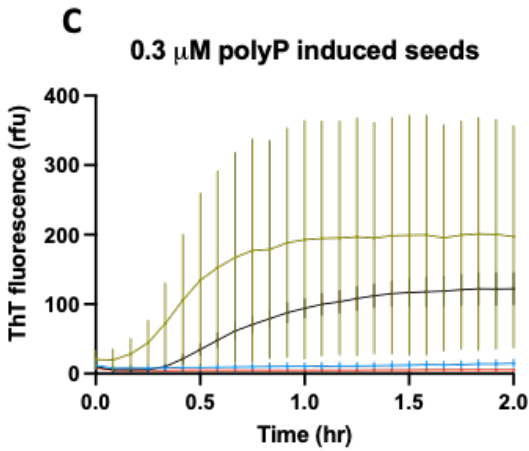
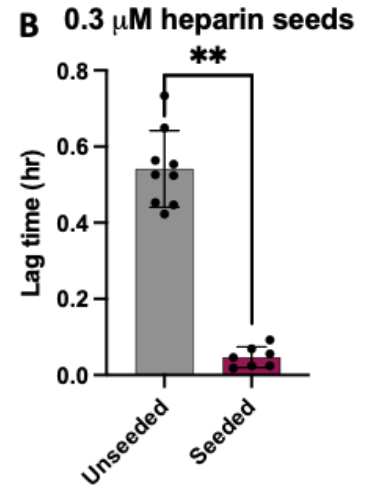
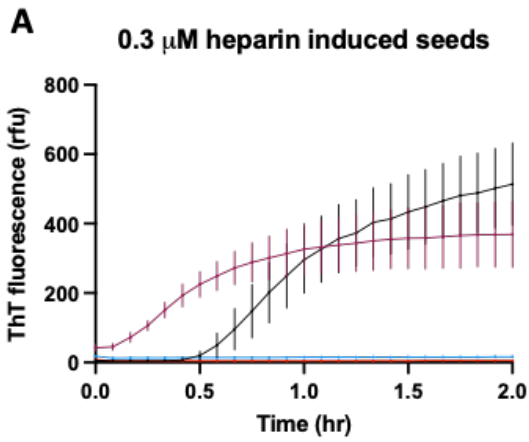
A Images of cells seeded with differentially induced aggregates (0.1 μm), packaged with (+) or without (-) lipofectamine.

B-D Quantification of total number of cells with aggregates at the indicated concentrations. mean \pm SD plotted, n = 3 replicates per experiment, and experiments repeated in triplicate.

E Images showing growth of cells seeded with heparin induced fibrils at different concentrations (0-0.3 μM).

F Fluorescent microscope images of uninduced tau monomer and ethanol induced seed (0.1 μm) controls.

G-H Quantification of uninduced and ethanol induced controls. Mean \pm SD, n = 3 replicates per experiment, and experiments repeated in triplicate.



(continued)

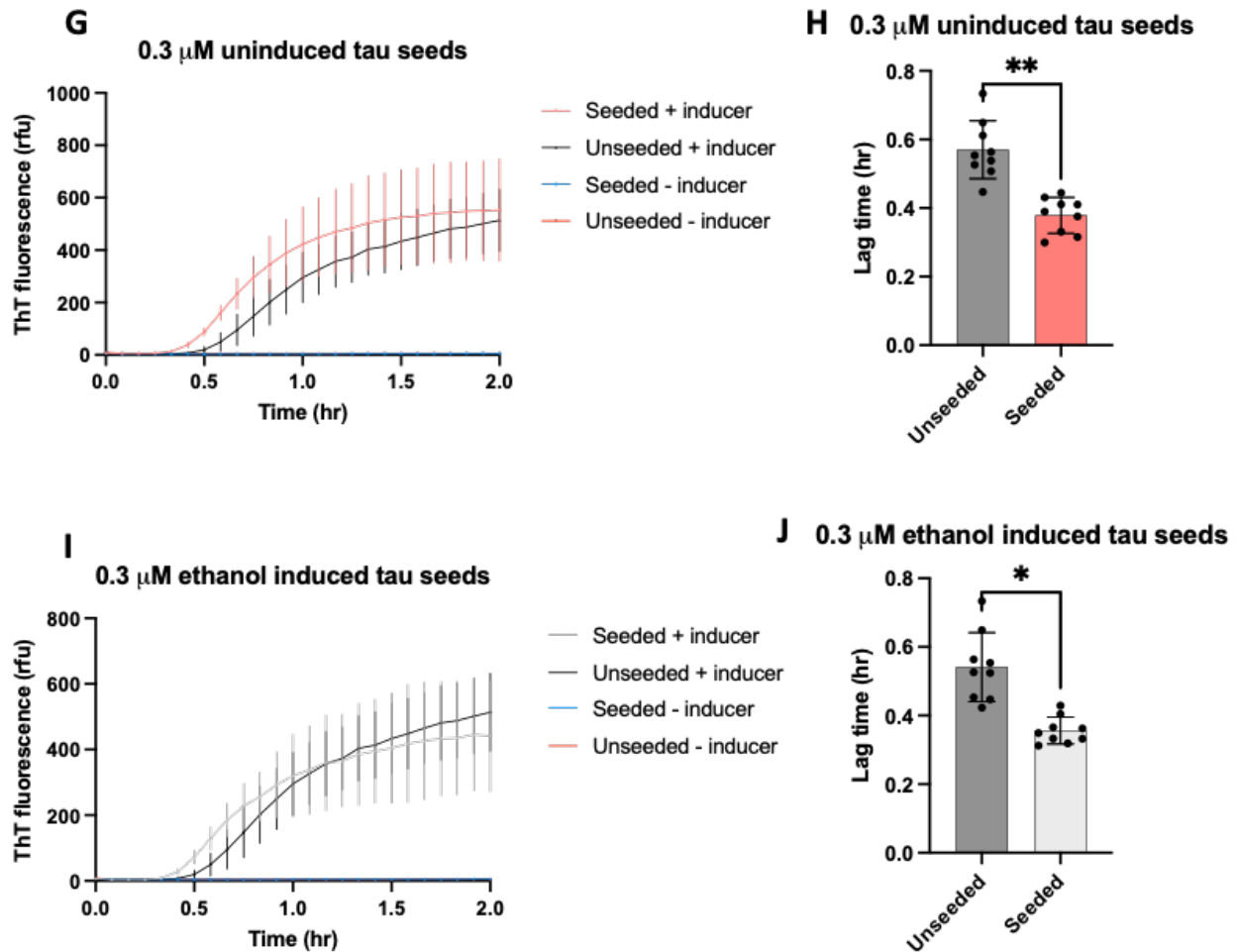


Figure 3.7. Efficiency of tau aggregation based on inducer *in vitro*

In vitro kinetic assays performed with P301L tau and monitored with ThT fluorescence over the course of 24 hours. Pre-formed aggregate seeds generated with different inducers (or controls) were used as seeding material (0.3 μM), with DPBS acting as a control.

Heparin (A), polyP (B), and Ara (C) induced aggregates along with uninduced (G), and ethanol induced (I) tau controls are represented by kinetic curves. DPBS serves as a control (- inducer).

B, D, F, H, J Quantification of lag time in kinetic assays seeded with differently induced tau aggregates or controls. Values determined using Welch's T-Test. ** p-value < 0.0001, * p-value = 0.0004

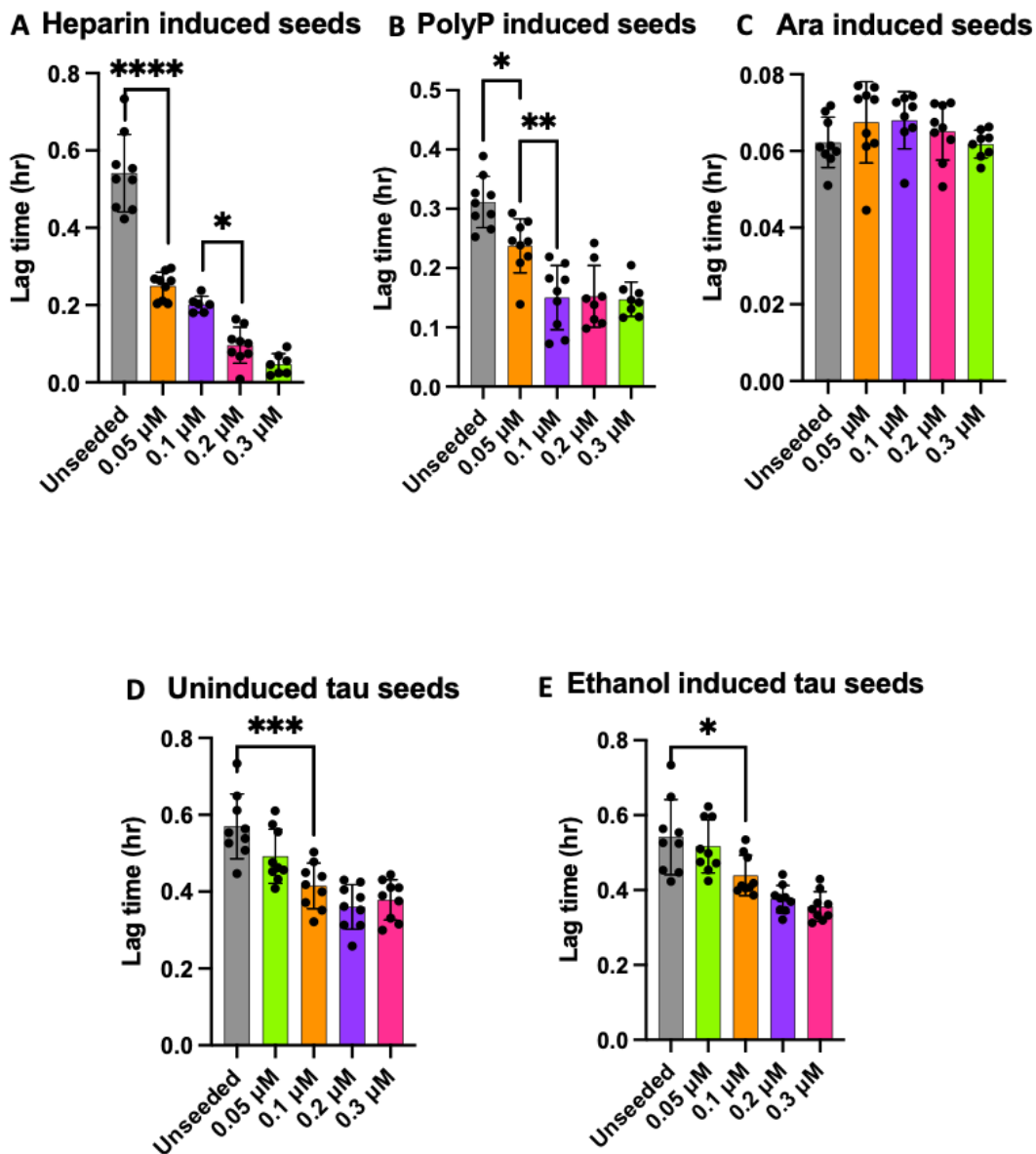
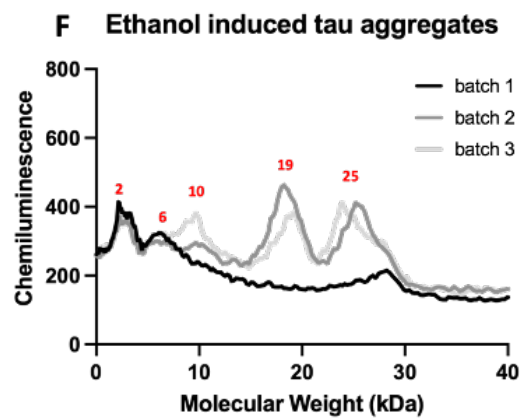
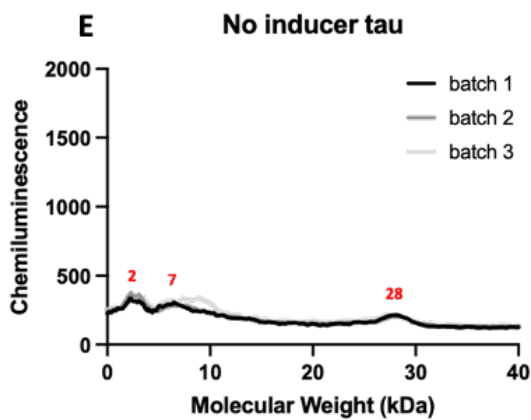
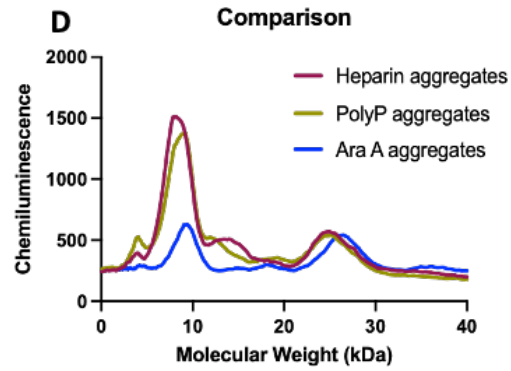
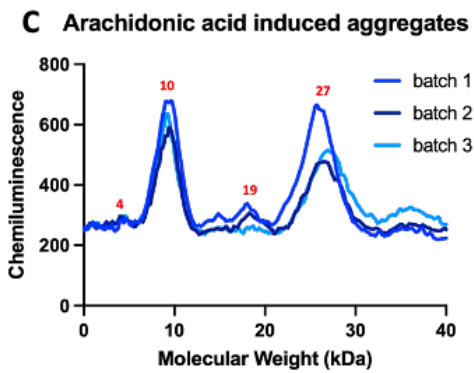
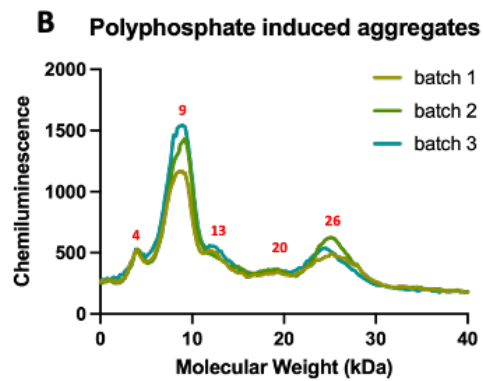
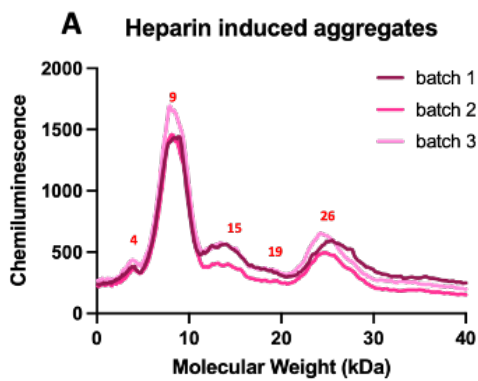


Figure 3.8. Efficiency of tau aggregation based on seed concentration *in vitro*

A-E Bar graphs showing aggregation lag time of P301L-tau monomer when 0-0.3 μM of differently induced aggregates (A-C) or controls (D, E) were added to the reaction as seeding material. Values determined using one-way ANOVA test. **** p-value < 0.0001 *** p-value = 0.0001, ** p-value = 0.002, * p-value = 0.01.



(continued)

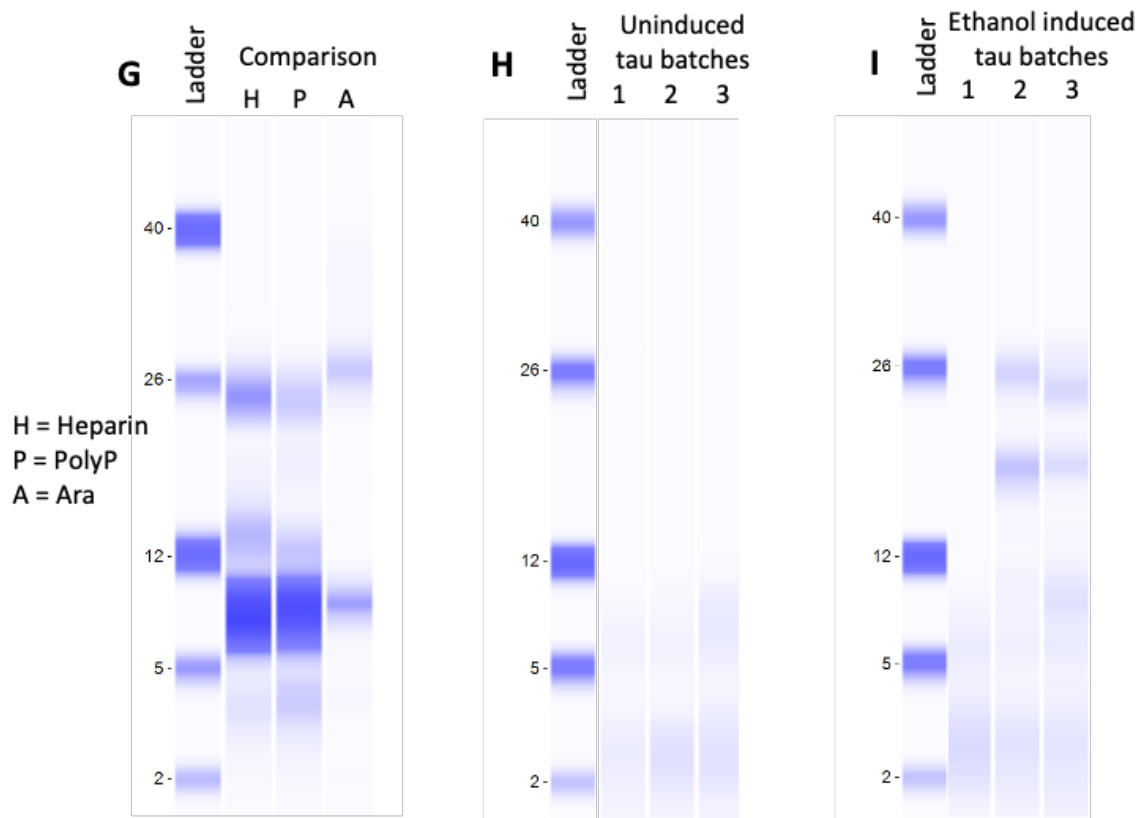


Figure 3.9. Evidence of structural differences between tau aggregates generated with heparin, polyP, or Ara

A-C Chromatogram outputs for capillary gel electrophoresis of trypsin digested tau aggregates induced with heparin (**A**), polyP (**B**), and Ara (**C**). Three independently generated aggregate samples (batch # 1 – 3) were analyzed for each experimental group. Chromatograms display the band intensities according to their molecular weight, with molecular weights of major peaks labeled in red.

D Chromatograms comparing the trypsin digest profiles of aggregates generated using the three different inducers.

E-F Chromatograms of uninduced tau (**E**), and ethanol induced tau (**F**) processed as described in **A-C**.

G-I Corresponding lane view versions of the chromatograms shown in **D-F**.

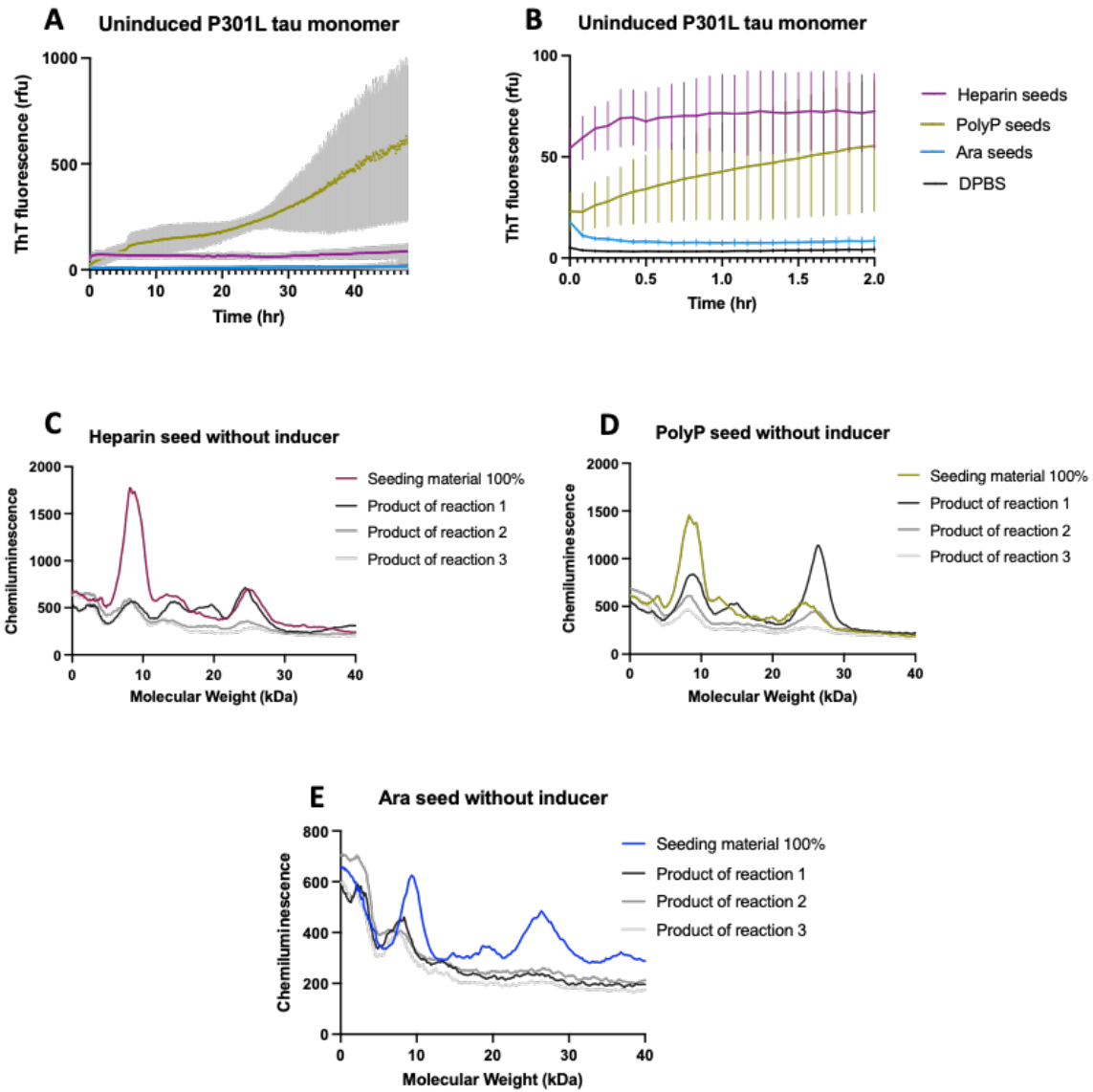


Figure 3.10. PolyP induced aggregates can seed tau monomer without the addition of an inducer

A-B In vitro kinetic aggregation curves obtained from seeding P301L-tau monomer with 10 % seeding material, and the absence of an inducer. Seeding material was R-tau aggregates generated with either heparin, polyp, or Ara. Aggregation reaction was carried out over 48 hours (**A**), and ThT signal changes are visible within the first two hours (**B**).

C-E Chromatogram outputs for capillary gel electrophoresis of trypsin digested tau aggregates from the original reaction (seeding material 100 %), and the products of the seeding reaction (1-3). Digests were carried out on seeding material and reaction products from aggregates generated with heparin (**A**), polyp (**B**), and Ara (**C**).

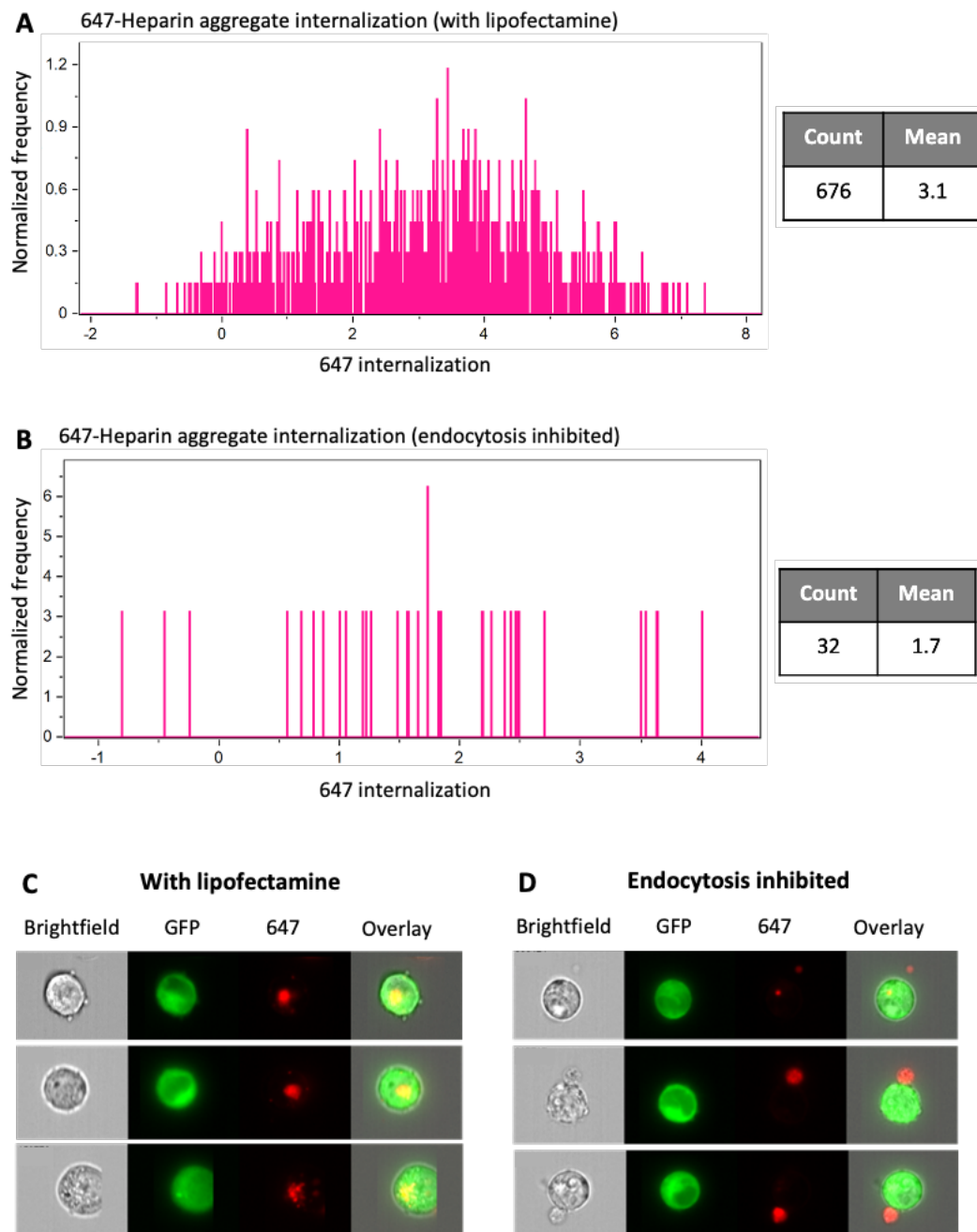


Figure 3.11. Heparin induced aggregates are internalized by cells

A HEK293 cells induced with 10 ng dox for 72 hours were seeded with Alexa fluor 647-labeled heparin induced tau aggregates packaged with lipofectamine. Internalization measured with imaging flow cytometry, 4 hours post seeding. Bar graph representing frequency of Alexa fluor 647 internalization events with respect to distance from cell perimeter is plotted. Total cells counted and mean of internalization shown in table.

B Control group in which cells pretreated on ice for 45 min to prevent endocytosis were seeded with lipofectamine packaged tau aggregates then analyzed as described in (A).

C-D Representative images of internalized Alexa fluor 647-aggregates in the presence of lipofectamine (C), or when endocytosis is inhibited (D).

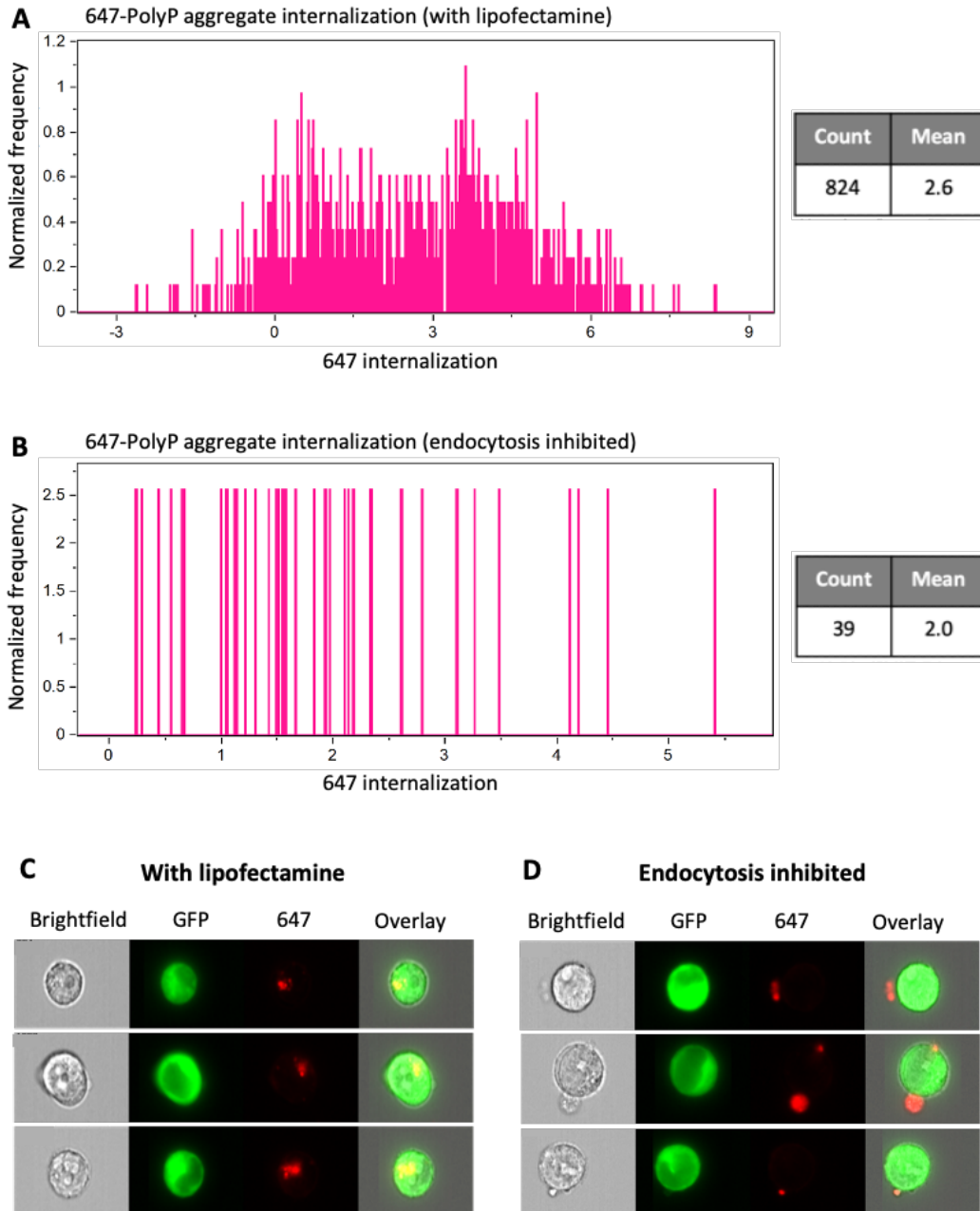


Figure 3.12. PolyP induced aggregates are internalized by cells

A HEK293 cells induced with 10 ng dox for 72 hours were seeded with Alexa fluor 647-labeled polyP induced tau aggregates packaged with lipofectamine. Internalization measured with imaging flow cytometry, 4 hours post seeding. Bar graph representing frequency of Alexa fluor 647 internalization events with respect to distance from cell perimeter is plotted. Total cells counted and mean of internalization shown in table.

B Control group in which cells pretreated on ice for 45 min to prevent endocytosis were seeded with lipofectamine packaged tau aggregates then analyzed as described in (A).

C-D Representative images of internalized Alexa fluor 647-aggregates in the presence of lipofectamine (C), or when endocytosis is inhibited (D).

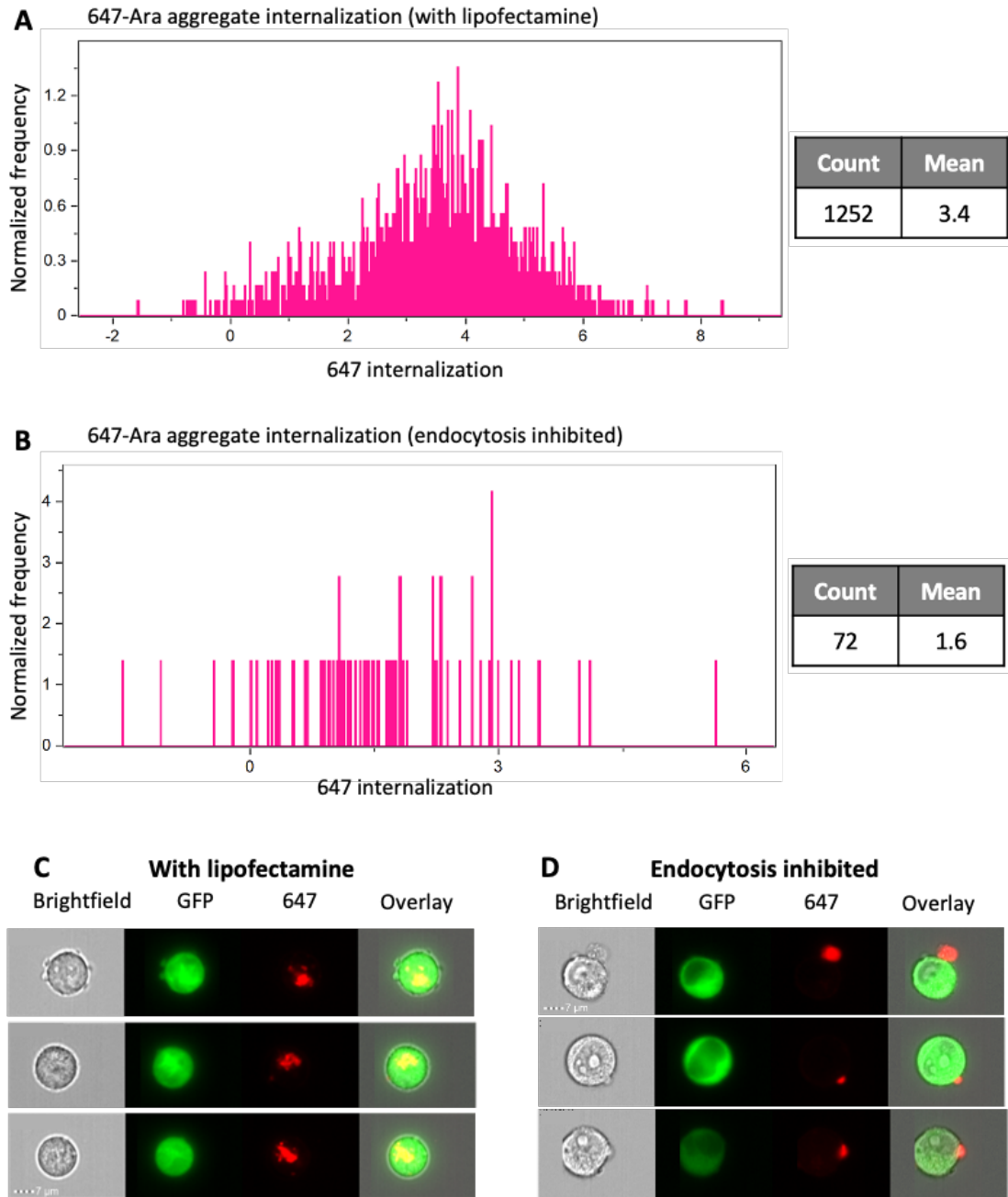


Figure 3.13. Ara induced aggregates are internalized by cells

A HEK293 cells induced with 10 ng dox for 72 hours were seeded with Alexa fluor 647-labeled Ara induced tau aggregates packaged with lipofectamine. Internalization measured with imaging flow cytometry, 4 hours post seeding. Bar graph representing frequency of Alexa fluor 647 internalization events with respect to distance from cell perimeter is plotted. Total cells counted and mean of internalization shown in table.

B Control group in which cells pretreated on ice for 45 min to prevent endocytosis were seeded with lipofectamine packaged tau aggregates then analyzed as described in (A).

C-D Representative images of internalized Alexa fluor 647-aggregates in the presence of lipofectamine (C), or when endocytosis is inhibited (D).

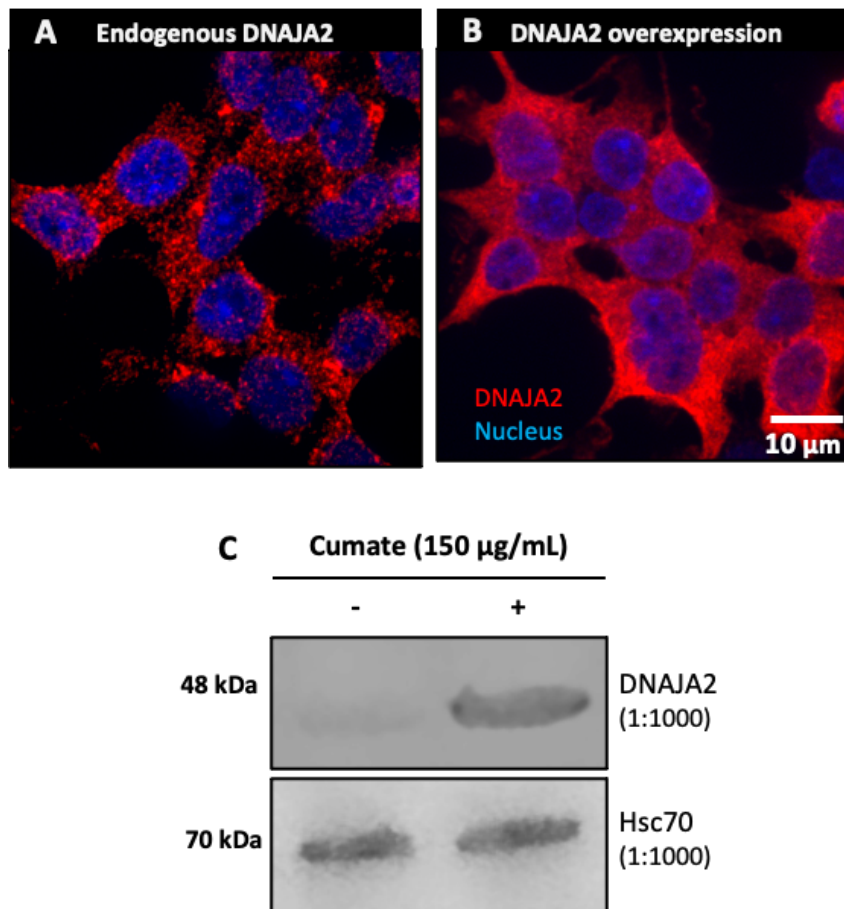


Figure 3.14 HEK293 cell transfection with cumate inducible expression vector

A-B HEK293 cells expressing only endogenous levels of DNAJA2 (A), and overexpressing DNAJA2 due to the presence of the cumate inducible expression vector and induction with cumate for 48 hours prior to imaging (B). Cells were induced with Hoechst stain 2 hours prior to fixation and imaging. Cell images were obtained using the WaveFx1 confocal microscope at 60X magnification.

C Western blot of HEK293 cells transfected with the cumate inducible expression vector both before and after a 24-hour induction with 150 μ g/mL cumate.

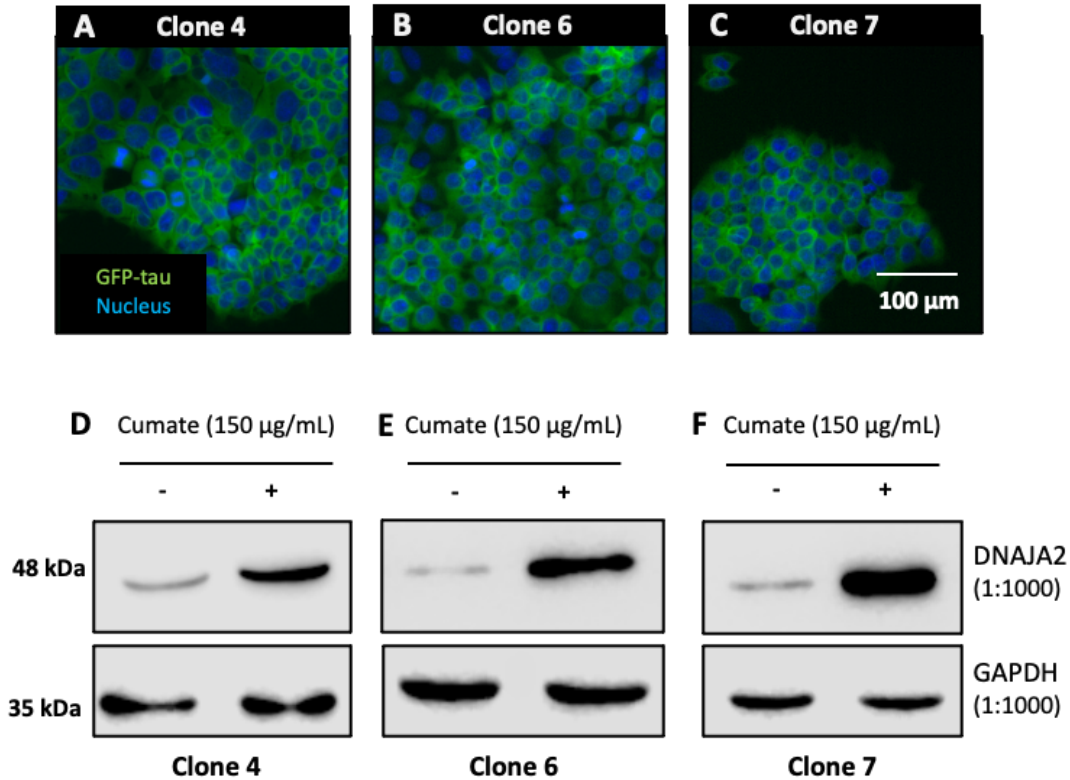


Figure 3.15 Single cell clones contain the cumate inducible expression vector, and express GFP-tau

A-B Single cell clones selected after puromycin treatment of HEK293 cells transfected with the cumate inducible expression vector were induced with 10 ng dox for 72 hours. 2 hours prior to imaging, 1 µg/mL Hoechst stain was applied to cells and images were acquired using a high content screening microscope (Molecular Devices) at 10X magnification. The three clones imaged were clones 4 (A), 6 (B), and 7 (C).

D-F Western blots showing clones 4 (D), 6 (E), and 7 (F) obtained through single cell selection, both before and after a 48-hour induction with 150 µg/mL cumate.

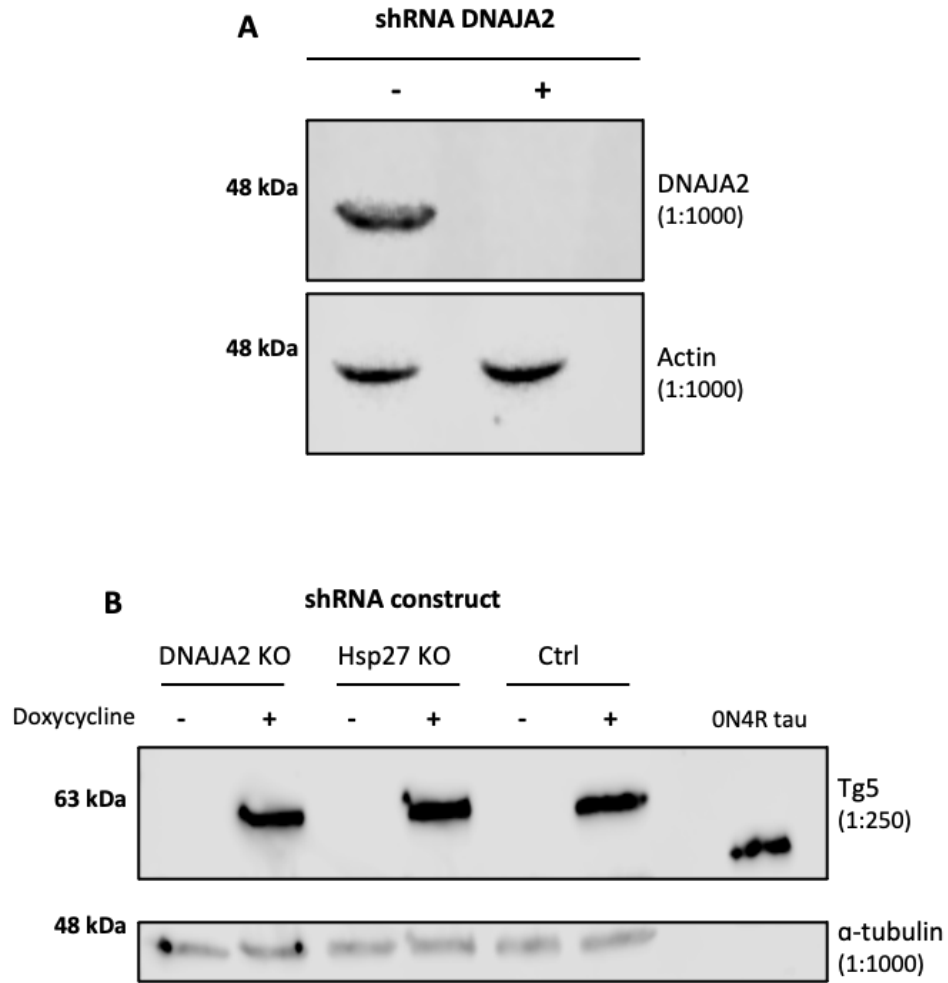


Figure 3.16 Characterization of the shRNA transfected HEK293 cell lines

A Western blot of HEK293 cell lysates both without and with the addition of the DNAJA2 shRNA vector,

B Western blot of HEK293 cells transfected with shRNA constructs (DNAJA2, hsp27, and control) that had been induced with 10 ng dox for 72 hours prior to lysis. 0N4R served as a positive control.

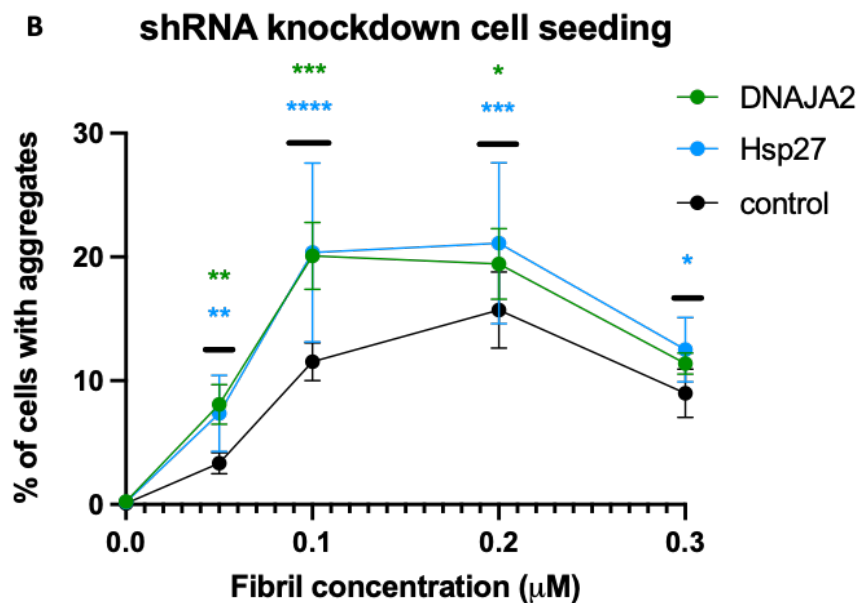
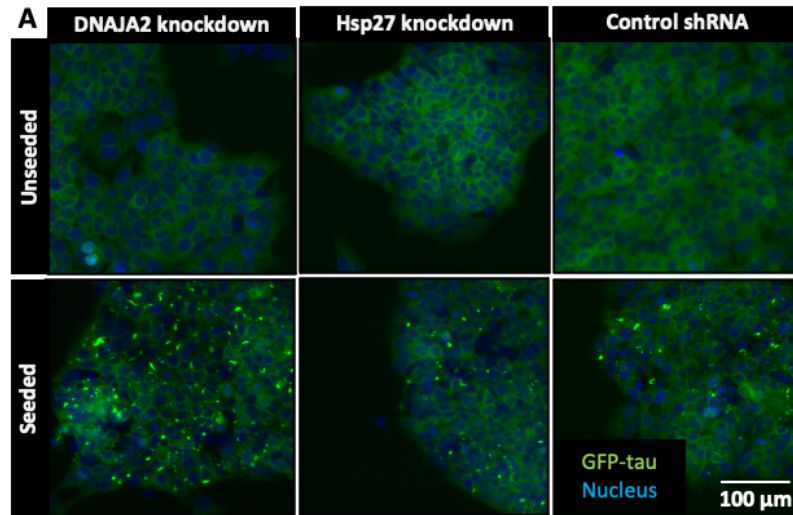


Figure 3.17 Seeding in HEK293 cells transfected with shRNA constructs

A HEK293 cells expressing different shRNA constructs were treated with dox to induce GFP-tau expression 72 hours prior to seeding with heparin induced aggregates, or lipofectamine only control. Cellular aggregates at 48 hours post-seeding were observed via live cell imaging. Cell nuclei were stained with Hoechst (1 μg/mL) 2 hour prior to imaging. Fluorescent microscope images were acquired using a high content screening microscope (Molecular Devices) at 10 X magnification.

B Quantification of total number of cells with aggregates at the indicated concentrations, for each shRNA construct cell line. mean ± SD plotted, n = 3 replicates per experiment, and experiments repeated in triplicate. Values determined using two-way ANOVA.

DNAJA2 significance values (green): * p-value = 0.03, ** p-value = 0.004, *** p-value < 0.0001
Hsp27 significance values (blue): * p-value = 0.04, ** p-value = 0.02, *** p-value = 0.001, *** p-value < 0.0001

CHAPTER FOUR: DISCUSSION

4.1. R-tau aggregates generated with various inducers have different seeding abilities in cells

Our lab makes use of R-tau aggregates generated *in vitro* to study the tau aggregation process and associated pathobiology. R-tau monomers are induced to form aggregates *in vitro* through the use of different inducers, and can then be applied to both cellular and *in vitro* assays. Consistent with previous findings, we have demonstrated that heparin, polyP, and Ara are all capable of promoting tau aggregation (**Figure 3.4**) (Cremers et al., 2016; Mok et al., 2018; Sibille et al., 2006; Voss et al., 2012).

Our HEK293 cell model utilizes a dox inducible system to express GFP-tagged 0N4R tau with a P301L mutation. The GFP-tau expressed by our cells mimics the physiological role of tau by binding to MTs (Hernández & Avila, 2007) (**Figure 3.3**), and does not spontaneously form aggregates. The goal with our R-tau aggregates was to use them as seeding material, to induce aggregate formation in our cellular assays (**Figure 2.2**). Upon addition of the differently induced aggregates to our cells (in the presence and absence of lipofectamine), it became apparent that only heparin induced aggregates generated a significant seeding effect, while polyP induced aggregates generated 8-fold less aggregation, and Ara induced aggregates had no observable seeding effect (**Figure 3.6**). Curiously, aggregates generated with heparin and polyP were capable of seeding monomeric tau *in vitro* in the presence of their respective inducers, which was observed by a reduction in lag time compared to DPBS controls (**Figure 3.7**). Heparin induced aggregates were able to reduce the lag time by 5-fold, while polyP aggregates reduced the lag time by 2.5-fold (**Figure 3.7 A-D**). The effect of Ara induced aggregates *in vitro* could not be determined due to the rapid tau aggregation generated by the Ara inducer, which showed aggregation happening at the first time point measured (5 minutes) and thus an effect could not be teased out (**Figure 3.7 E-**

F). The fast aggregation of Ara may be a limiting factor, which requires us to take even earlier time points in the future.

We next sought out to determine why differently induced aggregates were showing variable seeding abilities in cells. Misfolded tau is thought to replicate in a prion-like manner, by serving as a template for other monomers to undergo a misfolding process (Aguzzi et al., 2007; Brunello et al., 2020; Hosokawa et al., 2021; Lasagna-Reeves et al., 2012). By doing this, tau not only propagates its structural conformation, but also other unique traits such as seeding ability, transmissibility, and lag time (Aguzzi et al., 2007; Sanders et al., 2014). In this way, tau is suspected to have different ‘strains’, similar to the prion protein (Aguzzi et al., 2007; Vaquer-Alicea et al., 2021). There can also be certain barriers that accompany these strains. The best example would be the species barrier present in prion diseases. A classic example of this species barrier occurs between mice and hamster prions (Aguzzi et al., 2007). When samples obtained from PrPSc infected hamster brains were inoculated into mice, it did not elicit disease or further PrPSc buildup (Aguzzi et al., 2007). When these inoculated mice brains were re-introduced to hamsters however, the result was lethal (Aguzzi et al., 2007). Although our studies are not a case of species barriers modulating transmission, perhaps it can be likened to a “cellular barrier” in which the conformation of polyP or Ara induced aggregates are not compatible with GFP-tau templating in cells.

Given the importance of tau aggregate structure and seed origin on its ability to template in the literature (Clavaguera, Akatsu, et al., 2013; Sanders et al., 2014; Woerman et al., 2016), our next step was to analyze the structure of our differentially induced aggregates. Since the amyloid tau cores are protease-resistant (Aguzzi et al., 2007), fragmentation of the protein via trypsin digestion allowed us to look specifically at sizes and regions of the core by capillary gel electrophoresis.

Results revealed that 1) differently induced aggregates are amyloid in nature due to the existence of protease-resistant fragments following digestion, and 2) structural differences do exist between the differently induced aggregates (**Figure 3.9**). While both polyP and Ara induced aggregates have some structural overlap with heparin induced aggregates, Ara induced aggregates appear to be the most structurally different, which is consistent with them having the least ability to seed aggregation in cells. Furthermore, the ability of the differently induced aggregates to propagate their own structure relies on the presence of their respective inducer in the reaction (**Figure 3.10** and **Appendix**). PolyP induced aggregates are able to seed *in vitro* tau aggregation without the addition of an inducer, however the product of the reaction only generates an amyloid product in one-third of the replicates. These findings suggest that 10% of seeding material in relation to the tau monomer may not be enough to generate a significant seeding effect for heparin and Ara induced aggregates *in vitro*. PolyP induced aggregates however, have the potential to seed tau monomers *in vitro* when present as 10% of total tau in the reaction, though the newly aggregated tau does not maintain the original seed's structure. This perhaps points to issues with the polyP induced aggregates ability to serve as a good template for monomeric tau and to continue to generate the same amyloid product, which could translate to what we're seeing in our cell model. However, this does not explain why heparin induced aggregates can template in the absence of an inducer in our cell model while polyP induced aggregates cannot. This could be due to cellular factors that are able to assist in templating, similar to our heparin and polyP inducers, and the structure of heparin induced aggregates may be more compatible with this system.

Lastly, to rule out the possibility that polyP and Ara induced aggregates were simply not being taken up into the cells, we used fluorescently labeled tau aggregates to monitor their internalization. Using this technique, we determined that heparin, polyP, and Ara induced

aggregates are able to be similarly taken up into GFP-tau expressing cells when incubated with lipofectamine (**Figures 3.11-3.13**). Their uptake was measured using a calculated “mean value of internalization”, where a higher number is associated with a more central localization of the Alexa fluor 647-labeled tau puncta within the GFP-tau expressing cell. Heparin, polyP, and Ara induced aggregates had mean internalization values of 3.1, 2.6, and 3.4, while their endocytosis inhibited controls had values of 1.7, 2.0, and 1.6 respectively. Additionally, preliminary ThT fluorescent staining of the differently induced aggregates reveal no apparent size differences (**Appendix D**). Since their internalization into cells does not appear to be an issue, the current reasoning behind the varying cell seeding ability of differently induced aggregates points to aggregate structure. The specific conformation of polyP and Ara induced tau aggregate cores may not be compatible with GFP-tagged 0N4R P301L-tau templating in cells.

This finding reinforces the importance of structure in relation to templating and spread, and gives credence to the existence of tau strains. Additionally, it gives us insight into how common aggregation inducers may affect experimental outcome.

4.2 DNAJA2 knockdown leads to increased aggregation in cells

DNAJA2 exhibited inhibitory effects on tau aggregation *in vitro* (Mok et al., 2018). Additionally, fixed brain samples revealed that DNAJA2 levels were increased in 7 patients with MCI or AD compared to non-demented controls and levels of DNAJB4 (Mok et al., 2018). Specifically, protein levels were detected using a DNAJA2 specific antibody and their observable upregulation in neurons was correlated with tau pathology (determined by increased phospho-tau staining) (Mok et al., 2018).

This prompted us to study the effects of DNAJA2 on tau aggregation in a human cell model, which had not yet been undertaken. Specifically, we wanted to investigate the effects of DNAJA2 knockdown (using shRNA), as well as the overexpression of DNAJA2 (using a cumate inducible expression vector) on tau's ability to seed in HEK293 cells upon the addition of R-tau aggregates. The successful transfection of our HEK293 cell model with the cumate inducible DNAJA2 expression vector was confirmed via immunofluorescence and Western blot, both of which showed an increased expression of DNAJA2 upon transfection and induction with cumate (**Figure 3.14**). Single cell clones were selected from the heterogeneous transfected population, leaving us with 3 clones positive for both GFP-tau expression and DNAJA2 overexpression confirmed with fluorescent live cell imaging and Western blotting respectively (**Figure 3.15**). While two of the positive clones, clones 6 and 7, were relatively similar to one another, clone 4 was inconsistent in its overexpression of DNAJA2 so we decided to exclude it from future use in the DNAJA2 overexpression assays.

With successful clones established, the current task is to set up cell lines expressing cumate inducible control vectors. These control cell lines should show no differences in percent cells with aggregates when cumate is present or absent. This will confirm that both our construct components and the small molecule inducer, cumate, are having no effect on any observed seeding phenotype. We are in the process of generating multiple cell lines stably integrated with cumate inducible control constructs. The control proteins expressed include mCherry (a non-chaperone, well folded, fluorescent protein), and two DNAJA2 deletion mutants: missing the J-domain (ΔJ) or dimerization domain (ΔCT). Since DNAJA2 binds aggregated tau via CBD2 (Irwin et al., 2021), the ΔJ mutant should behave similar to WT DNAJA2 since both constructs contain this domain. The ΔCT mutant, however, should have no effect on tau seeding since it is lacking CBD2.

In contrast to DNAJA2 overexpression, we used shRNA constructs to knockdown the endogenous expression of DNAJA2 in our cells. In addition to the DNAJA2 shRNA construct, we also transfected our cells with an Hsp27 shRNA construct and a non-targeting control shRNA construct (see section 2.2.2). The Hsp27 construct was expected to behave as a positive control, since Hsp27 is known to modulate tau aggregation, and thus a knockdown of its expression should show a detrimental effect on tau seeding in our cells. The control shRNA sequence does not have a gene target, and thus it would be expected to act as a negative control with no effect on cell seeding activity. When heparin induced aggregates were used to seed the shRNA cell lines, it appeared that aggregation was made worse by knocking down DNAJA2 and Hsp27, which was shown by the higher percentage of cells with aggregates present compared to the control (**Figure 3.17**).

As previously mentioned, Hsp27 modulates tau aggregation and was previously shown to rescue neuronal dysfunction in transgenic mice expressing human P301L-tau (Abisambra et al., 2010). Thus, our Hsp27 knockdown cell line exhibiting a higher percentage of total cells with aggregates compared to the control group is expected, since its potentially protective anti-aggregation activity is being removed. In the case of DNAJA2 knockdown, previous research has shown that DNAJA2 is capable of inhibiting tau aggregation *in vitro* (Mok et al., 2018) and it has been shown to bind to both monomeric and aggregated tau (Irwin et al., 2021), making tau one of its potential targets. Our results support that DNAJA2 may have a beneficial effect on tau seeding in a human cell model, and that significantly decreasing its expression leads to a higher level of aggregate positive cells. Additionally, it was confirmed that GFP-tau expression levels upon induction with 10 ng/mL dox for 72 hours did not change between shRNA cell lines (**Figure 3.16 B**). This finding eliminates the possibility that altered tau expression is responsible for the increase in aggregate positive cells seen in the Hsp27 and DNAJA2 knockdown cells.

CHAPTER FIVE: CONCLUSIONS AND FUTURE DIRECTIONS

5.1 Conclusions

The original hypotheses of this thesis were as follows:

1. *I hypothesize that different inducers may generate aggregates with different structures, therefore making them more or less seeding potent in cellular assays.*
2. *I hypothesize that an overexpression of DNAJA2 will reduce or inhibit the number of aggregates formed in our cell model upon seeding.*

Though many areas remain to be explored, both hypotheses have been addressed.

Firstly, the generation of R-tau aggregates using different inducers did indeed alter their ability to seed GFP-tau aggregation in our HEK293 cell model (**Figure 3.6**). While this variability existed in a cellular setting, the differently induced aggregates showed promising seeding ability *in vitro* (**Figure 3.7**). After investigating this effect using trypsin digestion assays, it was revealed that structural differences existed between aggregates generated using different inducers (**Figure 3.9**). Additionally, fluorescently labeled aggregates revealed that our HEK293 cells were capable of internalizing all three types of differently induced aggregates (**Figure 3.11-3.13**). The mystery behind the varying cell seeding ability of the aggregates points towards a structural difference that renders cellular GFP-tau unable to template and propagate.

Secondly, while looking directly at the effects of DNAJA2 overexpression on tau seeding in cells remains to be done, we did have success in generating the molecular tools necessary to accomplish this in the future. Insight into DNAJA2's role in relation to tau aggregate seeding was able to be

analyzed using complementary knockdown experiments with shRNAs. The results of seeding in DNAJA2 knockdown cells demonstrated that decreased levels of DNAJA2 lead to an increase in cells positive for seeded tau aggregates (**Figure 3.17**). This suggests that DNAJA2 may have a beneficial effect on tau aggregation in human cells by directly acting to inhibit or reduce tau aggregate formation, which is consistent with results seen *in vitro* (Mok et al., 2018).

5.2 Future directions

Moving forward, testing tau mutants with a similar trypsin digestion pattern to our differently induced aggregates would be a critical step in reinforcing that the structure of our aggregates is what is causing the seeding variability observed in cells. Additionally, using heparin, polyP, or Ara to generate aggregates using WT tau, or other mutants, may give us insight into the role of the inducer in the formation of structure.

It should also be looked into whether or not the inducer itself plays a role in seeding variability. To accomplish this, one strategy would be to incubate preformed R-tau aggregates with different inducers than they were generated with. The application of these cross-inducer aggregates to cells should give us insight into whether or not the inducer itself is generating a seeding effect. Additionally, testing inducer only controls in conjunction with lipofectamine will give us insight into their direct effects on seeding.

In regards to DNAJA2, it is crucial to establish control cell lines that do not exhibit an effect on tau seeding phenotypes in cells in the presence or absence of the cumate inducer. Once these controls are established, we can use these same seeding conditions (cumate concentration, cumate incubation time) on clones 6 and 7 overexpressing DNAJA2 to observe the effect that DNAJA2 overexpression has on tau aggregation in cells.

Bibliography

- Abisambra, J. F., Blair, L. J., Hill, S. E., Jones, J. R., Kraft, C., Rogers, J., Koren, J., Jinwal, U. K., Lawson, L., Johnson, A. G., Wilcock, D., O'Leary, J. C., Jansen-West, K., Muschol, M., Golde, T. E., Weeber, E. J., Banko, J., & Dickey, C. A. (2010). Phosphorylation Dynamics Regulate Hsp27-Mediated Rescue of Neuronal Plasticity Deficits in Tau Transgenic Mice. *Journal of Neuroscience*, *30*(46), 15374–15382.
<https://doi.org/10.1523/JNEUROSCI.3155-10.2010>
- Abraha, A., Ghoshal, N., Gamblin, C. T., Cryns, V., Berry, R. W., Kuret, J., & Binder, L. I. (2000). C-terminal inhibition of tau assembly in vitro and in Alzheimer's disease. *Journal of Cell Science* *113*, 3737-3745.
- Achbergerová, L., & Nahálka, J. (2011). Polyphosphate—An ancient energy source and active metabolic regulator. *Microbial Cell Factories*, *10*(1), 63. <https://doi.org/10.1186/1475-2859-10-63>
- Agadjanyan, M. G., Zagorski, K., Petrushina, I., Davtyan, H., Kazarian, K., Antonenko, M., Davis, J., Bon, C., Blurton-Jones, M., Cribbs, D. H., & Ghochikyan, A. (2017). Humanized monoclonal antibody armanezumab specific to N-terminus of pathological tau: Characterization and therapeutic potency. *Molecular Neurodegeneration*, *12*(1), 33.
<https://doi.org/10.1186/s13024-017-0172-1>
- Aguzzi, A., Heikenwalder, M., & Polymenidou, M. (2007). Insights into prion strains and neurotoxicity. *Nature Reviews Molecular Cell Biology*, *8*(7), 552–561.
<https://doi.org/10.1038/nrm2204>
- Alquwaizani, M., Buckley, L., Adams, C., & Fanikos, J. (2013). Anticoagulants: A Review of the Pharmacology, Dosing, and Complications. *Current Emergency and Hospital Medicine Reports*, *1*(2), 83–97. <https://doi.org/10.1007/s40138-013-0014-6>
- Alzheimer Society of Canada. (2016). *Dementia numbers in Canada*. Alzheimer Society.

https://alzheimer.ca/en/about-dementia/what-dementia/dementia-numbers-canada?gclid=CjwKCAjwxZqSBhAHEiwASr9n9BkfyfXFy9SrB6LczQXRPuYeGx_-pTa9dlqi9JavnK0k0D8-0dtLQhoCMigQAvD_BwE

Arrasate, M., Pérez, M., Armas-Portela, R., & Ávila, J. (1999). Polymerization of tau peptides into fibrillar structures. The effect of FTDP-17 mutations. *FEBS Letters*, *446*(1), 199–202. [https://doi.org/10.1016/S0014-5793\(99\)00210-0](https://doi.org/10.1016/S0014-5793(99)00210-0)

Baaklini, I., Wong, M. J. H., Hantouche, C., Patel, Y., Shrier, A., & Young, J. C. (2012). The DNAJA2 Substrate Release Mechanism Is Essential for Chaperone-mediated Folding. *Journal of Biological Chemistry*, *287*(50), 41939–41954. <https://doi.org/10.1074/jbc.M112.413278>

Baas, P. W., & Qiang, L. (2019). Tau: It's Not What You Think. *Trends in Cell Biology*, *29*(6), 452–461. <https://doi.org/10.1016/j.tcb.2019.02.007>

Ben-Zvi, A., Miller, E. A., & Morimoto, R. I. (2009). Collapse of proteostasis represents an early molecular event in *Caenorhabditis elegans* aging. *Proceedings of the National Academy of Sciences*, *106*(35), 14914–14919. <https://doi.org/10.1073/pnas.0902882106>

Berriman, J., Serpell, L. C., Oberg, K. A., Fink, A. L., Goedert, M., & Crowther, R. A. (2003). Tau filaments from human brain and from *in vitro* assembly of recombinant protein show cross- β structure. *Proceedings of the National Academy of Sciences*, *100*(15), 9034–9038. <https://doi.org/10.1073/pnas.1530287100>

Braak, H., & Braak, E. (1991). Neuropathological staging of Alzheimer-related changes. *Acta Neuropathologica*, *82*(4), 239–259. <https://doi.org/10.1007/BF00308809>

Brehme, M., Voisine, C., Rolland, T., Wachi, S., Soper, J. H., Zhu, Y., Orton, K., Villella, A., Garza, D., Vidal, M., Ge, H., & Morimoto, R. I. (2014). A Chaperome Subnetwork Safeguards Proteostasis in Aging and Neurodegenerative Disease. *Cell Reports*, *9*(3), 1135–1150. <https://doi.org/10.1016/j.celrep.2014.09.042>

Brunello, C. A., Merezhko, M., Uronen, R.-L., & Huttunen, H. J. (2020). Mechanisms of

- secretion and spreading of pathological tau protein. *Cellular and Molecular Life Sciences*, 77(9), 1721–1744. <https://doi.org/10.1007/s00018-019-03349-1>
- Calafate, S., Buist, A., Miskiewicz, K., Vijayan, V., Daneels, G., de Strooper, B., de Wit, J., Verstreken, P., & Moechars, D. (2015). Synaptic Contacts Enhance Cell-to-Cell Tau Pathology Propagation. *Cell Reports*, 11(8), 1176–1183. <https://doi.org/10.1016/j.celrep.2015.04.043>
- Cantero, J. L., Hita-Yañez, E., Moreno-Lopez, B., Portillo, F., Rubio, A., & Avila, J. (2010). Tau Protein Role in Sleep-Wake Cycle. *Journal of Alzheimer's Disease*, 21(2), 411–421. <https://doi.org/10.3233/JAD-2010-100285>
- Carlson, S. W., Branden, M., Voss, K., Sun, Q., Rankin, C. A., & Gamblin, T. C. (2007). A Complex Mechanism for Inducer Mediated Tau Polymerization. *Biochemistry*, 46(30), 8838–8849. <https://doi.org/10.1021/bi700403a>
- Chen, J. J., Nathaniel, D. L., Raghavan, P., Nelson, M., Tian, R., Tse, E., Hong, J. Y., See, S. K., Mok, S.-A., Hein, M. Y., Southworth, D. R., Grinberg, L. T., Gestwicki, J. E., Leonetti, M. D., & Kampmann, M. (2019). Compromised function of the ESCRT pathway promotes endolysosomal escape of tau seeds and propagation of tau aggregation. *Journal of Biological Chemistry*, 294(50), 18952–18966. <https://doi.org/10.1074/jbc.RA119.009432>
- Chen, X., Li, Y., Wang, C., Tang, Y., Mok, S.-A., Tsai, R. M., Rojas, J. C., Karydas, A., Miller, B. L., Boxer, A. L., Gestwicki, J. E., Arkin, M., Cuervo, A. M., & Gan, L. (2020). Promoting tau secretion and propagation by hyperactive p300/CBP via autophagy-lysosomal pathway in tauopathy. *Molecular Neurodegeneration*, 15(1), 2. <https://doi.org/10.1186/s13024-019-0354-0>
- Chirita, C. N., Necula, M., & Kuret, J. (2003). Anionic Micelles and Vesicles Induce Tau Fibrillization in Vitro. *Journal of Biological Chemistry*, 278(28), 25644–25650. <https://doi.org/10.1074/jbc.M301663200>

- Cisse, S., Perry, G., Lacoste-Royal, G., Cabana, T., & Gauvreau, D. (1993). Immunochemical identification of ubiquitin and heat-shock proteins in corpora amylacea from normal aged and Alzheimer's disease brains. *Acta Neuropathologica*, *85*(3).
<https://doi.org/10.1007/BF00227716>
- Clavaguera, F., Akatsu, H., Fraser, G., Crowther, R. A., Frank, S., Hench, J., Probst, A., Winkler, D. T., Reichwald, J., Staufenbiel, M., Ghetti, B., Goedert, M., & Tolnay, M. (2013). Brain homogenates from human tauopathies induce tau inclusions in mouse brain. *Proceedings of the National Academy of Sciences*, *110*(23), 9535–9540.
<https://doi.org/10.1073/pnas.1301175110>
- Clavaguera, F., Bolmont, T., Crowther, R. A., Abramowski, D., Frank, S., Probst, A., Fraser, G., Stalder, A. K., Beibel, M., Staufenbiel, M., Jucker, M., Goedert, M., & Tolnay, M. (2009). Transmission and spreading of tauopathy in transgenic mouse brain. *Nature Cell Biology*, *11*(7), 909–913. <https://doi.org/10.1038/ncb1901>
- Clavaguera, F., Hench, J., Goedert, M., & Tolnay, M. (2015). Invited review: Prion-like transmission and spreading of tau pathology: Prion-like transmission and spreading of tau pathology. *Neuropathology and Applied Neurobiology*, *41*(1), 47–58.
<https://doi.org/10.1111/nan.12197>
- Clavaguera, F., Lavenir, I., Falcon, B., Frank, S., Goedert, M., & Tolnay, M. (2013). “Prion-Like” Templated Misfolding in Tauopathies: Tau and Templated Misfolding. *Brain Pathology*, *23*(3), 342–349. <https://doi.org/10.1111/bpa.12044>
- Cohen, E., Bieschke, J., Perciavalle, R. M., Kelly, J. W., & Dillin, A. (2006). Opposing Activities Protect Against Age-Onset Proteotoxicity. *Science*, *313*(5793), 1604–1610.
<https://doi.org/10.1126/science.1124646>
- Cohen, F. E., & Prusiner, S. B. (1998). PATHOLOGIC CONFORMATIONS OF PRION PROTEINS. *Annual Review of Biochemistry*, *67*(1), 793–819.
<https://doi.org/10.1146/annurev.biochem.67.1.793>

- Combs, B., & Gamblin, T. C. (2012). FTDP-17 Tau Mutations Induce Distinct Effects on Aggregation and Microtubule Interactions. *Biochemistry*, 51(43), 8597–8607.
<https://doi.org/10.1021/bi3010818>
- Cowan, C. M., & Mudher, A. (2013). Are Tau Aggregates Toxic or Protective in Tauopathies? *Frontiers in Neurology*, 4. <https://doi.org/10.3389/fneur.2013.00114>
- Craig, E. A., & Marszalek, J. (2017). How Do J-Proteins Get Hsp70 to Do So Many Different Things? *Trends in Biochemical Sciences*, 42(5), 355–368.
<https://doi.org/10.1016/j.tibs.2017.02.007>
- Cremers, C. M., Knoefler, D., Gates, S., Martin, N., Dahl, J.-U., Lempart, J., Xie, L., Chapman, M. R., Galvan, V., Southworth, D. R., & Jakob, U. (2016). Polyphosphate: A Conserved Modifier of Amyloidogenic Processes. *Molecular Cell*, 63(5), 768–780.
<https://doi.org/10.1016/j.molcel.2016.07.016>
- Crowe, A., Ballatore, C., Hyde, E., Trojanowski, J. Q., & Lee, V. M.-Y. (2007). High throughput screening for small molecule inhibitors of heparin-induced tau fibril formation. *Biochemical and Biophysical Research Communications*, 358(1), 1–6.
<https://doi.org/10.1016/j.bbrc.2007.03.056>
- Crowther, R. A., & Goedert, M. (2000). Abnormal Tau-Containing Filaments in Neurodegenerative Diseases. *Journal of Structural Biology*, 130(2–3), 271–279.
<https://doi.org/10.1006/jsbi.2000.4270>
- Cyr, D. M. (1995). *Cooperation of the molecular chaperone Ydj1 with specific Hsp70 homologs to suppress protein aggregation*. 4.
- Drepper, F., Biernat, J., Kaniyappan, S., Meyer, H. E., Mandelkow, E. M., Warscheid, B., & Mandelkow, E. (2020). *Combinatorial native MS and LC-MS/MS approach reveals high intrinsic phosphorylation of human Tau but minimal levels of other key modifications* [Preprint]. Neuroscience. <https://doi.org/10.1101/2020.09.03.281907>
- Dujardin, S., Bégard, S., Caillierez, R., Lachaud, C., Delattre, L., Carrier, S., Loyens, A., Galas,

- M.-C., Bousset, L., Melki, R., Aurégan, G., Hantraye, P., Brouillet, E., Buée, L., & Colin, M. (2014). Ectosomes: A New Mechanism for Non-Exosomal Secretion of Tau Protein. *PLoS ONE*, 9(6), e100760. <https://doi.org/10.1371/journal.pone.0100760>
- Eckermann, K., Mocanu, M.-M., Khlistunova, I., Biernat, J., Nissen, A., Hofmann, A., Schönig, K., Bujard, H., Haemisch, A., Mandelkow, E., Zhou, L., Rune, G., & Mandelkow, E.-M. (2007). The β -Propensity of Tau Determines Aggregation and Synaptic Loss in Inducible Mouse Models of Tauopathy. *Journal of Biological Chemistry*, 282(43), 31755–31765. <https://doi.org/10.1074/jbc.M705282200>
- Falcon, B., Cavallini, A., Angers, R., Glover, S., Murray, T. K., Barnham, L., Jackson, S., O'Neill, M. J., Isaacs, A. M., Hutton, M. L., Szekeres, P. G., Goedert, M., & Bose, S. (2015). Conformation Determines the Seeding Potencies of Native and Recombinant Tau Aggregates. *Journal of Biological Chemistry*, 290(2), 1049–1065. <https://doi.org/10.1074/jbc.M114.589309>
- Falcon, B., Zhang, W., Murzin, A. G., Murshudov, G., Garringer, H. J., Vidal, R., Crowther, R. A., Ghetti, B., Scheres, S. H. W., & Goedert, M. (2018). Structures of filaments from Pick's disease reveal a novel tau protein fold. *Nature*, 561(7721), 137–140. <https://doi.org/10.1038/s41586-018-0454-y>
- Falcon, B., Zivanov, J., Zhang, W., Murzin, A. G., Garringer, H. J., Vidal, R., Crowther, R. A., Newell, K. L., Ghetti, B., Goedert, M., & Scheres, S. H. W. (2019). Novel tau filament fold in chronic traumatic encephalopathy encloses hydrophobic molecules. *Nature*, 568(7752), 420–423. <https://doi.org/10.1038/s41586-019-1026-5>
- Fitzpatrick, A. W. P., Falcon, B., He, S., Murzin, A. G., Murshudov, G., Garringer, H. J., Crowther, R. A., Ghetti, B., Goedert, M., & Scheres, S. H. W. (2017). Cryo-EM structures of tau filaments from Alzheimer's disease. *Nature*, 547(7662), 185–190. <https://doi.org/10.1038/nature23002>
- Fitzpatrick, A. W., & Saibil, H. R. (2019). Cryo-EM of amyloid fibrils and cellular aggregates.

Current Opinion in Structural Biology, 58, 34–42.

<https://doi.org/10.1016/j.sbi.2019.05.003>

Friedhoff, P., Schneider, A., Mandelkow, E.-M., & Mandelkow, E. (1998). Rapid Assembly of Alzheimer-like Paired Helical Filaments from Microtubule-Associated Protein Tau Monitored by Fluorescence in Solution. *Biochemistry*, 37(28), 10223–10230.

<https://doi.org/10.1021/bi980537d>

Friedhoff, P., von Bergen, M., Mandelkow, E.-M., Davies, P., & Mandelkow, E. (1998). A nucleated assembly mechanism of Alzheimer paired helical filaments. *Proceedings of the National Academy of Sciences*, 95(26), 15712–15717.

<https://doi.org/10.1073/pnas.95.26.15712>

Frost, B., Jacks, R. L., & Diamond, M. I. (2009). Propagation of Tau Misfolding from the Outside to the Inside of a Cell. *Journal of Biological Chemistry*, 284(19), 12845–12852.

<https://doi.org/10.1074/jbc.M808759200>

Frost, B., Ollesch, J., Wille, H., & Diamond, M. I. (2009). Conformational Diversity of Wild-type Tau Fibrils Specified by Templated Conformation Change. *Journal of Biological Chemistry*, 284(6), 3546–3551. <https://doi.org/10.1074/jbc.M805627200>

Fuster, V. (2017). Changing Demographics. *Journal of the American College of Cardiology*, 69(24), 3002–3005. <https://doi.org/10.1016/j.jacc.2017.05.013>

Fuster-Matanzo, A., Hernández, F., & Ávila, J. (2018). Tau Spreading Mechanisms; Implications for Dysfunctional Tauopathies. *International Journal of Molecular Sciences*, 19(3), 645.

<https://doi.org/10.3390/ijms19030645>

Gerson, J. E., & Kaye, R. (2013). Formation and Propagation of Tau Oligomeric Seeds.

Frontiers in Neurology, 4. <https://doi.org/10.3389/fneur.2013.00093>

Ghag, G., Bhatt, N., Cantu, D. V., Guerrero-Munoz, M. J., Ellsworth, A., Sengupta, U., & Kaye, R. (2018). Soluble tau aggregates, not large fibrils, are the toxic species that display seeding and cross-seeding behavior: Generation of tau aggregates via sonication.

- Protein Science*, 27(11), 1901–1909. <https://doi.org/10.1002/pro.3499>
- Glabe, C. (2001). Intracellular Mechanisms of Amyloid Accumulation and Pathogenesis in Alzheimer's Disease. *Journal of Molecular Neuroscience*, 17(2), 137–145.
<https://doi.org/10.1385/JMN:17:2:137>
- Goedert, M., Jakes, R., & Crowther, R. A. (1999). Effects of frontotemporal dementia FTDP-17 mutations on heparin-induced assembly of tau filaments. *FEBS Letters*, 450(3), 306–311. [https://doi.org/10.1016/S0014-5793\(99\)00508-6](https://doi.org/10.1016/S0014-5793(99)00508-6)
- Götz, J., Halliday, G., & Nisbet, R. M. (2019). Molecular Pathogenesis of the Tauopathies. *Annual Review of Pathology: Mechanisms of Disease*, 14(1), 239–261.
<https://doi.org/10.1146/annurev-pathmechdis-012418-012936>
- Gunawardana, C. G., Mehrabian, M., Wang, X., Mueller, I., Lubambo, I. B., Jonkman, J. E. N., Wang, H., & Schmitt-Ulms, G. (2015). *The Human Tau Interactome: Binding to the Ribonucleoproteome, and Impaired Binding of the Proline-to-Leucine Mutant at Position 301 (P301L) to Chaperones and the Proteasome**□S. 15.
- Guo, J. L., Buist, A., Soares, A., Callaerts, K., Calafate, S., Stevenaert, F., Daniels, J. P., Zoll, B. E., Crowe, A., Brunden, K. R., Moechars, D., & Lee, V. M. Y. (2016). The Dynamics and Turnover of Tau Aggregates in Cultured Cells. *Journal of Biological Chemistry*, 291(25), 13175–13193. <https://doi.org/10.1074/jbc.M115.712083>
- Guo, J. L., & Lee, V. M. Y. (2013). Neurofibrillary tangle-like tau pathology induced by synthetic tau fibrils in primary neurons over-expressing mutant tau. *FEBS Letters*, 587(6), 717–723. <https://doi.org/10.1016/j.febslet.2013.01.051>
- Guo, J. L., & Lee, V. M.-Y. (2011). Seeding of Normal Tau by Pathological Tau Conformers Drives Pathogenesis of Alzheimer-like Tangles. *Journal of Biological Chemistry*, 286(17), 15317–15331. <https://doi.org/10.1074/jbc.M110.209296>
- Hageman, J., Rujano, M. A., van Waarde, M. A. W. H., Kakkar, V., Dirks, R. P., Govorukhina, N., Oosterveld-Hut, H. M. J., Lubsen, N. H., & Kampinga, H. H. (2010). A DNAJB

- Chaperone Subfamily with HDAC-Dependent Activities Suppresses Toxic Protein Aggregation. *Molecular Cell*, 37(3), 355–369.
<https://doi.org/10.1016/j.molcel.2010.01.001>
- Harris, C. R., Millman, K. J., van der Walt, S. J., Gommers, R., Virtanen, P., Cournapeau, D., Wieser, E., Taylor, J., Berg, S., Smith, N. J., Kern, R., Picus, M., Hoyer, S., van Kerkwijk, M. H., Brett, M., Haldane, A., del Río, J. F., Wiebe, M., Peterson, P., ... Oliphant, T. E. (2020). Array programming with NumPy. *Nature*, 585(7825), 357–362.
<https://doi.org/10.1038/s41586-020-2649-2>
- Hartl, F. U., Bracher, A., & Hayer-Hartl, M. (2011). Molecular chaperones in protein folding and proteostasis. *Nature*, 475(7356), 324–332. <https://doi.org/10.1038/nature10317>
- Hernández, F., & Avila, J. (2007). Tauopathies. *Cellular and Molecular Life Sciences*, 64(17), 2219–2233. <https://doi.org/10.1007/s00018-007-7220-x>
- Hipp, M. S., Kasturi, P., & Hartl, F. U. (2019). The proteostasis network and its decline in ageing. *Nature Reviews Molecular Cell Biology*, 20(7), 421–435.
<https://doi.org/10.1038/s41580-019-0101-y>
- Hipp, M. S., Park, S.-H., & Hartl, F. U. (2014). Proteostasis impairment in protein-misfolding and -aggregation diseases. *Trends in Cell Biology*, 24(9), 506–514.
<https://doi.org/10.1016/j.tcb.2014.05.003>
- Hosokawa, M., Masuda-Suzukake, M., Shitara, H., Shimozawa, A., Suzuki, G., Kondo, H., Nonaka, T., Campbell, W., Arai, T., & Hasegawa, M. (2021). Development of a novel tau propagation mouse model endogenously expressing 3 and 4 repeat tau isoforms. *Brain*, awab289. <https://doi.org/10.1093/brain/awab289>
- Hsu, A.-L., Murphy, C. T., & Kenyon, C. (2003). Regulation of Aging and Age-Related Disease by DAF-16 and Heat-Shock Factor. *Science*, 300(5622), 1142–1145.
<https://doi.org/10.1126/science.1083701>
- Iba, M., Guo, J. L., McBride, J. D., Zhang, B., Trojanowski, J. Q., & Lee, V. M.-Y. (2013).

- Synthetic Tau Fibrils Mediate Transmission of Neurofibrillary Tangles in a Transgenic Mouse Model of Alzheimer's-Like Tauopathy. *Journal of Neuroscience*, 33(3), 1024–1037. <https://doi.org/10.1523/JNEUROSCI.2642-12.2013>
- Irwin, R., Faust, O., Petrovic, I., Wolf, S. G., Hofmann, H., & Rosenzweig, R. (2021). Hsp40s play complementary roles in the prevention of tau amyloid formation. *ELife*, 10, e69601. <https://doi.org/10.7554/eLife.69601>
- Jackson, S. J., Kerridge, C., Cooper, J., Cavallini, A., Falcon, B., Cella, C. V., Landi, A., Szekeres, P. G., Murray, T. K., Ahmed, Z., Goedert, M., Hutton, M., O'Neill, M. J., & Bose, S. (2016). Short Fibrils Constitute the Major Species of Seed-Competent Tau in the Brains of Mice Transgenic for Human P301S Tau. *The Journal of Neuroscience*, 36(3), 762–772. <https://doi.org/10.1523/JNEUROSCI.3542-15.2016>
- Jahn, T. R., & Radford, S. E. (2005). The Yin and Yang of protein folding: The Yin and Yang of protein folding. *FEBS Journal*, 272(23), 5962–5970. <https://doi.org/10.1111/j.1742-4658.2005.05021.x>
- Jeganathan, S., von Bergen, M., Brutlach, H., Steinhoff, H.-J., & Mandelkow, E. (2006). Global Hairpin Folding of Tau in Solution. *Biochemistry*, 45(7), 2283–2293. <https://doi.org/10.1021/bi0521543>
- Jiang, Y., Rossi, P., & Kalodimos, C. G. (2019). *Structural basis for client recognition and activity of Hsp40 chaperones*. 7.
- Jiménez, J., Bru, S., Ribeiro, M. P. C., & Clotet, J. (2017). Polyphosphate: Popping up from oblivion. *Current Genetics*, 63(1), 15–18. <https://doi.org/10.1007/s00294-016-0611-5>
- Kadavath, H., Hofele, R. V., Biernat, J., Kumar, S., Tepper, K., Urlaub, H., Mandelkow, E., & Zweckstetter, M. (2015). Tau stabilizes microtubules by binding at the interface between tubulin heterodimers. *Proceedings of the National Academy of Sciences*, 112(24), 7501–7506. <https://doi.org/10.1073/pnas.1504081112>
- Kampers, T., Friedhoff, P., Biernat, J., Mandelkow, E.-M., & Mandelkow, E. (1996). RNA

- stimulates aggregation of microtubule-associated protein tau into Alzheimer-like paired helical filaments. *FEBS Letters*, 399(3), 344–349. [https://doi.org/10.1016/S0014-5793\(96\)01386-5](https://doi.org/10.1016/S0014-5793(96)01386-5)
- Kampinga, H. H., & Craig, E. A. (2010). The HSP70 chaperone machinery: J proteins as drivers of functional specificity. *Nature Reviews Molecular Cell Biology*, 11(8), 579–592. <https://doi.org/10.1038/nrm2941>
- Kampmann, M., Bassik, M. C., & Weissman, J. S. (2013). Integrated platform for genome-wide screening and construction of high-density genetic interaction maps in mammalian cells. *Proceedings of the National Academy of Sciences*, 110(25). <https://doi.org/10.1073/pnas.1307002110>
- Kampmann, M., Bassik, M. C., & Weissman, J. S. (2014). Functional genomics platform for pooled screening and generation of mammalian genetic interaction maps. *Nature Protocols*, 9(8), 1825–1847. <https://doi.org/10.1038/nprot.2014.103>
- Kang, S.-G., Han, Z. Z., Daude, N., McNamara, E., Wohlgemuth, S., Molina-Porcel, L., Safar, J. G., Mok, S.-A., & Westaway, D. (2021). Pathologic tau conformer ensembles induce dynamic, liquid-liquid phase separation events at the nuclear envelope. *BMC Biology*, 19(1), 199. <https://doi.org/10.1186/s12915-021-01132-y>
- Kar, A., Kuo, D., He, R., Zhou, J., & Wu, J. Y. (2007). *Tau Alternative Splicing and Frontotemporal Dementia*. 15.
- Kim Chiaw, P., Hantouche, C., Wong, M. J. H., Matthes, E., Robert, R., Hanrahan, J. W., Shrier, A., & Young, J. C. (2019). Hsp70 and DNAJA2 limit CFTR levels through degradation. *PLOS ONE*, 14(8), e0220984. <https://doi.org/10.1371/journal.pone.0220984>
- Kim, Y. E., Hipp, M. S., Bracher, A., Hayer-Hartl, M., & Ulrich Hartl, F. (2013). Molecular Chaperone Functions in Protein Folding and Proteostasis. *Annual Review of Biochemistry*, 82(1), 323–355. <https://doi.org/10.1146/annurev-biochem-060208-092442>
- Kovacs, G. G. (2018). Tauopathies. In *Handbook of Clinical Neurology* (Vol. 145, pp. 355–368).

Elsevier. <https://doi.org/10.1016/B978-0-12-802395-2.00025-0>

- Lasagna-Reeves, C. A., Castillo-Carranza, D. L., Sengupta, U., Guerrero-Munoz, M. J., Kiritoshi, T., Neugebauer, V., Jackson, G. R., & Kaye, R. (2012). Alzheimer brain-derived tau oligomers propagate pathology from endogenous tau. *Scientific Reports*, 2(1), 700. <https://doi.org/10.1038/srep00700>
- Le Corre, S., Klafki, H. W., Plesnila, N., Hübinger, G., Obermeier, A., Sahagún, H., Monse, B., Seneci, P., Lewis, J., Eriksen, J., Zehr, C., Yue, M., McGowan, E., Dickson, D. W., Hutton, M., & Roder, H. M. (2006). An inhibitor of tau hyperphosphorylation prevents severe motor impairments in tau transgenic mice. *Proceedings of the National Academy of Sciences*, 103(25), 9673–9678. <https://doi.org/10.1073/pnas.0602913103>
- Lee, H., Perry, G., Moreira, P. I., Garrett, M. R., Liu, Q., Zhu, X., Takeda, A., Nunomura, A., & Smith, M. A. (2005). Tau phosphorylation in Alzheimer's disease: Pathogen or protector? *Trends in Molecular Medicine*, 11(4), 164–169. <https://doi.org/10.1016/j.molmed.2005.02.008>
- Lim, S., Haque, Md. M., Kim, D., Kim, D. J., & Kim, Y. K. (2014). Cell-based Models To Investigate Tau Aggregation. *Computational and Structural Biotechnology Journal*, 12(20–21), 7–13. <https://doi.org/10.1016/j.csbj.2014.09.011>
- Linke, K., Wolfram, T., Bussemer, J., & Jakob, U. (2003). The Roles of the Two Zinc Binding Sites in DnaJ. *Journal of Biological Chemistry*, 278(45), 44457–44466. <https://doi.org/10.1074/jbc.M307491200>
- Liu, E. Y., Cali, C. P., & Lee, E. B. (2017). RNA metabolism in neurodegenerative disease. *Disease Models & Mechanisms*, 10(5), 509–518. <https://doi.org/10.1242/dmm.028613>
- Lövestam, S., Koh, F. A., van Knippenberg, B., Kotecha, A., Murzin, A. G., Goedert, M., & Scheres, S. H. (2022). Assembly of recombinant tau into filaments identical to those of Alzheimer's disease and chronic traumatic encephalopathy. *eLife*, 11, e76494. <https://doi.org/10.7554/eLife.76494>

- Lovestone, S. (2002). Protein aggregates and dementia: Is there a common toxicity? *Journal of Neurology, Neurosurgery & Psychiatry*, 72(2), 152–161.
<https://doi.org/10.1136/jnnp.72.2.152>
- Mandelkow, E.-M., Schweers, O., Drewes, G., Biernat, J., Gustke, N., Trinczek, B., & Mandelkow, E. (1996). Structure, Microtubule Interactions, and Phosphorylation of Tau Proteins. *Annals of the New York Academy of Sciences*, 777(1), 96–106.
<https://doi.org/10.1111/j.1749-6632.1996.tb34407.x>
- Margulis, B., Tsimokha, A., Zubova, S., & Guzhova, I. (2020). Molecular Chaperones and Proteolytic Machineries Regulate Protein Homeostasis in Aging Cells. *Cells*, 9(5), 1308.
<https://doi.org/10.3390/cells9051308>
- Meacham, G. C. (1999). The Hdj-2/Hsc70 chaperone pair facilitates early steps in CFTR biogenesis. *The EMBO Journal*, 18(6), 1492–1505.
<https://doi.org/10.1093/emboj/18.6.1492>
- Melková, K., Zapletal, V., Narasimhan, S., Jansen, S., Hritz, J., Škrabana, R., Zweckstetter, M., Ringkjøbing Jensen, M., Blackledge, M., & Žídek, L. (2019). Structure and Functions of Microtubule Associated Proteins Tau and MAP2c: Similarities and Differences. *Biomolecules*, 9(3), 105. <https://doi.org/10.3390/biom9030105>
- Meraz-Ríos, M. A., Lira-De León, K. I., Campos-Peña, V., De Anda-Hernández, M. A., & Mena-López, R. (2010). Tau oligomers and aggregation in Alzheimer's disease. *Journal of Neurochemistry*, 112(6), 1353–1367. <https://doi.org/10.1111/j.1471-4159.2009.06511.x>
- Min, S.-W., Chen, X., Tracy, T. E., Li, Y., Zhou, Y., Wang, C., Shirakawa, K., Minami, S. S., Defensor, E., Mok, S. A., Sohn, P. D., Schilling, B., Cong, X., Ellerby, L., Gibson, B. W., Johnson, J., Krogan, N., Shamloo, M., Gestwicki, J., ... Gan, L. (2015). Critical role of acetylation in tau-mediated neurodegeneration and cognitive deficits. *Nature Medicine*, 21(10), 1154–1162. <https://doi.org/10.1038/nm.3951>
- Min, S.-W., Sohn, P. D., Li, Y., Devidze, N., Johnson, J. R., Krogan, N. J., Masliah, E., Mok, S.-

- A., Gestwicki, J. E., & Gan, L. (2018). SIRT1 Deacetylates Tau and Reduces Pathogenic Tau Spread in a Mouse Model of Tauopathy. *The Journal of Neuroscience*, 38(15), 3680–3688. <https://doi.org/10.1523/JNEUROSCI.2369-17.2018>
- Mirbaha, H., Chen, D., Morazova, O. A., Ruff, K. M., Sharma, A. M., Liu, X., Goodarzi, M., Pappu, R. V., Colby, D. W., Mirzaei, H., Joachimiak, L. A., & Diamond, M. I. (2018). Inert and seed-competent tau monomers suggest structural origins of aggregation. *ELife*, 7, e36584. <https://doi.org/10.7554/eLife.36584>
- Mocanu, M.-M., Nissen, A., Eckermann, K., Khlistunova, I., Biernat, J., Drexler, D., Petrova, O., Schonig, K., Bujard, H., Mandelkow, E., Zhou, L., Rune, G., & Mandelkow, E.-M. (2008). The Potential for β -Structure in the Repeat Domain of Tau Protein Determines Aggregation, Synaptic Decay, Neuronal Loss, and Coassembly with Endogenous Tau in Inducible Mouse Models of Tauopathy. *Journal of Neuroscience*, 28(3), 737–748. <https://doi.org/10.1523/JNEUROSCI.2824-07.2008>
- Mok, S.-A., Condello, C., Freilich, R., Gillies, A., Arhar, T., Oroz, J., Kadavath, H., Julien, O., Assimon, V. A., Rauch, J. N., Duniak, B. M., Lee, J., Tsai, F. T. F., Wilson, M. R., Zweckstetter, M., Dickey, C. A., & Gestwicki, J. E. (2018). Mapping interactions with the chaperone network reveals factors that protect against tau aggregation. *Nature Structural & Molecular Biology*, 25(5), 384–393. <https://doi.org/10.1038/s41594-018-0057-1>
- Moran, L. A., Horton, R. H., Scrimgeour, G. K., & Perry, M. D. (2013). *Principles of Biochemistry* (Second custom edition for University of Alberta). Prentice Hall.
- Morozova, O. A., March, Z. M., Robinson, A. S., & Colby, D. W. (2013). Conformational Features of Tau Fibrils from Alzheimer's Disease Brain Are Faithfully Propagated by Unmodified Recombinant Protein. *Biochemistry*, 52(40), 6960–6967. <https://doi.org/10.1021/bi400866w>
- Morrissey, J. H., Choi, S. H., & Smith, S. A. (2012). Polyphosphate: An ancient molecule that

- links platelets, coagulation, and inflammation. *Blood*, 119(25), 5972–5979.
<https://doi.org/10.1182/blood-2012-03-306605>
- Mroczo, Groblewska, & Litman-Zawadzka. (2019). The Role of Protein Misfolding and Tau Oligomers (TauOs) in Alzheimer's Disease (AD). *International Journal of Molecular Sciences*, 20(19), 4661. <https://doi.org/10.3390/ijms20194661>
- Mutreja, Y., & Gamblin, T. C. (2017). Optimization of in vitro conditions to study the arachidonic acid induction of 4R isoforms of the microtubule-associated protein tau. In *Methods in Cell Biology* (Vol. 141, pp. 65–88). Elsevier. <https://doi.org/10.1016/bs.mcb.2017.06.007>
- Nachman, E., Wentink, A. S., Madiona, K., Bousset, L., Katsinelos, T., Allinson, K., Kampinga, H., McEwan, W. A., Jahn, T. R., Melki, R., Mogk, A., Bukau, B., & Nussbaum-Krammer, C. (2020). Disassembly of Tau fibrils by the human Hsp70 disaggregation machinery generates small seeding-competent species. *Journal of Biological Chemistry*, 295(28), 9676–9690. <https://doi.org/10.1074/jbc.RA120.013478>
- Nie, C. L., Wang, X. S., Liu, Y., Perrett, S., & He, R. Q. (2007). Amyloid-like aggregates of neuronal tau induced by formaldehyde promote apoptosis of neuronal cells. *BMC Neuroscience*, 8(1), 9. <https://doi.org/10.1186/1471-2202-8-9>
- Nillegoda, N. B., Kirstein, J., Szlachcic, A., Berynskyy, M., Stank, A., Stengel, F., Arnsburg, K., Gao, X., Scior, A., Aebersold, R., Guilbride, D. L., Wade, R. C., Morimoto, R. I., Mayer, M. P., & Bukau, B. (2015). Crucial HSP70 co-chaperone complex unlocks metazoan protein disaggregation. *Nature*, 524(7564), 247–251.
<https://doi.org/10.1038/nature14884>
- Nillegoda, N. B., Stank, A., Malinverni, D., Alberts, N., Szlachcic, A., Barducci, A., De Los Rios, P., Wade, R. C., & Bukau, B. (2017). Evolution of an intricate J-protein network driving protein disaggregation in eukaryotes. *eLife*, 6, e24560.
<https://doi.org/10.7554/eLife.24560>
- Nonaka, T., Watanabe, S. T., Iwatsubo, T., & Hasegawa, M. (2010). Seeded Aggregation and

- Toxicity of α -Synuclein and Tau. *Journal of Biological Chemistry*, 285(45), 34885–34898.
<https://doi.org/10.1074/jbc.M110.148460>
- Park, S. A., Ahn, S. I., & Gallo, J.-M. (2016). Tau mis-splicing in the pathogenesis of neurodegenerative disorders. *BMB Reports*, 49(8), 405–413.
<https://doi.org/10.5483/BMBRep.2016.49.8.084>
- Patterson, K. R., Remmers, C., Fu, Y., Brooker, S., Kanaan, N. M., Vana, L., Ward, S., Reyes, J. F., Philibert, K., Glucksman, M. J., & Binder, L. I. (2011). Characterization of Prefibrillar Tau Oligomers in Vitro and in Alzheimer Disease. *Journal of Biological Chemistry*, 286(26), 23063–23076. <https://doi.org/10.1074/jbc.M111.237974>
- Paudel, H. K., & Li, W. (1999). Heparin-induced Conformational Change in Microtubule-associated Protein Tau as Detected by Chemical Cross-linking and Phosphopeptide Mapping. *Journal of Biological Chemistry*, 274(12), 8029–8038.
<https://doi.org/10.1074/jbc.274.12.8029>
- Perez, N., Sugar, J., Charya, S., Johnson, G., Merrill, C., Bierer, L., Perl, D., Haroutunian, V., & Wallace, W. (1991). Increased synthesis and accumulation of heat shock 70 proteins in Alzheimer's disease. *Molecular Brain Research*, 11(3–4), 249–254.
[https://doi.org/10.1016/0169-328X\(91\)90033-T](https://doi.org/10.1016/0169-328X(91)90033-T)
- Pickhardt, M., Gazova, Z., von Bergen, M., Khlistunova, I., Wang, Y., Hascher, A., Mandelkow, E.-M., Biernat, J., & Mandelkow, E. (2005). Anthraquinones Inhibit Tau Aggregation and Dissolve Alzheimer's Paired Helical Filaments in Vitro and in Cells. *Journal of Biological Chemistry*, 280(5), 3628–3635. <https://doi.org/10.1074/jbc.M410984200>
- Piette, B. L., Alerasool, N., Lin, Z.-Y., Lacoste, J., Lam, M. H. Y., Qian, W. W., Tran, S., Larsen, B., Campos, E., Peng, J., Gingras, A.-C., & Taipale, M. (2021). Comprehensive interactome profiling of the human Hsp70 network highlights functional differentiation of J domains. *Molecular Cell*, 81(12), 2549-2565.e8.
<https://doi.org/10.1016/j.molcel.2021.04.012>

- Polanco, J. C., Hand, G. R., Briner, A., Li, C., & Götz, J. (2021). Exosomes induce endolysosomal permeabilization as a gateway by which exosomal tau seeds escape into the cytosol. *Acta Neuropathologica*, 141(2), 235–256. <https://doi.org/10.1007/s00401-020-02254-3>
- Prusiner, S. B., Scott, M. R., DeArmond, S. J., & Cohen, F. E. (1998). Prion Protein Biology. *Cell*, 93(3), 337–348. [https://doi.org/10.1016/S0092-8674\(00\)81163-0](https://doi.org/10.1016/S0092-8674(00)81163-0)
- Ramachandran, G., & Udgaonkar, J. B. (2011). Understanding the Kinetic Roles of the Inducer Heparin and of Rod-like Protofibrils during Amyloid Fibril Formation by Tau Protein. *Journal of Biological Chemistry*, 286(45), 38948–38959. <https://doi.org/10.1074/jbc.M111.271874>
- Rampelt, H., Kirstein-Miles, J., Nillegoda, N. B., Chi, K., Scholz, S. R., Morimoto, R. I., & Bukau, B. (2012). Metazoan Hsp70 machines use Hsp110 to power protein disaggregation: Disaggregation by animal Hsp110-Hsp70-Hsp40. *The EMBO Journal*, 31(21), 4221–4235. <https://doi.org/10.1038/emboj.2012.264>
- Rauch, J. N., Chen, J. J., Sorum, A. W., Miller, G. M., Sharf, T., See, S. K., Hsieh-Wilson, L. C., Kampmann, M., & Kosik, K. S. (2018). Tau Internalization is Regulated by 6-O Sulfation on Heparan Sulfate Proteoglycans (HSPGs). *Scientific Reports*, 8(1), 6382. <https://doi.org/10.1038/s41598-018-24904-z>
- Renkawek, K., Bosman, G. J. C. G., & Gaestel, M. (1993). Increased expression of heat-shock protein 27 kDa in Alzheimer disease: A preliminary study. *NeuroReport*, 5, 14–16.
- Requena, J. R., & Wille, H. (2014). The structure of the infectious prion protein: Experimental data and molecular models. *Prion*, 8(1), 60–66. <https://doi.org/10.4161/pri.28368>
- Requena, J. R., & Wille, H. (2017). The Structure of the Infectious Prion Protein and Its Propagation. In *Progress in Molecular Biology and Translational Science* (Vol. 150, pp. 341–359). Elsevier. <https://doi.org/10.1016/bs.pmbts.2017.06.009>
- Rosenzweig, R., Nillegoda, N. B., Mayer, M. P., & Bukau, B. (2019). The Hsp70 chaperone

- network. *Nature Reviews Molecular Cell Biology*, 20(11), 665–680.
<https://doi.org/10.1038/s41580-019-0133-3>
- Sanders, D. W., Kaufman, S. K., DeVos, S. L., Sharma, A. M., Mirbaha, H., Li, A., Barker, S. J., Foley, A. C., Thorpe, J. R., Serpell, L. C., Miller, T. M., Grinberg, L. T., Seeley, W. W., & Diamond, M. I. (2014). Distinct Tau Prion Strains Propagate in Cells and Mice and Define Different Tauopathies. *Neuron*, 82(6), 1271–1288.
<https://doi.org/10.1016/j.neuron.2014.04.047>
- SantaCruz, K., Lewis, J., Spires, T., Paulson, J., Kotilinek, L., Ingelsson, M., Guimaraes, A., DeTure, M., Ramsden, M., McGowan, E., Forster, C., Yue, M., Orne, J., Janus, C., Mariash, A., Kuskowski, M., Hyman, B., Hutton, M., & Ashe, K. H. (2005). Tau Suppression in a Neurodegenerative Mouse Model Improves Memory Function. *Science*, 309(5733), 476–481. <https://doi.org/10.1126/science.1113694>
- Scheres, S., & Lövestam, S. (2022). High-throughput cryo-EM structure determination of amyloids. *bioRxiv*. <https://doi.org/10.1101/2022.02.07.479378>
- Scheres, S. H., Zhang, W., Falcon, B., & Goedert, M. (2020). Cryo-EM structures of tau filaments. *Current Opinion in Structural Biology*, 64, 17–25.
<https://doi.org/10.1016/j.sbi.2020.05.011>
- Shammas, S. L., Garcia, G. A., Kumar, S., Kjaergaard, M., Horrocks, M. H., Shivji, N., Mandelkow, E., Knowles, T. P. J., Mandelkow, E., & Klenerman, D. (2015). A mechanistic model of tau amyloid aggregation based on direct observation of oligomers. *Nature Communications*, 6(1), 7025. <https://doi.org/10.1038/ncomms8025>
- Sharon, R., Bar-Joseph, I., Mirick, G. E., Serhan, C. N., & Selkoe, D. J. (2003). Altered Fatty Acid Composition of Dopaminergic Neurons Expressing α -Synuclein and Human Brains with α -Synucleinopathies. *Journal of Biological Chemistry*, 278(50), 49874–49881.
<https://doi.org/10.1074/jbc.M309127200>
- Shinohara, H., Inaguma, Y., Goto, S., Inagaki, T., & Kato, K. (1993). Alpha B crystallin and

- Hsp28 are enhanced in the cerebral cortex of patients with Alzheimer's disease. *Journal of the Neurological Sciences*, 119, 203–208.
- Sibille, N., Sillen, A., Leroy, A., Wieruszeski, J.-M., Mulloy, B., Landrieu, I., & Lippens, G. (2006). Structural Impact of Heparin Binding to Full-Length Tau As Studied by NMR Spectroscopy. *Biochemistry*, 45(41), 12560–12572. <https://doi.org/10.1021/bi060964o>
- Smith, S. A., Mutch, N. J., Baskar, D., Rohloff, P., Docampo, R., & Morrissey, J. H. (2006). Polyphosphate modulates blood coagulation and fibrinolysis. *Proceedings of the National Academy of Sciences*, 103(4), 903–908. <https://doi.org/10.1073/pnas.0507195103>
- Snowden, S. G., Ebshiana, A. A., Hye, A., An, Y., Pletnikova, O., O'Brien, R., Troncoso, J., Legido-Quigley, C., & Thambisetty, M. (2017). Association between fatty acid metabolism in the brain and Alzheimer disease neuropathology and cognitive performance: A nontargeted metabolomic study. *PLOS Medicine*, 14(3), e1002266. <https://doi.org/10.1371/journal.pmed.1002266>
- Söti, C., & Csermely (2000). Molecular chaperones and the aging process. *Biogerontology*, 1, 225-233.
- Söti, C., & Csermely, P. (2002). Chaperones and aging: Role in neurodegeneration and in other civilizational diseases. *Neurochemistry International*, 41(6), 383–389. [https://doi.org/10.1016/S0197-0186\(02\)00043-8](https://doi.org/10.1016/S0197-0186(02)00043-8)
- Soto, C. (2003). Unfolding the role of protein misfolding in neurodegenerative diseases. *Nature Reviews Neuroscience*, 4(1), 49–60. <https://doi.org/10.1038/nrn1007>
- Soto, C., & Castaño, E. M. (1996). The conformation of Alzheimer's β peptide determines the rate of amyloid formation and its resistance to proteolysis. *Biochemical Journal*, 314(2), 701–707. <https://doi.org/10.1042/bj3140701>
- Soto, C., & Pritzkow, S. (2018). Protein misfolding, aggregation, and conformational strains in neurodegenerative diseases. *Nature Neuroscience*, 21(10), 1332–1340.

<https://doi.org/10.1038/s41593-018-0235-9>

- Spires, T. L., Orne, J. D., SantaCruz, K., Pitstick, R., Carlson, G. A., Ashe, K. H., & Hyman, B. T. (2006). Region-specific Dissociation of Neuronal Loss and Neurofibrillary Pathology in a Mouse Model of Tauopathy. *The American Journal of Pathology*, *168*(5), 1598–1607. <https://doi.org/10.2353/ajpath.2006.050840>
- Stege, G. J. J., Renkawek, K., Overkamp, P. S. G., Verschuure, P., van Rijk, A. F., Reijnen-Aalbers, A., & Boelens, W. C. (1999). The Molecular Chaperone β -crystallin Enhances Amyloid β Neurotoxicity. *BIOCHEMICAL AND BIOPHYSICAL RESEARCH COMMUNICATIONS*, *262*(1), 5.
- Tallima, H., & El Ridi, R. (2018). Arachidonic acid: Physiological roles and potential health benefits – A review. *Journal of Advanced Research*, *11*, 33–41. <https://doi.org/10.1016/j.jare.2017.11.004>
- Taniguchi, S., Suzuki, N., Masuda, M., Hisanaga, S., Iwatsubo, T., Goedert, M., & Hasegawa, M. (2005). Inhibition of Heparin-induced Tau Filament Formation by Phenothiazines, Polyphenols, and Porphyrins. *Journal of Biological Chemistry*, *280*(9), 7614–7623. <https://doi.org/10.1074/jbc.M408714200>
- Terada, K., & Mori, M. (2000). Human DnaJ Homologs dj2 and dj3, and bag-1 Are Positive Cochaperones of hsc70. *Journal of Biological Chemistry*, *275*(32), 24728–24734. <https://doi.org/10.1074/jbc.M002021200>
- Vaquer-Alicea, J., Diamond, M. I., & Joachimiak, L. A. (2021). Tau strains shape disease. *Acta Neuropathologica*, *142*(1), 57–71. <https://doi.org/10.1007/s00401-021-02301-7>
- von Bergen, M., Barghorn, S., Biernat, J., Mandelkow, E.-M., & Mandelkow, E. (2005). Tau aggregation is driven by a transition from random coil to beta sheet structure. *Biochimica et Biophysica Acta (BBA) - Molecular Basis of Disease*, *1739*(2–3), 158–166. <https://doi.org/10.1016/j.bbadis.2004.09.010>

- von Bergen, M., Barghorn, S., Li, L., Marx, A., Biernat, J., Mandelkow, E.-M., & Mandelkow, E. (2001). Mutations of Tau Protein in Frontotemporal Dementia Promote Aggregation of Paired Helical Filaments by Enhancing Local β -Structure. *Journal of Biological Chemistry*, 276(51), 48165–48174. <https://doi.org/10.1074/jbc.M105196200>
- von Bergen, M., Friedhoff, P., Biernat, J., Mandelkow, E.-M., & Mandelkow, E. (2000). Assembly of tau protein into Alzheimer paired helical filaments depends on a local motif (306VQIVYK311) forming beta structure. *PNAS*, 97(10), 5129–5134.
- Voss, K., Combs, B., Patterson, K. R., Binder, L. I., & Gamblin, T. C. (2012). Hsp70 Alters Tau Function and Aggregation in an Isoform Specific Manner. *Biochemistry*, 51(4), 888–898. <https://doi.org/10.1021/bi2018078>
- Wang, C., Fan, L., Zhan, L., Kodama, L., Liu, B., Chin, M., Li, Y., Le, D., Zhou, Y., Condello, C., Grinberg, L., Seeley, W. W., Miller, B., Mok, S.-A., Gestwicki, J., & Gan, L. (2021). *Microglial NF- κ B drives tau spreading and toxicity in a mouse model of tauopathy* [Preprint]. Neuroscience. <https://doi.org/10.1101/2021.02.22.432272>
- Ward, S. M., Himmelstein, D. S., Lancia, J. K., & Binder, L. I. (2012). Tau oligomers and tau toxicity in neurodegenerative disease. *Biochemical Society Transactions*, 40(4), 667–671. <https://doi.org/10.1042/BST20120134>
- Whitford, D. (2005). *Proteins: Structure and Function*. John Wiley & Sons. 1-5.
- Wickramasinghe, S. P., Lempart, J., Merens, H. E., Murphy, J., Huettemann, P., Jakob, U., & Rhoades, E. (2019). Polyphosphate Initiates Tau Aggregation through Intra- and Intermolecular Scaffolding. *Biophysical Journal*, 117(4), 717–728. <https://doi.org/10.1016/j.bpj.2019.07.028>
- Wilson, D. M., & Binder, L. I. (1997). Free Fatty Acids Stimulate the Polymerization of Tau and Amyloid B Peptides. *American Journal of Pathology* 150 (6), 2181-2195.
- Woerman, A. L., Aoyagi, A., Patel, S., Kazmi, S. A., Lobach, I., Grinberg, L. T., McKee, A. C.,

- Seeley, W. W., Olson, S. H., & Prusiner, S. B. (2016). Tau prions from Alzheimer's disease and chronic traumatic encephalopathy patients propagate in cultured cells. *Proceedings of the National Academy of Sciences*, 113(50).
<https://doi.org/10.1073/pnas.1616344113>
- Xie, L., & Jakob, U. (2019). Inorganic polyphosphate, a multifunctional polyanionic protein scaffold. *Journal of Biological Chemistry*, 294(6), 2180–2190.
<https://doi.org/10.1074/jbc.REV118.002808>
- Yan, W., & Craig, E. A. (1999). The Glycine-Phenylalanine-Rich Region Determines the Specificity of the Yeast Hsp40 Sis1. *Molecular and Cellular Biology*, 19(11), 7751–7758.
<https://doi.org/10.1128/MCB.19.11.7751>
- Yu, A., Fox, S. G., Cavallini, A., Kerridge, C., O'Neill, M. J., Wolak, J., Bose, S., & Morimoto, R. I. (2019). Tau protein aggregates inhibit the protein-folding and vesicular trafficking arms of the cellular proteostasis network. *Journal of Biological Chemistry*, 294(19), 7917–7930. <https://doi.org/10.1074/jbc.RA119.007527>
- Yu, H. Y., Ziegelhoffer, T., & Craig, E. A. (2015). Functionality of Class A and Class B J-protein co-chaperones with Hsp70. *FEBS Letters*, 589(19PartB), 2825–2830.
<https://doi.org/10.1016/j.febslet.2015.07.040>
- Zanier, E. R., Bertani, I., Sammali, E., Pischutta, F., Chiaravalloti, M. A., Vegliante, G., Masone, A., Corbelli, A., Smith, D. H., Menon, D. K., Stocchetti, N., Fiordaliso, F., De Simoni, M.-G., Stewart, W., & Chiesa, R. (2018). Induction of a transmissible tau pathology by traumatic brain injury. *Brain*. <https://doi.org/10.1093/brain/awy193>
- Zhang, W., Falcon, B., Murzin, A. G., Fan, J., Crowther, R. A., Goedert, M., & Scheres, S. H. (2019). Heparin-induced tau filaments are polymorphic and differ from those in Alzheimer's and Pick's diseases. *eLife*, 8, e43584. <https://doi.org/10.7554/eLife.43584>
- Zhang, W., Tarutani, A., Newell, K. L., Murzin, A. G., Matsubara, T., Falcon, B., Vidal, R., Garringer, H. J., Shi, Y., Ikeuchi, T., Murayama, S., Ghetti, B., Hasegawa, M., Goedert,

M., & Scheres, S. H. W. (2020). Novel tau filament fold in corticobasal degeneration. *Nature*, 580(7802), 283–287. <https://doi.org/10.1038/s41586-020-2043-0>

Appendix A: Signal from 10% seeding material in capillary gel electrophoresis

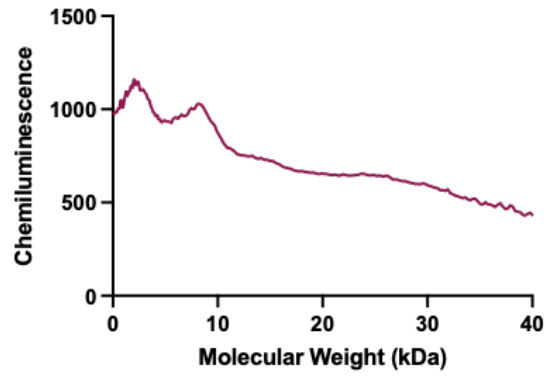
Signal from 10% seeding material in capillary gel electrophoresis

When analyzing results from the *in vitro* seeding assay with 10% seeding material and no addition of inducer (see section 3.2.5), we saw minimal signal in the products of the resulting reactions when heparin, polyP and Ara induced aggregates were used as seeding material (with the exception of one of the polyP aggregate reactions) (**Figure 3.10**). This prompted us to question whether or not the minimal trypsin resistant signal that we were seeing in most reactions was due to the signal from the original 10% seeding material itself. The 10% seeding material underwent trypsin digestion and was subsequently subjected to capillary gel electrophoresis with the goal of determining how much background signal was contributed by the seeding material itself. This experiment used the products of three wells combined, completed only once.

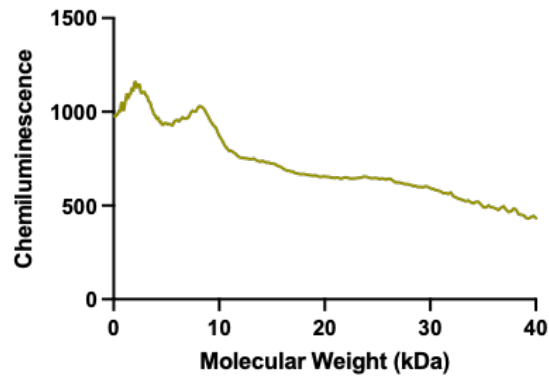
Results

Results indicate that 10% seeding material does indeed generate a minimal signal with peaks that resemble those seen in Figure 3.10. We can likely conclude that aside from the product of polyP reaction 1, the signal produced from the other products of seeding reactions is due to background from the original 10% seeding material.

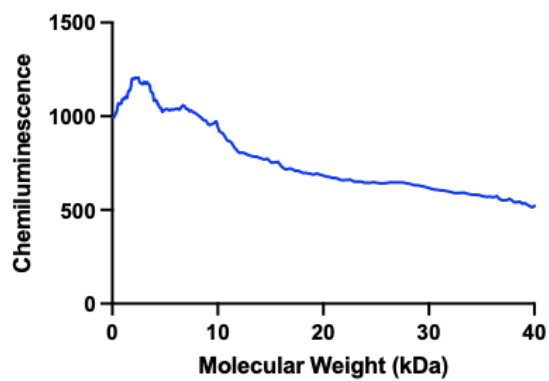
10% Heparin aggregate seeding material



10% PolyP aggregate seeding material



10% Ara aggregate seeding material



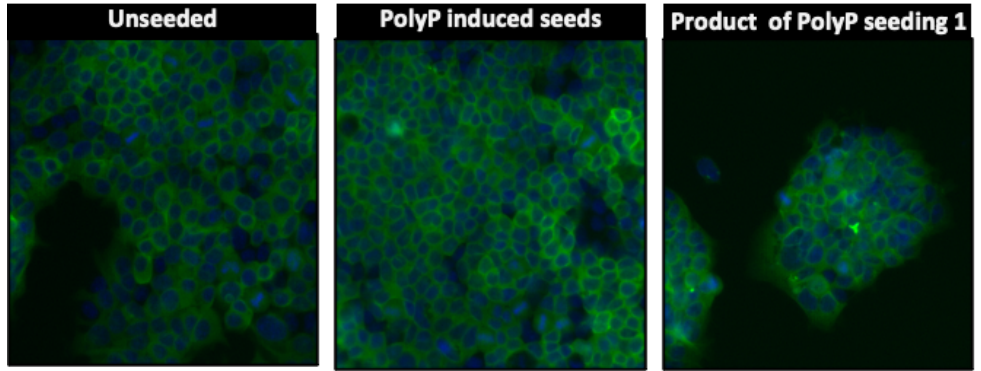
Appendix B: Trypsin resistant seeding product of polyP aggregation reaction

Trypsin resistant seeding product of polyP aggregation reaction

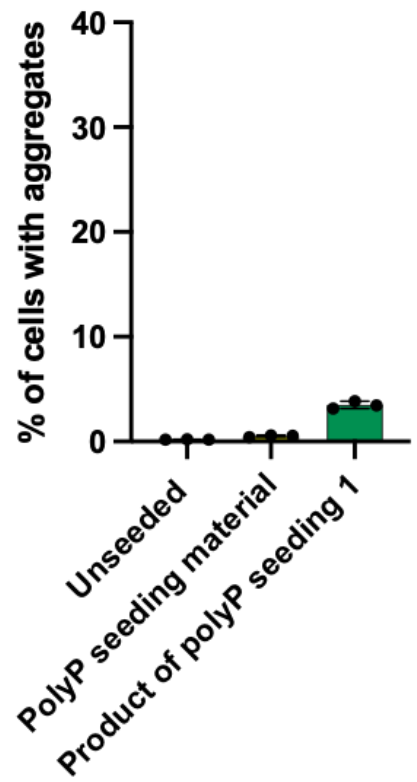
When 10% polyP induced aggregates were added to monomeric tau without the addition of an inducer in an *in vitro* aggregation assay, ThT signal increased over the course of 48 hours indicating the existence of a seeding event (**Figure 3.10 A+B**). Upon trypsin digestion of the three products of reaction, only one yielded a trypsin resistant product (**Figure 3.10 D**). It would be juvenile to assume that we would not want to apply this product to cells. Given that the *in vitro* reaction is carried out in such a small volume, we only had enough material to seed cells at 0.1 μM , a concentration that we chose based on its ability to achieve high seeding levels with heparin induced aggregates (**Figure 3.6**). This experiment was done in triplicate wells, in only one experiment.

Results

Upon addition of 0.1 μM of polyP aggregation product 1 to cells, very little seeding effect was observed. Product 1 led to a total of 3.5% of cells being positive for aggregates, while polyP induced aggregates themselves achieved only a level of 0.6%. While product 1 does achieve a higher seeding level than polyP induced aggregates themselves, it is nowhere close to the level of aggregation achieved when heparin induced aggregates act as seeds.



0.1 μM aggregate seeding in cells



Appendix C: *In vitro* seeding with differently induced aggregates in conjunction with their respective inducer

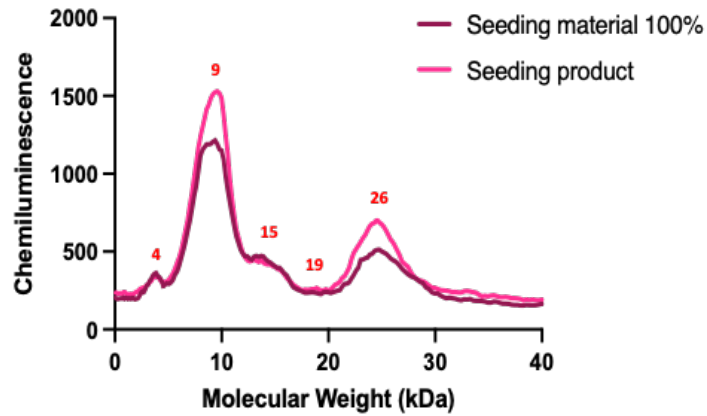
***In vitro* seeding with differently induced aggregates in conjunction with their respective inducer**

Since differently induced aggregates did not appear to have significant seeding effects without the addition of their inducers *in vitro* (with the exception of polyP product 1), we carried out a reaction with 3% seeding material with the addition of the respective inducers. The original differently induced aggregates and the products of each seeding reaction were subjected to trypsin digest and capillary gel electrophoresis. One *in vitro* experiment was carried out with wells repeated in triplicate. The triplicate wells were combined before addition of trypsin to yield enough reaction product.

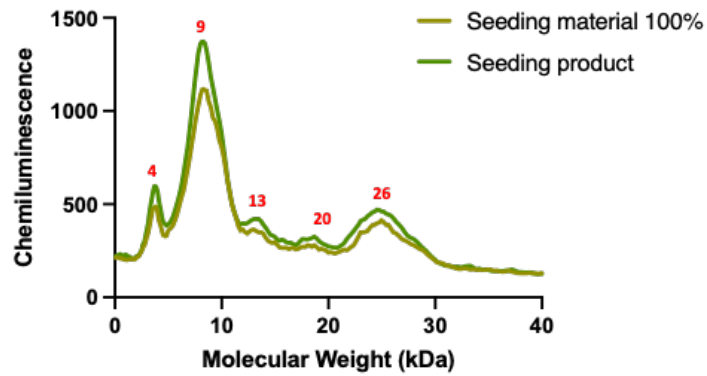
Results

Resulting chromatograms obtained from capillary gel electrophoresis show similar peaks between the original seeding material and the product of seeded reaction. This suggests that in the presence of their respective inducer, differently induced aggregates are able to carry out a seeding reaction that propagates their unique structure. A limitation of this experiment is that we cannot conclude that the inducer in the reaction itself isn't solely responsible for the structures of the resulting products.

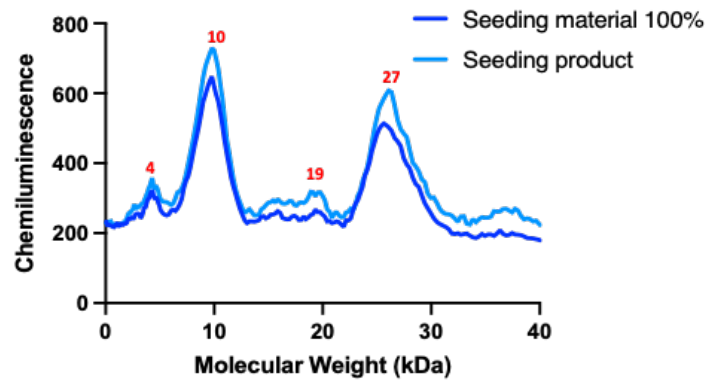
Seeding with heparin aggregates and inducer



Seeding with polyP aggregates and inducer



Seeding with Ara aggregates and inducer



Appendix D: ThT staining of differently induced aggregates

ThT staining of differently induced aggregates

To ensure that there were no significant size differences between differently induced aggregates that might be contributing to their seeding variability in cells, Pallabi Sil Paul of the Kar lab (Center for Prions and Protein Folding Disease, University of Alberta) stained our aggregates with ThT and visualized them using fluorescent microscopy. This experiment was only carried out once and is in the process of being optimized so that we can quantify the images to obtain exact measurements of the aggregates.

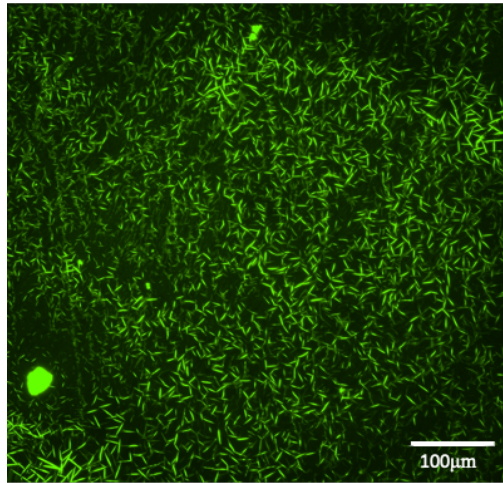
Protocol

Aggregates were spun down at 11,000 rpm for 10 minutes and resuspended in nuclease free water. 1:5 volume of ThT dye was added to 10 μ M of aggregates and allowed to incubate for 30 minutes at room temperature. 10 μ L of the final solution was loaded onto a glass slide and allowed to dry prior to imaging. Images were collected using a Nikon Eclipse 90i fluorescence microscope at 20 X magnification and processed using NIS Elements software.

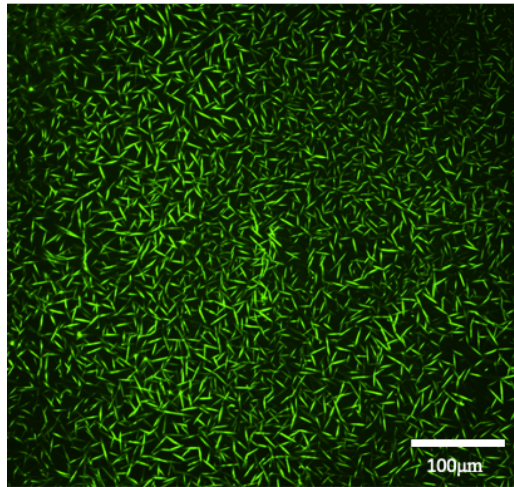
Results

Fluorescent images indicate that differently induced aggregates are all similar in size, and have relative size homogeneity within samples. The centrifugation step of this experiment may be limiting in that it selects for a particular size range of aggregates. In future experiments, we plan to eliminate the centrifugation step and dilute the aggregates so that the resulting images can be properly quantified using an analysis software.

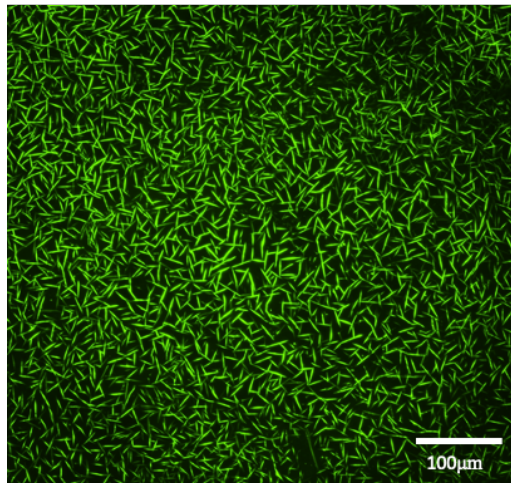
Heparin aggregates



PolyP aggregates



Ara aggregates



Staining and imaging done by Pallabi Sil Paul